International Journal of Mechanical Sciences 268 (2024) 109036

Contents lists available at ScienceDirect

International Journal of Mechanical Sciences

journal homepage: www.elsevier.com/locate/ijmecsci

The dependent coordinates in the linearization of constrained multibody systems: Handling and elimination

A.G. Agúndez [a,*], D. García-Vallejo [a], E. Freire [b], A. Mikkola [c]

[a] Department of Mechanical Engineering and Manufacturing, Universidad de Sevilla, Seville, Spain
[b] Department of Applied Mathematics II, Universidad de Sevilla, Seville, Spain
[c] Department of Mechanical Engineering, Lappeenranta University of Technology, Lappeenranta, Finland

ARTICLE INFO

Keywords:
Constrained multibody system
Linear stability analysis
Dependent coordinate elimination
Linearization approaches overview
Bicycle
e-scooter

ABSTRACT

In this paper, the handling of the dependent coordinates in the linearization of constrained multibody systems is clarified. To this end, a brief but comprehensive overview of linearization approaches used in the field of Multibody System Dynamics is presented. These procedures are illustrated by using a common notation and classified into four groups, depending on the initial form of the nonlinear equations of motion and the selection of the generalized coordinates (a redundant or a minimal set). The handling of the dependent coordinates in each of the procedures is discussed. The linearized equations of motion of constrained multibody systems are of great importance in several applications, such as linear stability and modal analyses, the design of linear state feedback controllers or the building of state and input estimators, like Kalman filters. When modeling a constrained multibody system, a number of coordinates greater than the number of degrees of freedom of the system is usually used. While some linearization approaches make use of the complete set of coordinates, several procedures are based on a coordinate partition in terms of independent and dependent coordinates to reduce the number of linearized equations of motion. In this latter scenario, the role of the dependent coordinates in the linearization is important and, in a general case, these dependent coordinates cannot be ignored to obtain the correct linearized equations of motion. This aspect, which may seem obvious, is not straightforward and is addressed in this work. The importance of considering the set of dependent coordinates in the linearization is demonstrated with a well-acknowledged bicycle benchmark multibody model and an electric kickscooter multibody model with rear and front suspensions. To this end, the Jacobian matrix and the linear stability results of these case studies are computed by considering different choices of independent and dependent coordinates.

1. Introduction

The equations of motion of constrained multibody systems are usually given by nonlinear Differential-Algebraic Equations (DAE) systems, whose correct linearization poses a challenge when the multibody system model consists of a large number of coordinates and constraints. The DAE system can be reduced to a system of Ordinary Differential Equations (ODE) by resorting to a coordinate partition in terms of independent and dependent coordinates [1–3]. In this case, the linearization must be conducted carefully and, in general, the dependent coordinates cannot be ignored in the computation of the correct linearized equations. In the field of Multibody System Dynamics, the number of works devoted to the linearization of the equations of motion has increased in recent years, due to its importance, for example, in the design of controllers and state observers. These linearization approaches differ from each other depending on the initial form of the nonlinear equations of motion, the selection of the generalized coordinates that they use (a redundant or a minimal set) or the structure of the linearized equations of motion, which is highly dependent on the selection of coordinates.

A first group of works intends to linearize the index-3 DAE equations of motion. The work of Negrut et al. [4] presents a linearization approach suitable for heterogeneous systems, that include nonholonomic constraints, friction, flexible bodies or user-defined differential equations. In this procedure, the governing equations are augmented and a set of sensitivities that provide the linearization of interest are computed. The approach was numerically tested with a nonuniform helicopter blade, a washing machine, an all terrain vehicle and a rotor-stator multibody models. Escalona et al. [5,6] also linearized the index-3 DAE equations of motion. In [5], the stability analysis of the steady curving of vehicles is addressed. An alternative stability analysis

* Corresponding author.
E-mail addresses: agarciaagundez@us.es (A.G. Agúndez), dgvallejo@us.es (D. García-Vallejo), efrem@us.es (E. Freire), aki.mikkola@lut.fi (A. Mikkola).

https://doi.org/10.1016/j.ijmecsci.2024.109036
Received 2 October 2023; Received in revised form 9 January 2024; Accepted 9 January 2024
Available online 15 January 2024

to the use of Floquet's theory, based on two coordinate projections, is presented. In particular, the linear stability of the circular steady motion of a simple wheeled mechanism is analyzed. The same approach is used in [6] to linearize the equations of motion of railroad vehicles moving on curved tracks. Another procedure devoted to the linearization of the index-3 DAE system is described by González et al. [7]. This approach, known as Redundant Coordinate Set (RCS) Formulation in [7], leads to the same structure of the linearized equations motion obtained in [5,6]. The properties of the approach are shown with the linearization of two numerical examples in static equilibrium: a multiple loop four-bar linkage and a flexible double pendulum. The work of González et al. [7] presents two other linearization procedures, whose properties are also assessed with these numerical examples. Recently, Pappalardo et al. [8] presented an approach to linearize the index-3 DAE form of the equations of motion of multibody systems with holonomic and nonholonomic constraints. The use of the procedure is illustrated with different numerical examples of multibody systems: a two-dimensional physical pendulum and wheeled inverted pendulum, a spinning top, a disk rolling without slipping on a horizontal plane and a Watt centrifugal governor model. The approach is also revisited in [9] and applied to study the stability of a bicycle multibody model [10]. Moreover, Xiong et al. [11] linearized the index-3 DAE equations of motion of the Whipple bicycle, moving on a revolution surface, along its circular steady motion. The resulting linearized equations of motion present the same structure obtained with the RCS approach of González et al. [7] and the approach of Escalona et al. [5,6]. Nevertheless, since these approaches result in a structure of the linearized system of equations that hinders the performance of a standard eigenvalue analysis, a reduced system of first-order ODEs is derived in [11]. All the linearization procedures of this group make use of a redundant set of coordinates.

A second group of approaches is based on the linearization of the index-1 form of the DAE system. The index-1 form is obtained by computing the constraints at acceleration level and assembling them with the dynamic equilibrium equations. A straightforward way to carry out the linearization of these nonlinear equations of motion is based on the isolation of the acceleration vector. Once the accelerations are obtained, a linear ODE system can be built. Nevertheless, this approach is impractical for complex multibody systems with large number of bodies, coordinates and constraints, due to the high computational cost required. Van Khang et al. [12] proposed a symbolic linearization procedure using redundant coordinates. The correctness of the approach is verified with a four-bar mechanism with an elastic connecting link. Agúndez et al. [13] developed three general procedures to linearize the equations of motion of constrained multibody systems. Among the procedures presented in [13], a direct linearization of the index-1 form of the DAE system of equations was presented. This procedure was validated with the stability results of the bicycle benchmark of Meijaard et al. [14].

The reduction of the DAE system to an ODE system, by using a coordinate partition in terms of independent and dependent coordinates, gives rise to a third group of linearization approaches. Some works describing the transformation of the nonlinear equations of motion of a constrained dynamical system in DAE form into an ODE system, expressed in terms of the independent coordinates, are the works of Wehage and Haug [1] and García de Jalón and Bayo [3]. The linearization of this ODE system of equations is performed by Cuadrado et al. [15,16] to compute the state-space Jacobian matrix, required for building continuous extended Kalman filters (CEKF). In [15,16], the derivatives of the independent accelerations with respect to the independent coordinates and velocities are required, and the size of the state-space Jacobian matrix is twice the number of degrees of freedom of the multibody system. These derivatives are also necessary in the construction of the state-transition matrix of discrete extended Kalman filters (DEKF) [17–19] and error-state extended Kalman filters [17,18,20–22]. A similar result to that of [15,16] is obtained by González et al. [7] with the procedure known as Minimal Coordinate Set (MCS) Formulation. In this work, a further development of the derivatives of the independent accelerations with respect to the independent positions and velocities are presented. In all these works, the state-space Jacobian matrix includes only the partial derivatives with respect to the independent positions and velocities. Nevertheless, some explanatory comments regarding the role of the dependent coordinates in these linearization approaches are required to compute the correct linearized equations of motion. As stated by Peterson et al. [23], where a linearization procedure is developed for equations of motion generated by Kane's method [24], the dependent coordinates and dependent velocities are functions of the independent coordinates and independent velocities. Therefore, the dependent states cannot be eliminated in general without considering this dependency with the independent ones. To the best of the authors' knowledge, no previous author makes this explicitly clear when presenting procedures for symbolically linearizing the equations of motion of constrained dynamical systems [23]. In some particular cases, one can intuitively find a set of independent coordinates that allows for eliminating the derivatives with respect to the dependent ones in the linearization. For example, Escalona et al. [25] analyzed the linear stability of the steady forward motion of a bicycle multibody model by resorting to a similar procedure to those of [15,16], considering only the derivatives with respect to the independent coordinates in the linearization. In [25], it is specified that the dependent coordinates are considered as null in the linearization, since, in the particular case of the bicycle multibody model, they do not have influence on the linear stability. Agúndez et al. [13] also performed the linearization of this ODE system. In this case, it is explicitly stated that the dependent coordinates are not ignored in the linearization and the resulting Jacobian matrix includes the derivatives with respect to the dependent coordinates. Moreover, a counterpart approach, which significantly reduces the computational cost for the computation of the Jacobian matrix, was presented in [13]. This counterpart approach also included the blocks associated with the dependent coordinates in the Jacobian matrix. While the approaches found in [7,15–17,25] transform the original nonlinear DAE system into a nonlinear ODE system of equations by using the coordinate partition, and subsequently perform the linearization, the counterpart approaches presented in [13] first linearize the DAE system and then carry out the reduction to a linear ODE system. The correctness of this procedure was validated with the linear stability results of the bicycle benchmark of Meijaard et al. [14].

Lastly, a fourth group of linearization approaches can be considered. As in the third group, these procedures make use of a coordinate partition in terms of independent and dependent coordinates. Nevertheless, these approaches achieve a linear ODE system of equations that is only expressed in terms of the independent coordinates. In this case, the influence of the dependent coordinates on the linearization is considered by resorting to the linearized constraints, which allows for obtaining an expression of the dependent coordinates in terms of the independent ones. In the case of a multibody system constrained only by holonomic constraints, the Jacobian matrix only includes the derivatives with respect to the independent variables, without ignoring the dependent ones, and presents a size twice the number of degrees of freedom of the multibody system (as in [15–17]). Bae [26] presents a linearization procedure in which the perturbed constraint equations are solved for variations of all the variables in terms of the independent ones. Subsequently, these relations are substituted into the variational dynamic equations to obtain the linearized equations of motion in terms of the independent variations. Agúndez et al. [13] proposed two linearization approaches that fall within this group. The first procedure transforms the original nonlinear DAE system into a nonlinear ODE system of equations by using a coordinate partition. Next, the linearization of the ODE system is carried out, including the dependency of the dependent coordinates with the independent ones by using the linearized holonomic constraints. A counterpart approach is

developed in [13], where the DAE system is first linearized, and then a reduction to a linear ODE system is performed with the coordinate partition, greatly reducing the computational cost. This strategy is also followed by Cossalter et al. [27], where a procedure for evaluating the stability of steady state solutions in straight running and on a curve of sports motorcycles is presented. The linearization approaches of this group achieve the maximum possible reduction of the Jacobian matrix.

In addition to the approaches already mentioned, there exist alternative procedures to linearize the equations of motion of multibody systems. An example is the third procedure presented by González et al. in [7], so-called Unconstrained Coordinate Set (UCS) Formulation. This approach is based on the Penalty method, in which a penalty-based relaxation of the constraints allows for transforming a DAE system into a set of ODEs [28]. Moreover, González et al. [29] identified two types of linearization problems: heavily constrained multibody systems, with a number of degrees of freedom much lower than the number of kinematic variables, and systems in which both numbers are similar. Other works are based on the linearization of the equations of motion of constrained multibody systems without Lagrange multipliers. Xiong et al. [30] derived the Gibbs–Appell equations [31,32] for the dynamic analysis of the Whipple bicycle, obtaining a minimal set of equations of motion without Lagrange multipliers. These equations are linearized and the stability analyses of the steady straight-line motion and the circular steady solution are performed. Xiong et al. [33] also applied Voronets equations [34] to the Whipple bicycle moving on a revolution surface, to obtain a seven-dimensional reduced dynamic system on the reduced constraint space. Two types of relative equilibria (static and dynamic) were studied and the stability of the bicycle was discussed. As previously mentioned, a linearization approach based on Kane's equations of motion [24] is presented by Peterson et al. [23]. Moreover, Saccon et al. [35] proposed, from the standpoint of Geometric Mechanics, a recursive and singularity-free linearization procedure for moving-based robot systems.

The linearized equations of multibody systems are also computed in other works devoted to the development of Kalman filters [36–38] and order reduction methods [39], where the system is modeled by using the nonlinear finite elements of absolute nodal coordinate formulation and then locally linearized at a series of quasi-static equilibrium configurations. The stability of complex multibody systems is addressed by Bauchau et al. [40,41], and Floquet theory [42,43] is the preferred methodology for assessing the linear stability of systems with periodic coefficients [44,45]. This kind of analysis requires the evaluation of the so-called Floquet multipliers, based on a monodromy matrix which follows by numerical integration of a linearized set of equations. Additional works include stability analyses of multibody systems as motorcycles [27,46–53], the waveboard [54,55] and other vehicles [56–59]. The stability analysis of nonlinear multibody systems, as rotorcraft systems, can be found in several works of Masarati et al. [60–66], which make use of Lyapunov characteristic exponents.

In a context of boom in electric single-person vehicles, bicycles and electric kickscooters play a major role in urban microbility. A review of history, development, design, research and rules for utilization of electric bicycles in some world areas was addressed by Hung et al. [67]. Ventura et al. [68] proposed a novel framework to assess the vibrational behavior of electric bicycles and kickscooters when driven by different users and exposed to the pavement irregularities. Eccarius et al. [69] presented a review of consumer adoption of electric motorcycles, and Manrique et al. [70] reviewed the main aspects concerning the kinematics, dynamics and control of two-wheeled vehicles, described within the multibody formulation. Several works in the literature are devoted to the stability of bicycles [14,71–78], the study of safety and injuries resulting from the use of electric kickscooters [79–86] and the stability of electric kickscooters [87–89]. As case studies to illustrate the role of the dependent coordinates in the linearization procedures outlined in this work, the linear stability results of a bicycle and an e-scooter multibody model have been utilized.

The novelty of this work lies in clarifying the handling of the dependent coordinates in the linearization of the equations of motion of multibody systems with holonomic and nonholonomic constraints. Despite the dependent coordinates can be ignored in some particular cases, they should generally be considered to compute the correct linearized equations of motion. To this end, a first contribution of this study is the presentation of a brief but comprehensive overview with some of the most notable linearization approaches developed in the field of Multibody System Dynamics, for constrained multibody systems with Lagrange multipliers. To the best knowledge of the authors, this has not been done in any previous work of the literature and constitutes an useful contribution for the MBS community, since the linearization approaches of previous works are summarized and illustrated by using a common notation. The role of the dependent coordinates in each of these procedures is discussed. The linearization procedures are classified into four groups: procedures based on the linearization of the index-3 DAE system, using a redundant set of coordinates; procedures based on the linearization of the index-1 DAE system, considering a redundant set of coordinates; procedures based on a coordinate partition in terms of independent and dependent coordinates, which lead to a reduced linear ODE system; and procedures that lead to the linearized equations of motion in ODE form, only expressed in terms of the independent coordinates, by means of the elimination of the holonomic constraints. It is important to highlight that this work is not intended to present a survey with all the existing linearization approaches that can be found in the literature of Multibody System Dynamics and a comparison between them. Another important contribution of this study is the detailed demonstration of the importance of considering the dependent coordinates in those linearization procedures that rely on a coordinate partition in terms of independent and dependent coordinates. This is illustrated through the linear stability results of a well-acknowledged bicycle benchmark multibody model and an electric kickscooter multibody model with rear and front suspensions. In this regard, different choices of independent and dependent coordinates are considered when computing the Jacobian matrices for both the bicycle and e-scooter.

The paper is organized as follows. Following the Introduction, Section 2 presents different forms of the nonlinear equations of motion of multibody systems, which give rise to the classification of the linearization procedures presented in Section 3. The main steps and the handling of the dependent coordinates in each approach are summarized in Section 3. Section 4 shows the importance of considering the derivatives with respect to the dependent coordinates in the linearization with the linear stability results of the bicycle and e-scooter multibody models. Finally, the main conclusions drawn from this work are summarized in Section 5.

2. Forms of the equations of motion

In this section, different forms of the nonlinear equations of motion of constrained multibody systems are summarized. These forms of the equations of motion lead to the classification of the linearization procedures presented in Section 3. First, the index-3 DAE form of the equations of motion of a multibody system with holonomic and nonholonomic constraints is presented. Next, the index-1 DAE form, given by the dynamic equations and the constraints at acceleration level, is shown. Subsequently, the DAE system is transformed into an ODE system of equations by using a coordinate partition in terms of independent and dependent coordinates. Lastly, this coordinate partition is also used to obtain a DAE system of equations without Lagrange multipliers.

2.1. Index-3 DAE form

The equations of motion of a multibody system, modeled with n coordinates, m holonomic and l nonholonomic constraints, are given by the following nonlinear index-3 DAE system:

$$\boldsymbol{M}(\boldsymbol{x})\,\ddot{\boldsymbol{x}} + \boldsymbol{D}^{\mathrm{T}}(\boldsymbol{x})\,\boldsymbol{\Lambda} = \boldsymbol{Q}(\boldsymbol{x},\dot{\boldsymbol{x}}), \tag{1}$$

$$\boldsymbol{C}(\boldsymbol{x}) = \boldsymbol{0}, \tag{2}$$

$$\boldsymbol{C}_{nh}(\boldsymbol{x},\dot{\boldsymbol{x}}) = \boldsymbol{B}(\boldsymbol{x})\,\dot{\boldsymbol{x}} = \boldsymbol{0}, \tag{3}$$

where $\boldsymbol{x} \in \mathbb{R}^n$ is the $n\times 1$ vector of coordinates; $\boldsymbol{\Lambda} \in \mathbb{R}^{m+l}$ is the $(m+l)\times 1$ vector of Lagrange multipliers; $\boldsymbol{M}(\boldsymbol{x})$ is the $n\times n$ mass matrix; $\boldsymbol{Q}(\boldsymbol{x},\dot{\boldsymbol{x}})$ is the $n\times 1$ vector of generalized forces; $\boldsymbol{C}(\boldsymbol{x})$ is the $m\times 1$ vector of holonomic constraints; and $\boldsymbol{C}_{nh}(\boldsymbol{x},\dot{\boldsymbol{x}})$ is the $l\times 1$ vector of nonholonomic constraints, which are assumed to be linearly dependent on velocities in this work. In this study, it is assumed that the constraints are scleronomic and do not explicitly depend on time. The matrices $\boldsymbol{B}(\boldsymbol{x})$ and $\boldsymbol{D}(\boldsymbol{x})$ are $l\times n$ and $(m+l)\times n$, respectively, and can be computed as:

$$\boldsymbol{B}(\boldsymbol{x}) = \frac{\partial \boldsymbol{C}_{nh}(\boldsymbol{x},\dot{\boldsymbol{x}})}{\partial \dot{\boldsymbol{x}}}, \qquad \boldsymbol{D}(\boldsymbol{x}) = \begin{pmatrix} \boldsymbol{C}_{\boldsymbol{x}}(\boldsymbol{x}) \\ \boldsymbol{B}(\boldsymbol{x}) \end{pmatrix}, \tag{4}$$

where $\boldsymbol{C}_{\boldsymbol{x}} = \frac{\partial \boldsymbol{C}}{\partial \boldsymbol{x}}$.

2.2. Index-1 DAE system

By differentiating the holonomic constraints in Eq. (2) with respect to time, and assembling them with the nonholonomic constraints of Eq. (3), the following index-2 DAE system is obtained:

$$\boldsymbol{M}(\boldsymbol{x})\,\ddot{\boldsymbol{x}} + \boldsymbol{D}^{\mathrm{T}}(\boldsymbol{x})\,\boldsymbol{\Lambda} = \boldsymbol{Q}(\boldsymbol{x},\dot{\boldsymbol{x}}), \tag{5}$$

$$\boldsymbol{D}(\boldsymbol{x})\,\dot{\boldsymbol{x}} = \boldsymbol{0}. \tag{6}$$

The velocity constraints in Eq. (6) can be differentiated once with respect to time, leading to the index-1 DAE system:

$$\begin{aligned} &\boldsymbol{M}(\boldsymbol{x})\,\ddot{\boldsymbol{x}} + \boldsymbol{D}^{\mathrm{T}}(\boldsymbol{x})\,\boldsymbol{\Lambda} = \boldsymbol{Q}(\boldsymbol{x},\dot{\boldsymbol{x}}), \\ &\boldsymbol{D}(\boldsymbol{x})\,\ddot{\boldsymbol{x}} = \boldsymbol{Q}_d(\boldsymbol{x},\dot{\boldsymbol{x}}), \end{aligned} \tag{7}$$

where $\boldsymbol{Q}_d(\boldsymbol{x},\dot{\boldsymbol{x}}) = -\dfrac{\partial(\boldsymbol{D}(\boldsymbol{x})\,\dot{\boldsymbol{x}})}{\partial \boldsymbol{x}}\dot{\boldsymbol{x}}$.

Alternately, Eqs. (7) can be written as:

$$\underbrace{\begin{pmatrix} \boldsymbol{M}(\boldsymbol{x}) & \boldsymbol{D}^{\mathrm{T}}(\boldsymbol{x}) \\ \boldsymbol{D}(\boldsymbol{x}) & \boldsymbol{0}_{(m+l)} \end{pmatrix}}_{\boldsymbol{A}(\boldsymbol{x})} \begin{pmatrix} \ddot{\boldsymbol{x}} \\ \boldsymbol{\Lambda} \end{pmatrix} = \begin{pmatrix} \boldsymbol{Q}(\boldsymbol{x},\dot{\boldsymbol{x}}) \\ \boldsymbol{Q}_d(\boldsymbol{x},\dot{\boldsymbol{x}}) \end{pmatrix}, \tag{8}$$

where $\boldsymbol{0}_{(m+l)}$ is a null square matrix of size $m+l$.

2.3. ODE system with coordinate partition in terms of independent and dependent coordinates

The equations of motion given by Eqs. (1)–(3) can be reduced by means of a coordinate partition at velocity level, based on $n-m-l$ independent velocities $\dot{\boldsymbol{x}}_{ai}$ and $m+l$ dependent velocities $\dot{\boldsymbol{x}}_{dd}$:

$$\dot{\boldsymbol{x}} = \begin{pmatrix} \dot{\boldsymbol{x}}_{ai} & \dot{\boldsymbol{x}}_{dd} \end{pmatrix}^{\mathrm{T}}. \tag{9}$$

Similarly, the corresponding partition at position level is defined:

$$\boldsymbol{x} = \begin{pmatrix} \boldsymbol{x}_{ai} & \boldsymbol{x}_{dd} \end{pmatrix}^{\mathrm{T}}. \tag{10}$$

By using this coordinate partition in the velocity constraints of Eq. (6), the following velocity transformation is obtained:

$$\dot{\boldsymbol{x}} = \boldsymbol{T}(\boldsymbol{x})\,\dot{\boldsymbol{x}}_{ai}, \tag{11}$$

where $\boldsymbol{T}$ is a transformation matrix, given by:

$$\boldsymbol{T}(\boldsymbol{x}) = \begin{pmatrix} \boldsymbol{I}_{(n-m-l)} \\ -\left(\boldsymbol{D}_{dd}(\boldsymbol{x})\right)^{-1}\boldsymbol{D}_{ai}(\boldsymbol{x}) \end{pmatrix}. \tag{12}$$

In Eq. (12), $\boldsymbol{I}_{(n-m-l)}$ is the identity matrix of size $n-m-l$; $\boldsymbol{D}_{dd}(\boldsymbol{x})$ is a $(m+l)$-square matrix, formed by the columns of matrix $\boldsymbol{D}(\boldsymbol{x})$ corresponding to the dependent coordinates; and $\boldsymbol{D}_{ai}(\boldsymbol{x})$ is a $(m+l)\times(n-m-l)$ matrix, defined by the columns of $\boldsymbol{D}(\boldsymbol{x})$ associated with the independent coordinates. The selection of independent coordinates can be obtained, in practice, using Gaussian elimination with column pivoting. Note that $\boldsymbol{T}(\boldsymbol{x})$ is the null-space of $\boldsymbol{D}(\boldsymbol{x})$, and therefore:

$$\boldsymbol{T}^{\mathrm{T}}(\boldsymbol{x})\,\boldsymbol{D}^{\mathrm{T}}(\boldsymbol{x}) = \boldsymbol{0}. \tag{13}$$

Differentiating with respect to time the velocity transformation of Eq. (11), the following acceleration transformation is obtained:

$$\ddot{\boldsymbol{x}} = \boldsymbol{T}(\boldsymbol{x})\,\ddot{\boldsymbol{x}}_{ai} + \dot{\boldsymbol{T}}(\boldsymbol{x})\,\dot{\boldsymbol{x}}_{ai}, \tag{14}$$

with $\dot{\boldsymbol{T}}(\boldsymbol{x})\,\dot{\boldsymbol{x}}_{ai} = \frac{\partial(\boldsymbol{T}\dot{\boldsymbol{x}}_{ai})}{\partial \boldsymbol{x}}\dot{\boldsymbol{x}}$.

Premultiplying the dynamic Eqs. (5) by $\boldsymbol{T}^{\mathrm{T}}(\boldsymbol{x})$, and using the velocity and acceleration transformations of Eqs. (11) and (14), respectively, in the dynamic Eqs. (5), the following reduced equations of motion in ODE form are obtained:

$$\boldsymbol{m}\left(\boldsymbol{x}_{ai},\boldsymbol{x}_{dd}\right)\ddot{\boldsymbol{x}}_{ai} = \boldsymbol{f}\left(\boldsymbol{x}_{ai},\boldsymbol{x}_{dd},\dot{\boldsymbol{x}}_{ai}\right), \tag{15}$$

$$\dot{\boldsymbol{x}}_{dd} = \boldsymbol{H}\left(\boldsymbol{x}_{ai},\boldsymbol{x}_{dd}\right)\dot{\boldsymbol{x}}_{ai}, \tag{16}$$

with

$$\begin{aligned} &\boldsymbol{m}\left(\boldsymbol{x}_{ai},\boldsymbol{x}_{dd}\right) = \boldsymbol{T}^{\mathrm{T}}\boldsymbol{M}\boldsymbol{T}, \\ &\boldsymbol{f}\left(\boldsymbol{x}_{ai},\boldsymbol{x}_{dd},\dot{\boldsymbol{x}}_{ai}\right) = \boldsymbol{T}^{\mathrm{T}}\left(\boldsymbol{Q} - \boldsymbol{M}\dot{\boldsymbol{T}}\dot{\boldsymbol{x}}_{ai}\right), \\ &\boldsymbol{H}\left(\boldsymbol{x}_{ai},\boldsymbol{x}_{dd}\right) = -\left(\boldsymbol{D}_{dd}\right)^{-1}\boldsymbol{D}_{ai}. \end{aligned} \tag{17}$$

Note that the Lagrange multipliers $\boldsymbol{\Lambda}$ of Eq. (5) are eliminated in Eq. (15) by virtue of Eq. (13).

An important clarification regarding the ODE equations of motion given by Eqs. (15)–(16) must be made. Note that, despite expressing the complete set of velocities and accelerations as a function of the independent velocities and accelerations by means of Eqs. (11) and (14), the equations of motion (15)–(16) are still a function of the dependent coordinates $\boldsymbol{x}_{dd}$. In general, this dependency at position level with the dependent coordinates cannot be eliminated, since the holonomic constraints are nonlinear algebraic equations that hinder obtaining an explicit expression of the dependent coordinates as a function of the independent ones. Moreover, the nonholonomic constraints are non-integrable first-order differential equations, which also impedes obtaining the dependent coordinates as a function of the independent ones. Therefore, the first-order differential Eqs. (16) are required.

2.4. Equations of motion in DAE form without Lagrange multipliers

Due to the m nonlinear holonomic constraints of Eq. (2) in the DAE system given by Eqs. (1)–(3), the n-coordinates vector can be partitioned in $n-m$ admissible coordinates $\boldsymbol{x}_a$ and m dependent coordinates $\boldsymbol{x}_d$, and therefore $\boldsymbol{x} = \begin{pmatrix} \boldsymbol{x}_a & \boldsymbol{x}_d \end{pmatrix}^{\mathrm{T}}$. Moreover, the l nonholonomic constraints in Eq. (3) allow the partition of the admissible velocities $\dot{\boldsymbol{x}}_a$ in l dependent admissible velocities $\dot{\boldsymbol{x}}_{ad}$ and $n-m-l$ independent admissible velocities $\dot{\boldsymbol{x}}_{ai}$, and thus $\dot{\boldsymbol{x}}_a = \begin{pmatrix} \dot{\boldsymbol{x}}_{ai} & \dot{\boldsymbol{x}}_{ad} \end{pmatrix}^{\mathrm{T}}$. The consideration of the same partition at position level leads to:

$$\boldsymbol{x} = \begin{pmatrix} \boldsymbol{x}_{ai} & \boldsymbol{x}_{ad} & \boldsymbol{x}_d \end{pmatrix}^{\mathrm{T}}. \tag{18}$$

The admissible dependent coordinates $\boldsymbol{x}_{ad}$ and the dependent coordinates $\boldsymbol{x}_d$ constitute the set $\boldsymbol{x}_{dd} = \begin{pmatrix} \boldsymbol{x}_{ad} & \boldsymbol{x}_d \end{pmatrix}^{\mathrm{T}}$, which was defined in Eq. (10).

The time derivative of the holonomic constraints in Eq. (2) leads to the following transformation at velocity level:

$$\boldsymbol{C}_{\boldsymbol{x}_d}(\boldsymbol{x})\,\dot{\boldsymbol{x}}_d + \boldsymbol{C}_{\boldsymbol{x}_a}(\boldsymbol{x})\,\dot{\boldsymbol{x}}_a = \boldsymbol{0} \rightarrow \dot{\boldsymbol{x}}_d = -\left(\boldsymbol{C}_{\boldsymbol{x}_d}(\boldsymbol{x})\right)^{-1}\boldsymbol{C}_{\boldsymbol{x}_a}(\boldsymbol{x})\,\dot{\boldsymbol{x}}_a, \tag{19}$$

and, therefore:

$$\dot{\boldsymbol{x}} = \boldsymbol{T}_h(\boldsymbol{x})\,\dot{\boldsymbol{x}}_a, \quad \text{with } \boldsymbol{T}_h(\boldsymbol{x}) = \begin{pmatrix} \boldsymbol{I}_{(n-m)} \\ -\left(\boldsymbol{C}_{\boldsymbol{x}_d}(\boldsymbol{x})\right)^{-1}\boldsymbol{C}_{\boldsymbol{x}_a}(\boldsymbol{x}) \end{pmatrix}. \tag{20}$$

Furthermore, the use of Eq. (20) in the nonholonomic constraints (3) leads to:

$$\boldsymbol{B}(\boldsymbol{x})\,\dot{\boldsymbol{x}} = \boldsymbol{0} \rightarrow \boldsymbol{B}(\boldsymbol{x})\,\boldsymbol{T}_h(\boldsymbol{x})\,\dot{\boldsymbol{x}}_a = \boldsymbol{0}. \tag{21}$$

Defining $\bar{\boldsymbol{B}}(\boldsymbol{x}) = \boldsymbol{B}(\boldsymbol{x})\,\boldsymbol{T}_h(\boldsymbol{x})$, the following transformation is found:

$$\bar{\boldsymbol{B}}_{ad}(\boldsymbol{x})\,\dot{\boldsymbol{x}}_{ad} + \bar{\boldsymbol{B}}_{ai}(\boldsymbol{x})\,\dot{\boldsymbol{x}}_{ai} = \boldsymbol{0} \rightarrow \dot{\boldsymbol{x}}_{ad} = -\left(\bar{\boldsymbol{B}}_{ad}(\boldsymbol{x})\right)^{-1}\bar{\boldsymbol{B}}_{ai}(\boldsymbol{x})\,\dot{\boldsymbol{x}}_{ai}. \tag{22}$$

Therefore, the equations of motion of the multibody system can be written as:

$$\boldsymbol{m}\left(\boldsymbol{x}_{ai}, \boldsymbol{x}_{ad}, \boldsymbol{x}_d\right)\ddot{\boldsymbol{x}}_{ai} = \boldsymbol{f}\left(\boldsymbol{x}_{ai}, \boldsymbol{x}_{ad}, \boldsymbol{x}_d, \dot{\boldsymbol{x}}_{ai}\right), \tag{23}$$

$$\boldsymbol{C}\left(\boldsymbol{x}_{ai}, \boldsymbol{x}_{ad}, \boldsymbol{x}_d\right) = \boldsymbol{0}, \tag{24}$$

$$\dot{\boldsymbol{x}}_{ad} = \boldsymbol{G}\left(\boldsymbol{x}_{ai}, \boldsymbol{x}_{ad}, \boldsymbol{x}_d\right)\dot{\boldsymbol{x}}_{ai}, \tag{25}$$

where $\boldsymbol{m}$ and $\boldsymbol{f}$ were defined in Eqs. (17), and $\boldsymbol{G}\left(\boldsymbol{x}_{ai}, \boldsymbol{x}_{ad}, \boldsymbol{x}_d\right) = -\left(\bar{\boldsymbol{B}}_{ad}\right)^{-1}\bar{\boldsymbol{B}}_{ai}$.

In the DAE system given by Eqs. (23)–(25), Eq. (23) corresponds to the $n - m - l$ reduced dynamic equations in ODE form presented in Eq. (15). These dynamic Eqs. (23) are not only a function of the independent coordinates $\boldsymbol{x}_{ai}$ and their time derivatives, but also depend on the coordinates $\boldsymbol{x}_{ad}$ and $\boldsymbol{x}_d$. The holonomic constraints (24) take into account the dependency at position level of the dependent coordinates $\boldsymbol{x}_d$ with $\boldsymbol{x}_{ai}$ and $\boldsymbol{x}_{ad}$. Eq. (25) corresponds to the nonholonomic constraints, which are non-integrable, and consider the dependency of the admissible dependent coordinates $\boldsymbol{x}_{ad}$ with the independent and dependent coordinates $\boldsymbol{x}_{ai}$ and $\boldsymbol{x}_d$.

In absence of nonholonomic constraints, the coordinates $\boldsymbol{x}_{ad}$ are not required and the coordinate partition of Eq. (18) becomes:

$$\boldsymbol{x} = \begin{pmatrix} \boldsymbol{x}_{ai} & \boldsymbol{x}_d \end{pmatrix}^{\mathrm{T}}. \tag{26}$$

In this case, the equations of motion (23)–(24) are expressed as:

$$\boldsymbol{m}\left(\boldsymbol{x}_{ai}, \boldsymbol{x}_d\right)\ddot{\boldsymbol{x}}_{ai} = \boldsymbol{f}\left(\boldsymbol{x}_{ai}, \boldsymbol{x}_d, \dot{\boldsymbol{x}}_{ai}\right), \tag{27}$$

$$\boldsymbol{C}\left(\boldsymbol{x}_{ai}, \boldsymbol{x}_d\right) = \boldsymbol{0}. \tag{28}$$

3. An overview of linearization approaches in multibody system dynamics

This section provides an overview of linearization approaches in Multibody System Dynamics. The approaches considered in this work are summarized in the chart of Fig. 1, which illustrates a classification into four groups. Group 1 encompasses procedures based on the linearization of the index-3 DAE, given by Eqs. (1)–(3), using a redundant set of coordinates. The linearization approaches considered in Group 1 are the procedure by Escalona et al. [5,6], the Redundant Coordinate Set (RCS) approach by González et al. [7], the procedure by Negrut et al. [4] and the linearization approach by Pappalardo et al. [8,9]. Group 2 comprises approaches based on the linearization of the index-1 DAE (Eq. (8)), using a redundant set of coordinates. The symbolic linearization of the index-1 DAE system, the approach by Van Khang et al. [12] and the first numerical procedure by Agúndez et al. [13] are considered in Group 2. Next, Group 3 includes linearization procedures based on the use of a coordinate partition in terms of independent and dependent coordinates. The procedures by Cuadrado et al. [15,16], the Minimal Coordinate Set (MCS) approach by González et al. [7], and the first symbolic and second numerical procedures by Agúndez et al. [13] are illustrated. Finally, Group 4 consists of procedures based on coordinate partitioning in terms of independent and dependent coordinates, with holonomic constraints elimination, resulting in a linear ODE system expressed solely in terms of the independent coordinates. The procedure by Bae et al. [26], the approach by Cossalter et al. [27] and the second symbolic and third numerical approaches by Agúndez et al. [13] are included in Group 4.

Consider a known reference solution of the DAE system given by Eqs. (1)–(3), defined by $\boldsymbol{x}^0(t)$, $\dot{\boldsymbol{x}}^0(t)$, $\ddot{\boldsymbol{x}}^0(t)$ and $\boldsymbol{\Lambda}^0(t)$. Therefore, the following holds:

$$\begin{aligned} &\boldsymbol{M}\left(\boldsymbol{x}^0\right)\ddot{\boldsymbol{x}}^0 + \boldsymbol{D}^{\mathrm{T}}\left(\boldsymbol{x}^0\right)\boldsymbol{\Lambda}^0 = \boldsymbol{Q}\left(\boldsymbol{x}^0, \dot{\boldsymbol{x}}^0\right), \\ &\boldsymbol{C}\left(\boldsymbol{x}^0\right) = \boldsymbol{0}, \\ &\boldsymbol{C}_{nh}\left(\boldsymbol{x}^0, \dot{\boldsymbol{x}}^0\right) = \boldsymbol{B}\left(\boldsymbol{x}^0\right)\dot{\boldsymbol{x}}^0 = \boldsymbol{0}, \end{aligned} \tag{29}$$

where the time dependence has been omitted for simplicity. The following variations with respect to the reference solution are introduced:

$$\begin{aligned} &\tilde{\boldsymbol{x}} = \boldsymbol{x} - \boldsymbol{x}^0, && \dot{\tilde{\boldsymbol{x}}} = \dot{\boldsymbol{x}} - \dot{\boldsymbol{x}}^0, \\ &\ddot{\tilde{\boldsymbol{x}}} = \ddot{\boldsymbol{x}} - \ddot{\boldsymbol{x}}^0, && \tilde{\boldsymbol{\Lambda}} = \boldsymbol{\Lambda} - \boldsymbol{\Lambda}^0. \end{aligned} \tag{30}$$

The linearization approaches presented in this section provide the linearized equations of motion along this reference solution.

3.1. Group 1: procedures based on the linearization of the index-3 DAE system, using a redundant set of coordinates

The first group of linearization approaches is based on the direct linearization of the index-3 DAE system. First, the procedures by Escalona et al. [5,6] and González et al. [7], under the name of Redundant Coordinate Set (RCS) Formulation in [7], are shown. Since [5–7] develop the approach for multibody systems with only holonomic constraints, the linearization procedure is described in this work without including nonholonomic constraints.

Procedure by Escalona et al. [5,6] and González et al. [7] (RCS Formulation)

Performing the Taylor expansion of Eqs. (1)–(2) with respect to the reference solution, retaining up to first-order terms and using Eq. (29), the following linear DAE system is obtained:

$$\begin{aligned} &\boldsymbol{M}\left(\boldsymbol{x}^0\right)\ddot{\tilde{\boldsymbol{x}}} + \left.\frac{\partial\left(\boldsymbol{M}(\boldsymbol{x})\,\ddot{\boldsymbol{x}}^0\right)}{\partial \boldsymbol{x}}\right|_0\tilde{\boldsymbol{x}} + \boldsymbol{C}_{\boldsymbol{x}}^{\mathrm{T}}\left(\boldsymbol{x}^0\right)\tilde{\boldsymbol{\Lambda}} + \left.\frac{\partial\left(\boldsymbol{C}_{\boldsymbol{x}}^{\mathrm{T}}(\boldsymbol{x})\,\boldsymbol{\Lambda}^0\right)}{\partial \boldsymbol{x}}\right|_0\tilde{\boldsymbol{x}} = \\ &\left.\frac{\partial \boldsymbol{Q}(\boldsymbol{x}, \dot{\boldsymbol{x}})}{\partial \boldsymbol{x}}\right|_0\tilde{\boldsymbol{x}} + \left.\frac{\partial \boldsymbol{Q}(\boldsymbol{x}, \dot{\boldsymbol{x}})}{\partial \dot{\boldsymbol{x}}}\right|_0\dot{\tilde{\boldsymbol{x}}}, \end{aligned} \tag{31}$$

$$\boldsymbol{C}_{\boldsymbol{x}}\left(\boldsymbol{x}^0\right)\tilde{\boldsymbol{x}} = \boldsymbol{0}, \tag{32}$$

where $(\cdot)|_0$ is henceforth used to indicate that the partial derivatives are evaluated for the reference solution. In Eqs. (31) and (32), $\boldsymbol{C}_{\boldsymbol{x}}\left(\boldsymbol{x}^0\right) = \left.\frac{\partial \boldsymbol{C}(\boldsymbol{x})}{\partial \boldsymbol{x}}\right|_0$.

Defining $\tilde{\boldsymbol{X}} = \begin{pmatrix} \tilde{\boldsymbol{x}} & \dot{\tilde{\boldsymbol{x}}} & \tilde{\boldsymbol{\Lambda}} \end{pmatrix}^{\mathrm{T}}$, the linear DAE system of Eqs. (31)–(32) can be expressed as the first-order ODE system:

$$\boldsymbol{\mathcal{A}}_0\dot{\tilde{\boldsymbol{X}}} = \boldsymbol{\mathcal{B}}_0\tilde{\boldsymbol{X}}, \tag{33}$$

where $\boldsymbol{\mathcal{A}}_0$ and $\boldsymbol{\mathcal{B}}_0$ are $(2n+m)\times(2n+m)$ matrices, whose detailed expressions can be found in Eqs. (136) and (137) of Appendix A.

As can be seen from the structure of matrix $\boldsymbol{\mathcal{A}}_0$ in Eq. (136), this matrix is singular, since the last m rows are null. Therefore, as stated by Escalona et al. [5,6] and González et al. [7], the system of Eqs. (33) cannot be solved with a standard eigenvalue analysis. Considering a solution of the form $\tilde{\boldsymbol{X}}(t) = \boldsymbol{X}_0 e^{\lambda t}$, where $\boldsymbol{X}_0$ is a constant vector, the generalized eigenvalue problem associated with the matrices $\boldsymbol{\mathcal{A}}_0$ and $\boldsymbol{\mathcal{B}}_0$ is:

$$\left(\boldsymbol{\mathcal{B}}_0 - \lambda\boldsymbol{\mathcal{A}}_0\right)\boldsymbol{X}_0 = \boldsymbol{0}. \tag{34}$$

The generalized eigenvalue analysis of the $2n+m$ linearized Eqs. (33) leads to $3m$ spurious eigenvalues [5–7], among which $2m$ are related to the m constrained dependent variables, and m are associated with the m Lagrange multipliers. The resulting $2(n-m)$ eigenvalues correspond to the spectrum of the constrained problem. In the particular case that the multibody system includes l nonholonomic constraints, a total of $2n+m+l$ eigenvalues are obtained, among which $2(n-m-l)$ correspond to the spectrum of the constrained problem and $3(m+l)$ are spurious eigenvalues.

Fig. 1. Linearization approaches in multibody dynamics considered in this work, classified into four groups. Group 1 (Section 3.1) encompasses the procedures based on the linearization of the index-3 DAE system, using a redundant set of coordinates. The linearization approaches considered in Group 1 are the procedure by Escalona et al. [5,6], the Redundant Coordinate Set (RCS) approach by González et al. [7], the procedure by Negrut et al. [4] and the linearization approach by Pappalardo et al. [8,9]. Group 2 (Section 3.2) includes those procedures based on the linearization of the index-1 DAE system, using a redundant set of coordinates. The symbolic linearization of the index-1 DAE system, the approach by Van Khang et al. [12] and the first numerical procedure by Agúndez et al. [13] are considered in Group 2. Group 3 (Section 3.3) comprises linearization procedures based on coordinate partitioning in terms of independent and dependent coordinates. The procedures by Cuadrado et al. [15,16], the Minimal Coordinate Set (MCS) approach by González et al. [7], and the first symbolic and second numerical procedures by Agúndez et al. [13] are included. Lastly, Group 4 (Section 3.4) includes linearization procedures, based on a coordinate partition in terms of independent and dependent coordinates, with holonomic constraints elimination. The procedure by Bae et al. [26], the approach by Cossalter et al. [27] and the second symbolic and third numerical approaches by Agúndez et al. [13] are considered in Group 4.

This linearization approach is based on the use of the redundant set of coordinates. As can be seen in Eq. (33), the variations of the complete set of coordinates $\tilde{\boldsymbol{x}}$ and their time derivatives $\dot{\tilde{\boldsymbol{x}}}$, $\ddot{\tilde{\boldsymbol{x}}}$ appear. In this case, no coordinate partition in terms of independent and dependent coordinates is made. Therefore, there is no ambiguity in the handling of the dependent coordinates in this approach.

Xiong et al. [11] follow a similar approach to linearize the index-3 DAE equations of motion of a Whipple bicycle multibody model, moving on a revolution surface, along its circular steady motion. The resulting linearized equations of motion present the same structure obtained with the RCS approach of González et al. [7] and Escalona et al. [5,6]. Nevertheless, since these linearized system of equations do not allow the performance of a standard eigenvalue analysis, a reduced system of first-order ODEs is derived in [11].

Procedure by Pappalardo et al. [8,9]

The procedure presented by Pappalardo et al. [8,9] performs the linearization of multibody systems with holonomic and nonholonomic constraints.

Computing the Taylor expansion of the nonlinear index-3 DAE system of Eqs. (1)–(3), retaining up to first-order terms and using Eq. (29), yields:

$$\begin{aligned} &\boldsymbol{M}\left(\boldsymbol{x}^0\right)\ddot{\tilde{\boldsymbol{x}}}+\left.\frac{\partial\left(\boldsymbol{M}\left(\boldsymbol{x}\right)\ddot{\boldsymbol{x}}^0\right)}{\partial\boldsymbol{x}}\right|_0\tilde{\boldsymbol{x}}+\boldsymbol{D}^{\mathrm{T}}\left(\boldsymbol{x}^0\right)\tilde{\boldsymbol{\Lambda}}+\left.\frac{\partial\left(\boldsymbol{D}^{\mathrm{T}}\left(\boldsymbol{x}\right)\boldsymbol{\Lambda}^0\right)}{\partial\boldsymbol{x}}\right|_0\tilde{\boldsymbol{x}}= \\ &\left.\frac{\partial\boldsymbol{Q}\left(\boldsymbol{x},\dot{\boldsymbol{x}}\right)}{\partial\boldsymbol{x}}\right|_0\tilde{\boldsymbol{x}}+\left.\frac{\partial\boldsymbol{Q}\left(\boldsymbol{x},\dot{\boldsymbol{x}}\right)}{\partial\dot{\boldsymbol{x}}}\right|_0\dot{\tilde{\boldsymbol{x}}}, \\ &\boldsymbol{E}_{\boldsymbol{x}}\big|_0\tilde{\boldsymbol{x}}+\boldsymbol{E}_{\dot{\boldsymbol{x}}}\big|_0\dot{\tilde{\boldsymbol{x}}}=\boldsymbol{0}, \end{aligned} \tag{35}$$

where $\boldsymbol{E}_{\boldsymbol{x}}|_0$ and $\boldsymbol{E}_{\dot{\boldsymbol{x}}}|_0$ are $(m+l)\times n$ matrices, given by:

$$\boldsymbol{E}_{\boldsymbol{x}}|_0 = \begin{pmatrix} \left.\dfrac{\partial \boldsymbol{C}(\boldsymbol{x})}{\partial \boldsymbol{x}}\right|_0 \\ \left.\dfrac{\partial \left(\boldsymbol{B}(\boldsymbol{x})\dot{\boldsymbol{x}}^0\right)}{\partial \boldsymbol{x}}\right|_0 \end{pmatrix}, \qquad \boldsymbol{E}_{\dot{\boldsymbol{x}}}|_0 = \begin{pmatrix} \boldsymbol{0}_{m\times n} \\ \boldsymbol{B}\left(\boldsymbol{x}^0\right) \end{pmatrix}. \tag{36}$$

In the absence of nonholonomic constraints, $\boldsymbol{E}_{\boldsymbol{x}}|_0 = \left.\dfrac{\partial \boldsymbol{C}(\boldsymbol{x})}{\partial \boldsymbol{x}}\right|_0$, $\boldsymbol{E}_{\dot{\boldsymbol{x}}}|_0 = \boldsymbol{0}_{m\times n}$ and $\boldsymbol{D}\left(\boldsymbol{x}^0\right) = \boldsymbol{C}_{\boldsymbol{x}}\left(\boldsymbol{x}^0\right)$.

Defining $\tilde{\boldsymbol{p}} = \begin{pmatrix} \tilde{\boldsymbol{x}} & \tilde{\boldsymbol{\Lambda}} \end{pmatrix}^{\mathrm{T}}$, the linear system given by Eqs. (35) can be rewritten as:

$$\bar{\boldsymbol{M}}_0\ddot{\tilde{\boldsymbol{p}}} + \bar{\boldsymbol{C}}_0\dot{\tilde{\boldsymbol{p}}} + \bar{\boldsymbol{K}}_0\tilde{\boldsymbol{p}} = \boldsymbol{0}, \tag{37}$$

where $\bar{\boldsymbol{M}}_0$, $\bar{\boldsymbol{C}}_0$ and $\bar{\boldsymbol{K}}_0$ are the $n+m+l$ composite mass, damping and stiffness matrices, respectively, whose detailed expressions can be found in Eqs. (138) of Appendix A.

As stated in [8,9], to carry out the stability analysis of the reference solution, a state-space reformulation of the linearized equations of motion (37) is necessary. To this end, by defining $\tilde{\boldsymbol{X}} = \begin{pmatrix} \tilde{\boldsymbol{p}} & \dot{\tilde{\boldsymbol{p}}} \end{pmatrix}^{\mathrm{T}}$, Eq. (37) can be expressed as the following first-order ODE system:

$$\boldsymbol{C}_0\dot{\tilde{\boldsymbol{X}}} = \boldsymbol{\mathcal{D}}_0\tilde{\boldsymbol{X}}, \tag{38}$$

where the matrices $\boldsymbol{C}_0$ and $\boldsymbol{\mathcal{D}}_0$ are given by Eqs. (139) of Appendix A.

As the matrix $\boldsymbol{\mathcal{A}}_0$ in Eq. (33), the matrix $\boldsymbol{C}_0$ of Eq. (38) is singular (see Eqs. (139)), since the last $m+l$ rows of $\bar{\boldsymbol{M}}_0$ are zero. Therefore, the system of Eqs. (38) cannot be solved with a standard eigenvalue analysis. Considering a solution of the form $\tilde{\boldsymbol{X}}(t) = \boldsymbol{X}_0 e^{\lambda t}$, where $\boldsymbol{X}_0$ is a constant vector, the generalized eigenvalue problem associated with the matrices $\boldsymbol{C}_0$ and $\boldsymbol{\mathcal{D}}_0$ is:

$$\left(\boldsymbol{\mathcal{D}}_0 - \lambda\boldsymbol{C}_0\right)\boldsymbol{X}_0 = \boldsymbol{0}. \tag{39}$$

The solution of Eq. (39) provides $2(n+m+l)$ eigenvalues. Given that the spectrum of the constrained problem consists of $2(n-m-l)$ eigenvalues, this approach results in $4(m+l)$ spurious eigenvalues. Among these spurious eigenvalues, $2(m+l)$ are associated with the $m+l$ dependent coordinates of the multibody model, and the remaining $2(m+l)$ are related to the $m+l$ Lagrange multipliers.

As in the linearization approach of Escalona et al. [5,6] and González et al. [7], the linearized equations of motion are expressed in terms of the variations of the redundant set of coordinates $\tilde{\boldsymbol{x}}$ and their time derivatives $\dot{\tilde{\boldsymbol{x}}}$, $\ddot{\tilde{\boldsymbol{x}}}$. There is no ambiguity in the handling of the dependent coordinates in this approach, since no coordinate partition in terms of independent and dependent coordinates is made.

Procedure by Negrut et al. [4]

Negrut et al. [4] also present a linearization approach for the index-3 DAE equations of motion. In this procedure, the governing equations are augmented and a set of sensitivities of interest that provide the linearization are computed. The approach presented in [4] is developed for heterogeneous multibody systems, including nonholonomic constraints, friction, flexible bodies or user-defined differential equations. Nevertheless, as in [4], it is assumed that the set of constraints are holonomic to keep the presentation of the approach simpler. Moreover, in [4], the vector of generalized velocities, denoted as $\boldsymbol{u}$, is not assumed to be the direct time derivative of the vector of position coordinates $\boldsymbol{x}$, and therefore:

$$\boldsymbol{u} = \boldsymbol{\mathcal{T}}(\boldsymbol{x})\dot{\boldsymbol{x}}, \tag{40}$$

where $\boldsymbol{\mathcal{T}}(\boldsymbol{x})$ is a transformation matrix. In this work, to present the linearization procedure in a clearer way (without losing any relevant information), it is assumed that $\boldsymbol{\mathcal{T}} = \boldsymbol{I}_n$, and therefore $\boldsymbol{u} = \dot{\boldsymbol{x}}$.

Negrut et al. [4] present the augmented equations of motion of the multibody system as follows:

$$\begin{aligned} &\boldsymbol{M}(\boldsymbol{x})\ddot{\boldsymbol{x}} + \boldsymbol{C}_{\boldsymbol{x}}^{\mathrm{T}}(\boldsymbol{x})\boldsymbol{\Lambda} - \boldsymbol{Q}(\boldsymbol{x},\dot{\boldsymbol{x}}) = \boldsymbol{0}, \\ &\ddot{\boldsymbol{C}}(\boldsymbol{x},\dot{\boldsymbol{x}},\ddot{\boldsymbol{x}}) = \boldsymbol{0}, \\ &\dot{\boldsymbol{C}}(\boldsymbol{x},\dot{\boldsymbol{x}}) = \boldsymbol{0}, \\ &\boldsymbol{C}(\boldsymbol{x}) = \boldsymbol{0}, \\ &\boldsymbol{B}_1\dot{\boldsymbol{x}} = \dot{\boldsymbol{x}}_{ai}, \\ &\boldsymbol{B}_0\boldsymbol{x} = \boldsymbol{x}_{ai}, \end{aligned} \tag{41}$$

where the constraints at velocity and acceleration levels are included. In Eqs. (41), $\boldsymbol{x}_{ai}$ and $\dot{\boldsymbol{x}}_{ai}$ are $n-m$ independent positions and velocities, respectively, arising from a coordinate partition of the complete set of coordinates $\boldsymbol{x}$ in dependent and independent coordinates. Moreover, $\boldsymbol{B}_1$ and $\boldsymbol{B}_0$ are $(n-m)\times n$ Boolean matrices. The nonlinear equations of motion (41) can be written as:

$$\boldsymbol{F}(\boldsymbol{x},\dot{\boldsymbol{x}},\ddot{\boldsymbol{x}},\boldsymbol{\Lambda}) = \boldsymbol{b}\left(\boldsymbol{x}_{ai},\dot{\boldsymbol{x}}_{ai}\right), \tag{42}$$

where $\boldsymbol{F}(\boldsymbol{x},\dot{\boldsymbol{x}},\ddot{\boldsymbol{x}},\boldsymbol{\Lambda})$ corresponds to the left-hand side of Eqs. (41), and $\boldsymbol{b}\left(\dot{\boldsymbol{x}}_{ai},\boldsymbol{x}_{ai}\right)$ to the right-hand side.

The main objective of this approach is the computation of several first-order sensitivities. In particular, the partial derivatives of the complete set of accelerations and velocities with respect to the independent velocities and positions are of interest in [4]: $\dfrac{\partial\ddot{\boldsymbol{x}}}{\partial\dot{\boldsymbol{x}}_{ai}}$, $\dfrac{\partial\dot{\boldsymbol{x}}}{\partial\boldsymbol{x}_{ai}}$, $\dfrac{\partial\dot{\boldsymbol{x}}}{\partial\dot{\boldsymbol{x}}_{ai}}$ and $\dfrac{\partial\dot{\boldsymbol{x}}}{\partial\boldsymbol{x}_{ai}}$. To this end, the partial derivatives $\dfrac{\partial\boldsymbol{F}}{\partial\dot{\boldsymbol{x}}_{ai}}$ and $\dfrac{\partial\boldsymbol{F}}{\partial\boldsymbol{x}_{ai}}$ are computed, verifying:

$$\frac{\partial\boldsymbol{F}}{\partial\dot{\boldsymbol{x}}_{ai}} = \frac{\partial\boldsymbol{b}}{\partial\dot{\boldsymbol{x}}_{ai}}, \tag{43}$$

$$\frac{\partial\boldsymbol{F}}{\partial\boldsymbol{x}_{ai}} = \frac{\partial\boldsymbol{b}}{\partial\boldsymbol{x}_{ai}}. \tag{44}$$

The detailed expressions of the partial derivatives $\dfrac{\partial\boldsymbol{F}}{\partial\dot{\boldsymbol{x}}_{ai}}$, $\dfrac{\partial\boldsymbol{F}}{\partial\boldsymbol{x}_{ai}}$, $\dfrac{\partial\boldsymbol{b}}{\partial\dot{\boldsymbol{x}}_{ai}}$ and $\dfrac{\partial\boldsymbol{b}}{\partial\boldsymbol{x}_{ai}}$ can be found in Eqs. (140), (141) and (143) of Appendix A.

Eqs. (43) and (44) can be assembled to build the following linear system:

$$\boldsymbol{\mathcal{A}}_1(\boldsymbol{x})\boldsymbol{X}_1 = \boldsymbol{b}_1, \tag{45}$$

where the definitions of $\boldsymbol{\mathcal{A}}_1$, $\boldsymbol{X}_1$ and $\boldsymbol{b}_1$ are presented in Eqs. (144) and Eqs. (145) of Appendix A. In Eq. (45), the assembly of Eqs. (43) and (44) is possible since both equations have the matrix $\boldsymbol{\mathcal{A}}_1(\boldsymbol{x})$ in common. Note that the linear system of Eqs. (45) provide the sensitivities of the velocities and accelerations with respect to the independent coordinates and velocities.

3.2. Group 2: procedures based on the linearization of the index-1 DAE system, using a redundant set of coordinates

The procedures summarized in this section are based on the linearization of the index-1 DAE system, given by Eq. (8). The symbolic linearization of the index-1 DAE system, the first numerical procedure of Agúndez et al. [13], the approach of Van Khang et al. [12] and a combination of the latter with the first numerical procedure of Agúndez et al. [13] are included in this group.

Symbolic linearization of the index-1 DAE system

A straightforward way to carry out the linearization of the DAE system in Eq. (8) is based on obtaining, first, the acceleration vector $\ddot{\boldsymbol{x}}$ from Eq. (8):

$$\begin{pmatrix} \ddot{\boldsymbol{x}} \\ \boldsymbol{\Lambda} \end{pmatrix} = \underbrace{\begin{pmatrix} \boldsymbol{M}(\boldsymbol{x}) & \boldsymbol{D}^{\mathrm{T}}(\boldsymbol{x}) \\ \boldsymbol{D}(\boldsymbol{x}) & \boldsymbol{0}_{(m+l)} \end{pmatrix}^{-1}}_{\boldsymbol{A}^{-1}(\boldsymbol{x})} \begin{pmatrix} \boldsymbol{Q}(\boldsymbol{x},\dot{\boldsymbol{x}}) \\ \boldsymbol{Q}_d(\boldsymbol{x},\dot{\boldsymbol{x}}) \end{pmatrix} = \boldsymbol{\mathcal{F}}(\boldsymbol{x},\dot{\boldsymbol{x}}), \tag{46}$$

where $\boldsymbol{\mathcal{F}}(\boldsymbol{x},\dot{\boldsymbol{x}})$ is a $(n+m+l)\times 1$ vector. Given that the symbolic computation of the inverse matrix $\boldsymbol{A}^{-1}(\boldsymbol{x})$ in Eq. (46) requires a high computational cost, this procedure is not valid for moderately complex multibody systems.

Denoting the first n components of $\boldsymbol{\mathcal{F}}(\boldsymbol{x},\dot{\boldsymbol{x}})$ as $\boldsymbol{F}_1(\boldsymbol{x},\dot{\boldsymbol{x}})$, and the last $m+l$ components by $\boldsymbol{F}_2(\boldsymbol{x},\dot{\boldsymbol{x}})$, Eq. (46) is rewritten as:

$$\ddot{\boldsymbol{x}} = \boldsymbol{F}_1(\boldsymbol{x},\dot{\boldsymbol{x}}), \tag{47}$$

$$\boldsymbol{\Lambda} = \boldsymbol{F}_2\left(\boldsymbol{x}, \dot{\boldsymbol{x}}\right). \tag{48}$$

Note that Eq. (48) corresponds to the expressions of the Lagrange multipliers $\boldsymbol{\Lambda}$, which do not provide information about the stability of the multibody system.

Performing the Taylor expansion of Eq. (47), retaining up to first-order terms and using that the reference motion verifies $\dot{\boldsymbol{x}}^0 = \boldsymbol{F}_1\left(\boldsymbol{x}^0, \dot{\boldsymbol{x}}^0\right)$, yield:

$$\ddot{\tilde{\boldsymbol{x}}} = \left.\frac{\partial \boldsymbol{F}_1}{\partial \boldsymbol{x}}\right|_0 \tilde{\boldsymbol{x}} + \left.\frac{\partial \boldsymbol{F}_1}{\partial \dot{\boldsymbol{x}}}\right|_0 \dot{\tilde{\boldsymbol{x}}}. \tag{49}$$

Defining $\tilde{\boldsymbol{X}} = \begin{pmatrix} \tilde{\boldsymbol{x}} & \dot{\tilde{\boldsymbol{x}}} \end{pmatrix}^{\mathrm{T}}$, the following first-order linear ODE system is obtained:

$$\dot{\tilde{\boldsymbol{X}}} = \boldsymbol{J}\tilde{\boldsymbol{X}}, \text{ with } \boldsymbol{J} = \begin{pmatrix} \boldsymbol{0}_n & \boldsymbol{I}_n \\ \left.\frac{\partial \boldsymbol{F}_1}{\partial \boldsymbol{x}}\right|_0 & \left.\frac{\partial \boldsymbol{F}_1}{\partial \dot{\boldsymbol{x}}}\right|_0 \end{pmatrix}. \tag{50}$$

The size of $\boldsymbol{J}$ is, in this case, $2n \times 2n$, obtaining $2n$ eigenvalues. Given that the real spectrum consists of $2(n-m-l)$ eigenvalues, associated with the $n_g = n-m-l$ degrees of freedom of the multibody system, this approach leads to $2(m+l)$ spurious null eigenvalues, arising from the $m+l$ dependent coordinates. Note that, as in the approaches based on the linearization of the index-3 DAE system (Section 3.1), the Jacobian matrix of Eq. (50) includes the partial derivatives with respect to the redundant set of coordinates $\boldsymbol{x}$. Therefore, no distinction between independent and dependent coordinates is made in this linearization approach.

Procedure by Agúndez et al. [13] (first numerical approach)

A counterpart procedure to the direct linearization of the index-1 DAE system was presented by Agúndez et al. [13]. It is the first of the numerical approaches developed in [13], and is labeled as numerical because it not only allows for symbolic calculation, but also for numerical implementation. The linearization of the index-1 DAE in Eq. (8) yields:

$$\boldsymbol{M}\left(\boldsymbol{x}^0\right)\ddot{\tilde{\boldsymbol{x}}} + \left.\frac{\partial\left(\boldsymbol{M}\left(\boldsymbol{x}\right)\ddot{\boldsymbol{x}}^0\right)}{\partial \boldsymbol{x}}\right|_0 \tilde{\boldsymbol{x}} + \boldsymbol{D}^{\mathrm{T}}\left(\boldsymbol{x}^0\right)\tilde{\boldsymbol{\Lambda}} + \left.\frac{\partial\left(\boldsymbol{D}^{\mathrm{T}}\left(\boldsymbol{x}\right)\boldsymbol{\Lambda}^0\right)}{\partial \boldsymbol{x}}\right|_0 \tilde{\boldsymbol{x}} = \left.\frac{\partial \boldsymbol{Q}\left(\boldsymbol{x}, \dot{\boldsymbol{x}}\right)}{\partial \boldsymbol{x}}\right|_0 \tilde{\boldsymbol{x}} + \left.\frac{\partial \boldsymbol{Q}\left(\boldsymbol{x}, \dot{\boldsymbol{x}}\right)}{\partial \dot{\boldsymbol{x}}}\right|_0 \dot{\tilde{\boldsymbol{x}}}, \tag{51}$$

$$\boldsymbol{D}\left(\boldsymbol{x}^0\right)\ddot{\tilde{\boldsymbol{x}}} + \left.\frac{\partial\left(\boldsymbol{D}\left(\boldsymbol{x}\right)\ddot{\boldsymbol{x}}^0\right)}{\partial \boldsymbol{x}}\right|_0 \tilde{\boldsymbol{x}} = \left.\frac{\partial \boldsymbol{Q}_d\left(\boldsymbol{x}, \dot{\boldsymbol{x}}\right)}{\partial \boldsymbol{x}}\right|_0 \tilde{\boldsymbol{x}} + \left.\frac{\partial \boldsymbol{Q}_d\left(\boldsymbol{x}, \dot{\boldsymbol{x}}\right)}{\partial \dot{\boldsymbol{x}}}\right|_0 \dot{\tilde{\boldsymbol{x}}}. \tag{52}$$

Eqs. (51) and (52) can be assembled to obtain the following linear index-1 DAE system:

$$\bar{\boldsymbol{\mathcal{A}}}_0 \begin{pmatrix} \ddot{\tilde{\boldsymbol{x}}} \\ \tilde{\boldsymbol{\Lambda}} \end{pmatrix} = \bar{\boldsymbol{\mathcal{B}}}_0 \begin{pmatrix} \tilde{\boldsymbol{x}} \\ \dot{\tilde{\boldsymbol{x}}} \end{pmatrix}, \tag{53}$$

where $\bar{\boldsymbol{\mathcal{A}}}_0$ and $\bar{\boldsymbol{\mathcal{B}}}_0$ are given by Eqs. (146) and (147) of Appendix A.

Eq. (53) is rewritten as follows:

$$\begin{pmatrix} \ddot{\tilde{\boldsymbol{x}}} \\ \tilde{\boldsymbol{\Lambda}} \end{pmatrix} = \boldsymbol{\mathcal{F}}_0 \begin{pmatrix} \tilde{\boldsymbol{x}} \\ \dot{\tilde{\boldsymbol{x}}} \end{pmatrix}, \tag{54}$$

where $\boldsymbol{\mathcal{F}}_0$ is a $(n+m+l) \times 2n$ matrix, given by $\boldsymbol{\mathcal{F}}_0 = \bar{\boldsymbol{\mathcal{A}}}_0^{-1}\bar{\boldsymbol{\mathcal{B}}}_0$. As in Eq. (47), where the first n equations of Eq. (46) were selected to obtain the acceleration vector $\ddot{\boldsymbol{x}}$, the first n equations of Eq. (54) provide the variations of the accelerations $\ddot{\tilde{\boldsymbol{x}}}$. The last $m+l$ equations of the linear index-1 DAE of Eq. (54) correspond to the variations of the Lagrange multipliers $\tilde{\boldsymbol{\Lambda}}$, which do not provide information about the stability of the multibody system. Note that, in contrast to Eq. (46), where the inverse matrix $\boldsymbol{A}^{-1}(\boldsymbol{x})$ is computed, the computation of $\boldsymbol{\mathcal{F}}_0$ in Eq. (54) requires the computation of $\bar{\boldsymbol{\mathcal{A}}}_0^{-1}$, which significantly reduces the computational cost.

Defining $\tilde{\boldsymbol{X}} = \begin{pmatrix} \tilde{\boldsymbol{x}} & \dot{\tilde{\boldsymbol{x}}} \end{pmatrix}^{\mathrm{T}}$, the following first-order linear ODE system is obtained:

$$\dot{\tilde{\boldsymbol{X}}} = \boldsymbol{J}\tilde{\boldsymbol{X}}, \text{ with } \boldsymbol{J} = \begin{pmatrix} \boldsymbol{0}_n & \boldsymbol{I}_n \\ \boldsymbol{J}_{21} & \boldsymbol{J}_{22} \end{pmatrix}. \tag{55}$$

In Eq. (55), $\boldsymbol{J}_{21}$ is the submatrix formed from rows 1 to n and columns 1 to n of $\boldsymbol{\mathcal{F}}_0$, and $\boldsymbol{J}_{22}$ is given by rows 1 to n and columns $n+1$ to $2n$ of $\boldsymbol{\mathcal{F}}_0$. In the case that the matrix $\boldsymbol{M}\left(\boldsymbol{x}^0\right)$ is not singular, explicit expressions for the submatrices $\boldsymbol{J}_{21}$ and $\boldsymbol{J}_{22}$ can be found, which are shown in detail in [78]. The size of $\boldsymbol{J}$ is $2n \times 2n$, leading to $2n$ eigenvalues. Among the $2n$ eigenvalues, $2(n-m-l)$ correspond to the real spectrum of the problem, and $2(m+l)$ are spurious eigenvalues, associated with the $m+l$ dependent coordinates. Note that the linear index-1 DAE system in Eq. (54) is expressed in terms of the variations of the redundant set of coordinates $\tilde{\boldsymbol{x}}$ and their time derivatives $\dot{\tilde{\boldsymbol{x}}}$ and $\ddot{\tilde{\boldsymbol{x}}}$. Therefore, no distinction between independent and dependent coordinates is made.

This approach was validated with the results of the bicycle benchmark model of Meijaard et al. [14] and used to perform the linear stability analysis of the steady forward motion of the waveboard [55].

Procedure by Van Khang et al. [12]

The approach of Van Khang et al. [12] is also based on the linearization of the index-1 DAE of Eq. (8). In this approach, the coordinate partition in $n-m-l$ independent and $m+l$ dependent coordinates, described in Section 2.3, is used. Using the transformation matrix $\boldsymbol{T}(\boldsymbol{x})$ presented in Eq. (11), and premultiplying the dynamic Eqs. (5) by $\boldsymbol{T}^{\mathrm{T}}(\boldsymbol{x})$, the index-1 DAE of Eq. (8) is transformed into the following ODE system:

$$\boldsymbol{T}^{\mathrm{T}}\left(\boldsymbol{x}\right)\boldsymbol{M}\left(\boldsymbol{x}\right)\ddot{\boldsymbol{x}} = \boldsymbol{T}^{\mathrm{T}}\left(\boldsymbol{x}\right)\boldsymbol{Q}\left(\boldsymbol{x}, \dot{\boldsymbol{x}}\right), \tag{56}$$

$$\boldsymbol{D}\left(\boldsymbol{x}\right)\ddot{\boldsymbol{x}} = \boldsymbol{Q}_d\left(\boldsymbol{x}, \dot{\boldsymbol{x}}\right). \tag{57}$$

Note that the Lagrange multipliers $\boldsymbol{\Lambda}$ in Eq. (8) are eliminated since $\boldsymbol{T}^{\mathrm{T}}(\boldsymbol{x})\,\boldsymbol{D}^{\mathrm{T}}(\boldsymbol{x}) = \boldsymbol{0}$. Presenting the following definitions:

$$\begin{aligned} \boldsymbol{f}_1\left(\boldsymbol{x}, \ddot{\boldsymbol{x}}\right) &= \boldsymbol{T}^{\mathrm{T}}\left(\boldsymbol{x}\right)\boldsymbol{M}\left(\boldsymbol{x}\right)\ddot{\boldsymbol{x}}, & \boldsymbol{k}_1\left(\boldsymbol{x}, \dot{\boldsymbol{x}}\right) &= \boldsymbol{T}^{\mathrm{T}}\left(\boldsymbol{x}\right)\boldsymbol{Q}\left(\boldsymbol{x}, \dot{\boldsymbol{x}}\right), \\ \boldsymbol{f}_2\left(\boldsymbol{x}, \ddot{\boldsymbol{x}}\right) &= \boldsymbol{D}\left(\boldsymbol{x}\right)\ddot{\boldsymbol{x}}, & \boldsymbol{k}_2\left(\boldsymbol{x}, \dot{\boldsymbol{x}}\right) &= \boldsymbol{Q}_d\left(\boldsymbol{x}, \dot{\boldsymbol{x}}\right), \end{aligned} \tag{58}$$

the nonlinear ODE system of Eqs. (56)–(57) can be written as:

$$\boldsymbol{f}_1\left(\boldsymbol{x}, \ddot{\boldsymbol{x}}\right) - \boldsymbol{k}_1\left(\boldsymbol{x}, \dot{\boldsymbol{x}}\right) = \boldsymbol{0}, \tag{59}$$

$$\boldsymbol{f}_2\left(\boldsymbol{x}, \ddot{\boldsymbol{x}}\right) - \boldsymbol{k}_2\left(\boldsymbol{x}, \dot{\boldsymbol{x}}\right) = \boldsymbol{0}. \tag{60}$$

The linearization of Eqs. (59)–(60) leads to:

$$\left.\frac{\partial \boldsymbol{f}_1}{\partial \ddot{\boldsymbol{x}}}\right|_0 \ddot{\tilde{\boldsymbol{x}}} - \left.\frac{\partial \boldsymbol{k}_1}{\partial \dot{\boldsymbol{x}}}\right|_0 \dot{\tilde{\boldsymbol{x}}} + \left(\left.\frac{\partial \boldsymbol{f}_1}{\partial \boldsymbol{x}}\right|_0 - \left.\frac{\partial \boldsymbol{k}_1}{\partial \boldsymbol{x}}\right|_0\right)\tilde{\boldsymbol{x}} = \boldsymbol{0}, \tag{61}$$

$$\left.\frac{\partial \boldsymbol{f}_2}{\partial \ddot{\boldsymbol{x}}}\right|_0 \ddot{\tilde{\boldsymbol{x}}} - \left.\frac{\partial \boldsymbol{k}_2}{\partial \dot{\boldsymbol{x}}}\right|_0 \dot{\tilde{\boldsymbol{x}}} + \left(\left.\frac{\partial \boldsymbol{f}_2}{\partial \boldsymbol{x}}\right|_0 - \left.\frac{\partial \boldsymbol{k}_2}{\partial \boldsymbol{x}}\right|_0\right)\tilde{\boldsymbol{x}} = \boldsymbol{0}. \tag{62}$$

The linear system of Eqs. (61)–(62) can be expressed as:

$$\bar{\boldsymbol{M}}\ddot{\tilde{\boldsymbol{x}}} + \bar{\boldsymbol{C}}\dot{\tilde{\boldsymbol{x}}} + \bar{\boldsymbol{K}}\tilde{\boldsymbol{x}} = \boldsymbol{0}, \tag{63}$$

where $\bar{\boldsymbol{M}}$, $\bar{\boldsymbol{C}}$ and $\bar{\boldsymbol{K}}$ are $n \times n$ matrices, representing the composite mass, damping and stiffness matrices, respectively, given by Eqs. (148) of Appendix A. The symbolic computation of matrices in Eqs. (148) is further developed in the work of Van Khang et al. [12].

Defining $\tilde{\boldsymbol{X}} = \begin{pmatrix} \tilde{\boldsymbol{x}} & \dot{\tilde{\boldsymbol{x}}} \end{pmatrix}^{\mathrm{T}}$, Eq. (63) can be written as the following first-order ODE system:

$$\dot{\tilde{\boldsymbol{X}}} = \boldsymbol{J}\tilde{\boldsymbol{X}}, \text{ with } \boldsymbol{J} = \begin{pmatrix} \boldsymbol{0}_n & \boldsymbol{I}_n \\ -\bar{\boldsymbol{M}}^{-1}\bar{\boldsymbol{K}} & -\bar{\boldsymbol{M}}^{-1}\bar{\boldsymbol{C}} \end{pmatrix}. \tag{64}$$

As in the previous two approaches, the resulting Jacobian matrix of Eq. (64) is $2n \times 2n$. This leads to $2n$ eigenvalues, among which $2(n-m-l)$ corresponds to the real spectrum of the problem, and $2(m+l)$ are spurious eigenvalues due to the $m+l$ dependent coordinates. Note that, despite this approach makes use of the coordinate partition in terms of independent and dependent coordinates described in Section 2.3, the resulting linearized equations of motion (63) are expressed in terms of the variations of the redundant set of coordinates $\tilde{\boldsymbol{x}}$ and their time derivatives $\dot{\tilde{\boldsymbol{x}}}$ and $\ddot{\tilde{\boldsymbol{x}}}$. Therefore, the dependent coordinates are not ignored in this approach.

Combination of Van Khang et al. [12] and Agúndez et al. [13]

To ease the analytical computation of the matrices $\bar{\boldsymbol{M}}$, $\bar{\boldsymbol{C}}$ and $\bar{\boldsymbol{K}}$ in Eqs. (148), the following counterpart procedure is proposed. Particularizing the transformation matrix $\boldsymbol{T}(\boldsymbol{x})$ of Eq. (11) for the reference solution $\boldsymbol{x}^0$, yields:

$$\boldsymbol{T}\left(\boldsymbol{x}^0\right) = \begin{pmatrix} \boldsymbol{I}_{(n-m-l)} \\ -\left(\boldsymbol{D}_{dd}\left(\boldsymbol{x}^0\right)\right)^{-1} \boldsymbol{D}_{ai}\left(\boldsymbol{x}^0\right) \end{pmatrix}. \tag{65}$$

Premultiplying the linearized dynamic Eqs. (51) by $\boldsymbol{T}^{\mathrm{T}}\left(\boldsymbol{x}^0\right)$, the variations of the Lagrange multipliers $\bar{\boldsymbol{\Lambda}}$ are eliminated, given that $\boldsymbol{T}^{\mathrm{T}}\left(\boldsymbol{x}^0\right)\boldsymbol{D}^{\mathrm{T}}\left(\boldsymbol{x}^0\right) = \boldsymbol{0}$. Therefore, the following linear system of equations is obtained:

$$\boldsymbol{T}_0^{\mathrm{T}}\boldsymbol{M}\left(\boldsymbol{x}^0\right)\ddot{\tilde{\boldsymbol{x}}} + \boldsymbol{T}_0^{\mathrm{T}}\left.\frac{\partial\left(\boldsymbol{M}(\boldsymbol{x})\,\ddot{\boldsymbol{x}}^0\right)}{\partial \boldsymbol{x}}\right|_0 \tilde{\boldsymbol{x}} + \boldsymbol{T}_0^{\mathrm{T}}\left.\frac{\partial\left(\boldsymbol{D}^{\mathrm{T}}(\boldsymbol{x})\,\boldsymbol{\Lambda}^0\right)}{\partial \boldsymbol{x}}\right|_0 \tilde{\boldsymbol{x}} = \boldsymbol{T}_0^{\mathrm{T}}\left.\frac{\partial \boldsymbol{Q}}{\partial \boldsymbol{x}}\right|_0 \tilde{\boldsymbol{x}} + \boldsymbol{T}_0^{\mathrm{T}}\left.\frac{\partial \boldsymbol{Q}}{\partial \dot{\boldsymbol{x}}}\right|_0 \dot{\tilde{\boldsymbol{x}}}, \tag{66}$$

$$\boldsymbol{D}\left(\boldsymbol{x}^0\right)\ddot{\tilde{\boldsymbol{x}}} + \left.\frac{\partial\left(\boldsymbol{D}(\boldsymbol{x})\,\ddot{\boldsymbol{x}}^0\right)}{\partial \boldsymbol{x}}\right|_0 \tilde{\boldsymbol{x}} = \left.\frac{\partial \boldsymbol{Q}_d}{\partial \boldsymbol{x}}\right|_0 \tilde{\boldsymbol{x}} + \left.\frac{\partial \boldsymbol{Q}_d}{\partial \dot{\boldsymbol{x}}}\right|_0 \dot{\tilde{\boldsymbol{x}}}, \tag{67}$$

where the transformation matrix $\boldsymbol{T}\left(\boldsymbol{x}^0\right)$ is denoted as $\boldsymbol{T}_0$ to simplify the notation. Eqs. (66)–(67) can be written in the form of Eq. (63), obtaining a detailed expression of the matrices $\bar{\boldsymbol{M}}$, $\bar{\boldsymbol{C}}$ and $\bar{\boldsymbol{K}}$ as shown in Eqs. (149) of Appendix A.

Defining $\tilde{\boldsymbol{X}} = \begin{pmatrix} \tilde{\boldsymbol{x}} & \dot{\tilde{\boldsymbol{x}}} \end{pmatrix}^{\mathrm{T}}$, a first-order ODE system of the form $\dot{\tilde{\boldsymbol{X}}} = \boldsymbol{J}\tilde{\boldsymbol{X}}$ is obtained, with the Jacobian matrix $\boldsymbol{J}$ having a structure as that of Eq. (64). As in Eqs. (50), (55) and (64), the Jacobian matrix is $2n \times 2n$.

The use of this approach greatly simplifies the analytical computation of the mass, damping and stiffness matrices of Van Khang et al. [12], given by Eqs. (148). Moreover, the expressions of the blocks $\left.\frac{\partial \boldsymbol{F}_1}{\partial \boldsymbol{x}}\right|_0$ and $\left.\frac{\partial \boldsymbol{F}_1}{\partial \dot{\boldsymbol{x}}}\right|_0$ in the Jacobian matrix of Eq. (50), and the blocks $\boldsymbol{J}_{21}$ and $\boldsymbol{J}_{22}$ in the Jacobian matrix of Eq. (55), are analytically derived with the Jacobian matrix of this approach.

It is important to mention that, despite the approach proposed by Van Khang et al. [12] makes use of a coordinate partition in independent and dependent coordinates and uses the transformation matrix of Eq. (12), the Jacobian matrix of Eq. (64) considers the complete set of coordinates, without eliminating the dependent coordinates. For this reason, and given that the procedure is based on the linearization of the index-1 DAE system, these approaches have been included in Section 3.2 instead of Section 3.3.

3.3. Group 3: procedures based on coordinate partitioning in terms of independent and dependent coordinates

The approaches included in this subsection are based on the linearization of the ODE system of Eqs. (15)–(16), expressed in terms of the independent and dependent coordinates. By virtue of the coordinate partition of Eq. (10), the reference solution $\boldsymbol{x}^0(t)$ and its time derivatives $\dot{\boldsymbol{x}}^0(t)$, $\ddot{\boldsymbol{x}}^0(t)$, presented in Section 3.1, can be expressed as:

$$\boldsymbol{x}_{ai}^0(t),\ \dot{\boldsymbol{x}}_{ai}^0(t),\ \ddot{\boldsymbol{x}}_{ai}^0(t),\ \boldsymbol{x}_{dd}^0(t),\ \dot{\boldsymbol{x}}_{dd}^0(t). \tag{68}$$

The following variations with respect to the reference solution of Eq. (68) are introduced:

$$\begin{aligned} &\tilde{\boldsymbol{x}}_{ai} = \boldsymbol{x}_{ai} - \boldsymbol{x}_{ai}^0, && \dot{\tilde{\boldsymbol{x}}}_{ai} = \dot{\boldsymbol{x}}_{ai} - \dot{\boldsymbol{x}}_{ai}^0, \\ &\ddot{\tilde{\boldsymbol{x}}}_{ai} = \ddot{\boldsymbol{x}}_{ai} - \ddot{\boldsymbol{x}}_{ai}^0, && \tilde{\boldsymbol{x}}_{dd} = \boldsymbol{x}_{dd} - \boldsymbol{x}_{dd}^0, \\ &\dot{\tilde{\boldsymbol{x}}}_{dd} = \dot{\boldsymbol{x}}_{dd} - \dot{\boldsymbol{x}}_{dd}^0. \end{aligned} \tag{69}$$

Procedure by Cuadrado et al. [15,16]

Cuadrado et al. [15,16] presented a linearization approach for multibody systems with holonomic constraints. In [15,16], the dynamic Eqs. (15) are written as the first-order ODE system:

$$\dot{\boldsymbol{x}}_{ai} = \boldsymbol{v}_{ai}, \tag{70}$$

$$\dot{\boldsymbol{v}}_{ai} = \left(\boldsymbol{m}\left(\boldsymbol{x}_{ai}, \boldsymbol{x}_{dd}\right)\right)^{-1} \boldsymbol{f}\left(\boldsymbol{x}_{ai}, \boldsymbol{x}_{dd}, \boldsymbol{v}_{ai}\right) = \boldsymbol{g}\left(\boldsymbol{x}_{ai}, \boldsymbol{x}_{dd}, \boldsymbol{v}_{ai}\right), \tag{71}$$

where the matrix $\boldsymbol{m}$ and the vector $\boldsymbol{f}$ were defined in Eq. (17). Defining $\boldsymbol{X} = \begin{pmatrix} \boldsymbol{x}_{ai} & \boldsymbol{v}_{ai} \end{pmatrix}^{\mathrm{T}}$, Eqs. (70)–(71) can be expressed in compact form as:

$$\dot{\boldsymbol{X}} = \boldsymbol{G}_1\left(\boldsymbol{x}_{ai}, \boldsymbol{x}_{dd}, \boldsymbol{v}_{ai}\right). \tag{72}$$

Introducing the vector of variations $\tilde{\boldsymbol{X}} = \begin{pmatrix} \tilde{\boldsymbol{x}}_{ai} & \tilde{\boldsymbol{v}}_{ai} \end{pmatrix}^{\mathrm{T}}$, the linearization of the first-order system of Eqs. (72) along the reference solution in Eq. (68) leads to a first-order linear ODE system of the form:

$$\dot{\tilde{\boldsymbol{X}}} = \boldsymbol{J}\tilde{\boldsymbol{X}}, \text{ with } \boldsymbol{J} = \left(\begin{array}{c|c} \boldsymbol{0}_{(n-m)} & \boldsymbol{I}_{(n-m)} \\ \hline \left.\frac{\partial \boldsymbol{g}}{\partial \boldsymbol{x}_{ai}}\right|_0 & \left.\frac{\partial \boldsymbol{g}}{\partial \dot{\boldsymbol{x}}_{ai}}\right|_0 \end{array}\right). \tag{73}$$

The state-space Jacobian matrix $\boldsymbol{J}$ of Eq. (73) is $2(n-m) \times 2(n-m)$, leading to $2(n-m)$ eigenvalues. These eigenvalues correspond to the real spectrum of the multibody system, which presents $n_g = n - m$ degrees of freedom.

This procedure can be found in several works. Cuadrado et al. [15, 16] and Sanjurjo et al. [17] followed this approach to construct the state-space Jacobian matrix, in order to build continuous extended Kalman filters.

Procedure by González et al. [7] (MCS Formulation)

A similar procedure is presented by González et al. [7], under the name of Minimal Coordinate Set (MCS) Formulation: Velocity Projection. As in the case of Cuadrado et al. [15,16], the approach is presented for multibody systems with holonomic constraints. The dynamic Eqs. (15) are written as:

$$\boldsymbol{H}_1 = \boldsymbol{m}\left(\boldsymbol{x}_{ai}, \boldsymbol{x}_{dd}\right)\ddot{\boldsymbol{x}}_{ai} - \boldsymbol{f}\left(\boldsymbol{x}_{ai}, \boldsymbol{x}_{dd}, \dot{\boldsymbol{x}}_{ai}\right) = \boldsymbol{0}, \tag{74}$$

where, according to Eq. (17), $\boldsymbol{m} = \boldsymbol{T}^{\mathrm{T}}\boldsymbol{M}\boldsymbol{T}$ and $\boldsymbol{f} = \boldsymbol{T}^{\mathrm{T}}\left(\boldsymbol{Q} - \boldsymbol{M}\dot{\boldsymbol{T}}\dot{\boldsymbol{x}}_{ai}\right)$.

The linearization of Eq. (74) along the reference solution yields:

$$\left.\frac{\partial \boldsymbol{H}_1}{\partial \boldsymbol{x}_{ai}}\right|_0 \tilde{\boldsymbol{x}}_{ai} + \left.\frac{\partial \boldsymbol{H}_1}{\partial \dot{\boldsymbol{x}}_{ai}}\right|_0 \dot{\tilde{\boldsymbol{x}}}_{ai} + \left.\frac{\partial \boldsymbol{H}_1}{\partial \ddot{\boldsymbol{x}}_{ai}}\right|_0 \ddot{\tilde{\boldsymbol{x}}}_{ai} = \boldsymbol{0}. \tag{75}$$

The expressions of the partial derivatives in Eq. (75) can be found in Eqs. (150)–(152) of Appendix A. By defining $\boldsymbol{M}_r = \left.\frac{\partial \boldsymbol{H}_1}{\partial \ddot{\boldsymbol{x}}_{ai}}\right|_0$, $\boldsymbol{C}_r = \left.\frac{\partial \boldsymbol{H}_1}{\partial \dot{\boldsymbol{x}}_{ai}}\right|_0$ and $\boldsymbol{K}_r = \left.\frac{\partial \boldsymbol{H}_1}{\partial \boldsymbol{x}_{ai}}\right|_0$, Eq. (75) can be expressed as:

$$\boldsymbol{M}_r\ddot{\tilde{\boldsymbol{x}}}_{ai} + \boldsymbol{C}_r\dot{\tilde{\boldsymbol{x}}}_{ai} + \boldsymbol{K}_r\tilde{\boldsymbol{x}}_{ai} = \boldsymbol{0}. \tag{76}$$

Eq. (76) leads to $2(n-m)$ eigenvalues, which represent the exact spectrum of the problem.

Cuadrado et al. [15,16] and González et al. [7] obtain a linear ODE system expressed in terms of the independent variables. In the computation of the Jacobian matrix of Eq. (73) and the linearized Eqs. (76), only the derivatives with respect to the independent coordinates are considered. Nevertheless, as explained in Section 2.3, the nonlinear dynamic Eqs. (15) are not only a function of the independent coordinates, but also the dependent coordinates $\boldsymbol{x}_{dd}$. In the present work, some clarifying comments regarding the handling of the dependent coordinates and their dependency with the independent ones are made. Escalona et al. [25] analyzed the linear stability of the steady forward motion of a bicycle multibody model resorting to a similar procedure to that found in Cuadrado et al. [15,16]. In [25], it is explicitly stated that the dependent coordinates are considered as null in the linearization, since, in the particular case of the bicycle multibody model, they do not have influence on the linear stability of the bicycle. While it is true for the stability analysis of the steady forward motion of the bicycle system, this is not true in general and the dependent coordinates are not always ignorable, being necessary in the computation of the exact linearized equations of motion. In the approaches of Section 3.4, it will be shown that the linearized holonomic constraints can be used to obtain a explicit relation between the variations of the dependent coordinates and the independent ones. Nevertheless, this is not possible in the case of nonholonomic constraints.

Peterson et al. [23] emphasized in their work the importance of the dependency of the dependent coordinates $\boldsymbol{x}_{dd}$ and dependent speeds $\dot{\boldsymbol{x}}_{dd}$ with the independent coordinates $\boldsymbol{x}_{ai}$ and independent speeds $\dot{\boldsymbol{x}}_{ai}$. The authors of this work stated: *That it is not immediately obvious that the chain rule needs to be applied is a byproduct of the commonly used notation which does not make it explicitly clear that dependent coordinates and dependent speeds are not only functions of time, but also functions of the independent coordinates and independent speeds. While this might seem obvious, no previous author makes this explicitly clear when presenting techniques for symbolically linearizing equations of motion that are subject to constraints. While the concept is simple in principle, correctly accounting for all quantities is tedious and error prone.* The linearization approach of Peterson et al. [23] was developed for equations of motion generated by Kane's method, without algebraically eliminating dependent states, and is compatible with multibody systems described by Ordinary Differential Equations (not Differential-Algebraic Equations).

Procedure by Agúndez et al. [13] (first symbolic approach)

Agúndez et al. [13] showed a linearization approach based on the direct linearization of the ODE system of Eqs. (15)–(16). The linearization of Eqs. (15)–(16) with respect to the reference solution in Eq. (68) leads to:

$$\begin{aligned} \boldsymbol{m}_0\ddot{\tilde{\boldsymbol{x}}}_{ai} &= \left.\frac{\partial\left(\boldsymbol{f}-\boldsymbol{m}\ddot{\boldsymbol{x}}_{ai}^0\right)}{\partial \boldsymbol{x}_{ai}}\right|_0 \tilde{\boldsymbol{x}}_{ai} + \left.\frac{\partial\left(\boldsymbol{f}-\boldsymbol{m}\ddot{\boldsymbol{x}}_{ai}^0\right)}{\partial \boldsymbol{x}_{dd}}\right|_0 \tilde{\boldsymbol{x}}_{dd} + \left.\frac{\partial \boldsymbol{f}}{\partial \dot{\boldsymbol{x}}_{ai}}\right|_0 \dot{\tilde{\boldsymbol{x}}}_{ai}, \\ \dot{\tilde{\boldsymbol{x}}}_{dd} &= \boldsymbol{H}_0\dot{\tilde{\boldsymbol{x}}}_{ai} + \left.\frac{\partial\left(\boldsymbol{H}\dot{\boldsymbol{x}}_{ai}^0\right)}{\partial \boldsymbol{x}_{ai}}\right|_0 \tilde{\boldsymbol{x}}_{ai} + \left.\frac{\partial\left(\boldsymbol{H}\dot{\boldsymbol{x}}_{ai}^0\right)}{\partial \boldsymbol{x}_{dd}}\right|_0 \tilde{\boldsymbol{x}}_{dd}, \end{aligned} \tag{77}$$

where the definitions $\boldsymbol{m}_0 = \boldsymbol{m}\left(\boldsymbol{x}_{ai}^0, \boldsymbol{x}_{dd}^0\right)$ and $\boldsymbol{H}_0 = \boldsymbol{H}\left(\boldsymbol{x}_{ai}^0, \boldsymbol{x}_{dd}^0\right)$ have been introduced.

Defining $\tilde{\boldsymbol{X}} = \begin{pmatrix} \tilde{\boldsymbol{x}}_{ai} & \dot{\tilde{\boldsymbol{x}}}_{ai} & \tilde{\boldsymbol{x}}_{dd} \end{pmatrix}^{\mathrm{T}}$, Eq. (77) is rewritten as a first-order linear ODE system of the form $\dot{\tilde{\boldsymbol{X}}} = \boldsymbol{J}\tilde{\boldsymbol{X}}$, where the expression of the Jacobian matrix $\boldsymbol{J}$ can be found in Eq. (153) of Appendix A. Note that the blocks associated with the dependent coordinates have been considered in the Jacobian matrix of Eq. (153). The linearized equations of motion (77) are not only expressed in terms of the independent variations $\tilde{\boldsymbol{x}}_{ai}$ and their time derivatives $\dot{\tilde{\boldsymbol{x}}}_{ai}$ and $\ddot{\tilde{\boldsymbol{x}}}_{ai}$, but also include the variations of the dependent coordinates $\tilde{\boldsymbol{x}}_{dd}$ and the time derivative $\dot{\tilde{\boldsymbol{x}}}_{dd}$. The approach is labeled as symbolic in [13], since Eq. (153) requires the symbolic computation of derivatives of inverse matrices, as matrix $\dot{\boldsymbol{T}}$ in Eq. (17).

Procedure by Agúndez et al. [13] (second numerical approach)

Given that the symbolic computation of the terms in the Jacobian matrix of (153) requires a high computational cost, Agúndez et al. [13] developed a counterpart procedure to their first symbolic approach. This procedure is the second numerical approach presented in [13]. Its accuracy is demonstrated with the linear stability results of the bicycle benchmark of Meijaard et al. [14]. This approach is labeled as numerical because it not only eases the symbolic computations, but also allows for numerical implementation.

The first symbolic approach of Agúndez et al. [13] is based on the transformation of the nonlinear DAE system given by Eqs. (1)–(3) into the nonlinear ODE system of Eqs. (15)–(16), and then the linearization is performed. In contrast, this counterpart approach first linearizes the DAE system, and then carries out the transformation into a linear ODE system.

The first key aspect of this approach is the premultiplication of the linearized dynamic Eqs. (51) by $\boldsymbol{T}^{\mathrm{T}}\left(\boldsymbol{x}^0\right)$ (the transformation matrix $\boldsymbol{T}\left(\boldsymbol{x}^0\right)$ was defined in Eq. (65)). This allows reducing the number of linearized dynamic equations from n to $n-m-l$ linear equations, and eliminating the variations of the Lagrange multipliers $\tilde{\boldsymbol{\Lambda}}$. Note that, in the same way that the relation $\boldsymbol{T}^{\mathrm{T}}(\boldsymbol{x})\,\boldsymbol{D}^{\mathrm{T}}(\boldsymbol{x}) = \boldsymbol{0}$ holds, this is also satisfied for the reference solution $\boldsymbol{x}^0$: $\boldsymbol{T}^{\mathrm{T}}\left(\boldsymbol{x}^0\right)\boldsymbol{D}^{\mathrm{T}}\left(\boldsymbol{x}^0\right) = \boldsymbol{0}$. Therefore, the linearized dynamic Eqs. (66) are obtained:

Next, a coordinate partition in terms of independent and dependent coordinates, as described in Section 2.3, is used. In this case, the coordinate partition is presented for the variations of the coordinates:

$$\tilde{\boldsymbol{x}} = \begin{pmatrix} \tilde{\boldsymbol{x}}_{ai} & \tilde{\boldsymbol{x}}_{dd} \end{pmatrix}^{\mathrm{T}}. \tag{78}$$

The objective is to express the reduced linearized dynamic Eqs. (66) in terms of the independent variations $\tilde{\boldsymbol{x}}_{ai}$ and their time derivatives $\dot{\tilde{\boldsymbol{x}}}_{ai}$ and $\ddot{\tilde{\boldsymbol{x}}}_{ai}$. For that purpose, the constraints at velocity and acceleration levels, given by Eqs. (6) and (7), are used.

The linearization of Eqs. (6) and (7) along the reference solution yields:

$$\boldsymbol{D}\left(\boldsymbol{x}^0\right)\dot{\tilde{\boldsymbol{x}}} + \left.\frac{\partial\left(\boldsymbol{D}(\boldsymbol{x})\,\dot{\boldsymbol{x}}^0\right)}{\partial \boldsymbol{x}}\right|_0 \tilde{\boldsymbol{x}} = \boldsymbol{0}, \tag{79}$$

$$\boldsymbol{D}\left(\boldsymbol{x}^0\right)\ddot{\tilde{\boldsymbol{x}}} + \left.\frac{\partial\left(\boldsymbol{D}(\boldsymbol{x})\,\ddot{\boldsymbol{x}}^0\right)}{\partial \boldsymbol{x}}\right|_0 \tilde{\boldsymbol{x}} = \left.\frac{\partial \boldsymbol{Q}_d}{\partial \boldsymbol{x}}\right|_0 \tilde{\boldsymbol{x}} + \left.\frac{\partial \boldsymbol{Q}_d}{\partial \dot{\boldsymbol{x}}}\right|_0 \dot{\tilde{\boldsymbol{x}}}. \tag{80}$$

From Eq. (79), the following relation between the variations of the dependent velocities $\dot{\tilde{\boldsymbol{x}}}_{dd}$ and the independent ones $\dot{\tilde{\boldsymbol{x}}}_{ai}$ is found:

$$\dot{\tilde{\boldsymbol{x}}}_{dd} = \boldsymbol{T}_{dd}\left(\boldsymbol{x}^0\right)\dot{\tilde{\boldsymbol{x}}}_{ai} + \bar{\boldsymbol{V}}\left(\boldsymbol{x}^0, \dot{\boldsymbol{x}}^0\right)\tilde{\boldsymbol{x}}, \tag{81}$$

where the expressions of matrices $\boldsymbol{T}_{dd}\left(\boldsymbol{x}^0\right)$ and $\bar{\boldsymbol{V}}\left(\boldsymbol{x}^0, \dot{\boldsymbol{x}}^0\right)$ can be found in Eqs. (154) of Appendix A.

The use of Eqs. (79) and (80) leads to the following transformations for the variations at velocity and acceleration levels $\dot{\tilde{\boldsymbol{x}}}$ and $\ddot{\tilde{\boldsymbol{x}}}$, respectively:

$$\dot{\tilde{\boldsymbol{x}}} = \boldsymbol{T}\left(\boldsymbol{x}^0\right)\dot{\tilde{\boldsymbol{x}}}_{ai} + \bar{\bar{\boldsymbol{V}}}\left(\boldsymbol{x}^0, \dot{\boldsymbol{x}}^0\right)\tilde{\boldsymbol{x}}, \tag{82}$$

$$\ddot{\tilde{\boldsymbol{x}}} = \boldsymbol{T}\left(\boldsymbol{x}^0\right)\ddot{\tilde{\boldsymbol{x}}}_{ai} + \boldsymbol{U}\left(\boldsymbol{x}^0, \dot{\boldsymbol{x}}^0\right)\dot{\tilde{\boldsymbol{x}}} + \boldsymbol{V}\left(\boldsymbol{x}^0, \dot{\boldsymbol{x}}^0, \ddot{\boldsymbol{x}}^0\right)\tilde{\boldsymbol{x}}, \tag{83}$$

where the matrices $\bar{\bar{\boldsymbol{V}}}\left(\boldsymbol{x}^0, \dot{\boldsymbol{x}}^0\right)$, $\boldsymbol{U}\left(\boldsymbol{x}^0, \dot{\boldsymbol{x}}^0\right)$ and $\boldsymbol{V}\left(\boldsymbol{x}^0, \dot{\boldsymbol{x}}^0, \ddot{\boldsymbol{x}}^0\right)$ are given by Eqs. (155)–(157) of Appendix A.

Finally, the coordinate partition of Eq. (78) results in the relation at position level:

$$\tilde{\boldsymbol{x}} = \boldsymbol{E}_{ai}\tilde{\boldsymbol{x}}_{ai} + \boldsymbol{E}_{dd}\tilde{\boldsymbol{x}}_{dd}, \tag{84}$$

where $\boldsymbol{E}_{ai}$ and $\boldsymbol{E}_{dd}$ are Boolean matrices, defined as:

$$\boldsymbol{E}_{ai} = \begin{pmatrix} \boldsymbol{I}_{(n-m-l)} \\ \boldsymbol{0}_{(m+l)\times(n-m-l)} \end{pmatrix}, \qquad \boldsymbol{E}_{dd} = \begin{pmatrix} \boldsymbol{0}_{(n-m-l)\times(m+l)} \\ \boldsymbol{I}_{(m+l)} \end{pmatrix}. \tag{85}$$

Substituting the relations for the variations at velocity, acceleration and position levels given by Eqs. (82), (83) and (84), respectively, in the linearized dynamic Eqs. (66), and using Eq. (81), yields:

$$\boldsymbol{m}_0\ddot{\tilde{\boldsymbol{x}}}_{ai} = \left(\boldsymbol{R}_0\bar{\bar{\boldsymbol{V}}}_0 + \boldsymbol{S}_0\right)\boldsymbol{E}_{ai}\tilde{\boldsymbol{x}}_{ai} + \boldsymbol{R}_0\boldsymbol{T}_0\dot{\tilde{\boldsymbol{x}}}_{ai} + \left(\boldsymbol{R}_0\bar{\bar{\boldsymbol{V}}}_0 + \boldsymbol{S}_0\right)\boldsymbol{E}_{dd}\tilde{\boldsymbol{x}}_{dd}, \tag{86}$$

$$\dot{\tilde{\boldsymbol{x}}}_{dd} = \bar{\boldsymbol{V}}_0\boldsymbol{E}_{ai}\tilde{\boldsymbol{x}}_{ai} + \boldsymbol{T}_{dd}\left(\boldsymbol{x}^0\right)\dot{\tilde{\boldsymbol{x}}}_{ai} + \bar{\boldsymbol{V}}_0\boldsymbol{E}_{dd}\tilde{\boldsymbol{x}}_{dd}, \tag{87}$$

where $\bar{\boldsymbol{V}}_0 = \bar{\boldsymbol{V}}\left(\boldsymbol{x}^0, \dot{\boldsymbol{x}}^0\right)$, $\bar{\bar{\boldsymbol{V}}}_0 = \bar{\bar{\boldsymbol{V}}}\left(\boldsymbol{x}^0, \dot{\boldsymbol{x}}^0\right)$, and the matrices $\boldsymbol{m}_0$, $\boldsymbol{R}_0$ and $\boldsymbol{S}_0$ are given by Eqs. (158) of Appendix A.

Defining $\tilde{\boldsymbol{X}} = \begin{pmatrix} \tilde{\boldsymbol{x}}_{ai} & \dot{\tilde{\boldsymbol{x}}}_{ai} & \tilde{\boldsymbol{x}}_{dd} \end{pmatrix}^{\mathrm{T}}$, a first-order linear ODE system of the form $\dot{\tilde{\boldsymbol{X}}} = \boldsymbol{J}\tilde{\boldsymbol{X}}$ is derived, where the expression of the Jacobian matrix $\boldsymbol{J}$ is detailed in Eq. (159) of Appendix A. The Jacobian matrices in Eqs. (153) and (159) are $(2n-m-l)\times(2n-m-l)$. Among the $2n-m-l$ eigenvalues obtained with these approaches, $2(n-m-l)$ correspond to the real spectrum of the problem, and $m+l$ are spurious eigenvalues, associated with the m holonomic constraints differentiated with respect to time and the l nonholonomic constraints.

Note that the resulting linearized equations of motion (86)–(87) present the same structure as Eq. (77). In this approach, the dependent coordinates are handled in the same way as in the symbolic counterpart. As in Eq. (77), the linearized equations of motion (86)–(87) are not only expressed in terms of the independent variations $\tilde{\boldsymbol{x}}_{ai}$ and their time derivatives $\dot{\tilde{\boldsymbol{x}}}_{ai}$ and $\ddot{\tilde{\boldsymbol{x}}}_{ai}$, but also include the variations of the dependent coordinates $\tilde{\boldsymbol{x}}_{dd}$ and the time derivatives $\dot{\tilde{\boldsymbol{x}}}_{dd}$.

3.4. Group 4: procedures based on coordinate partitioning in terms of independent and dependent coordinates, with holonomic constraints elimination

The procedures included in this subsection achieve a linear ODE system of equations expressed only in terms of the independent coordinates. The approach of Bae et al. [26], the second symbolic and

third numerical approaches of Agúndez et al. [13], and the linearization procedure of Cossalter et al. [27] are included in this group.

Procedure by Bae et al. [26]

Bae et al. [26] present a linearization approach for multibody systems with holonomic constraints. In absence of nonholonomic constraints, the coordinates $\boldsymbol{x}_{ad}$ are not required and the coordinate partition of Eq. (26) is used: $\boldsymbol{x} = \begin{pmatrix} \boldsymbol{x}_{ai} & \boldsymbol{x}_{d} \end{pmatrix}^{\mathrm{T}}$.

Computing the variational form of the holonomic constraints (28):

$$\delta \boldsymbol{C} = \boldsymbol{C}_{\boldsymbol{x}_d}(\boldsymbol{x})\,\delta \boldsymbol{x}_d + \boldsymbol{C}_{\boldsymbol{x}_{ai}}(\boldsymbol{x})\,\delta \boldsymbol{x}_{ai} = \boldsymbol{0}, \tag{88}$$

the variations of the dependent coordinates $\delta \boldsymbol{x}_d$ are obtained in terms of the independent ones as:

$$\delta \boldsymbol{x}_d = -\boldsymbol{C}_{\boldsymbol{x}_d}^{-1}(\boldsymbol{x})\,\boldsymbol{C}_{\boldsymbol{x}_{ai}}(\boldsymbol{x})\,\delta \boldsymbol{x}_{ai}. \tag{89}$$

Eq. (89) allows obtaining the following transformation:

$$\delta \boldsymbol{x} = \boldsymbol{T}(\boldsymbol{x})\,\delta \boldsymbol{x}_{ai}, \tag{90}$$

where $\boldsymbol{T}(\boldsymbol{x})$ is the transformation matrix defined in Eq. (12), for the particular case of a multibody system with only holonomic constraints: $\boldsymbol{D}_{dd}(\boldsymbol{x}) = \boldsymbol{C}_{\boldsymbol{x}_d}(\boldsymbol{x})$ and $\boldsymbol{D}_{ai}(\boldsymbol{x}) = \boldsymbol{C}_{\boldsymbol{x}_{ai}}(\boldsymbol{x})$.

Premultiplying the dynamic Eqs. (5) by $\boldsymbol{T}^{\mathrm{T}}$, $\boldsymbol{F}^{*}$ is defined as:

$$\boldsymbol{F}^{*}(\boldsymbol{x}, \dot{\boldsymbol{x}}, \ddot{\boldsymbol{x}}) = \boldsymbol{T}^{\mathrm{T}}(\boldsymbol{x})\,\boldsymbol{M}(\boldsymbol{x})\,\ddot{\boldsymbol{x}} - \boldsymbol{T}^{\mathrm{T}}(\boldsymbol{x})\,\boldsymbol{Q}(\boldsymbol{x}, \dot{\boldsymbol{x}}) = \boldsymbol{0}, \tag{91}$$

where the Lagrange multipliers $\boldsymbol{\Lambda}$ are eliminated, since $\boldsymbol{T}$ is the null space of $\boldsymbol{C}_{\boldsymbol{x}}$, and therefore $\boldsymbol{T}^{\mathrm{T}}(\boldsymbol{x})\,\boldsymbol{C}_{\boldsymbol{x}}^{\mathrm{T}}(\boldsymbol{x}) = \boldsymbol{0}$.

As stated by Bae et al. [26], $\boldsymbol{F}^{*}$ is a function of both the independent and dependent coordinates. Computing the variational form of Eq. (91):

$$\delta \boldsymbol{F}^{*} = \boldsymbol{F}^{*}_{\boldsymbol{x}}\delta \boldsymbol{x} + \boldsymbol{F}^{*}_{\dot{\boldsymbol{x}}}\delta \dot{\boldsymbol{x}} + \boldsymbol{F}^{*}_{\ddot{\boldsymbol{x}}}\delta \ddot{\boldsymbol{x}} = \boldsymbol{0}, \tag{92}$$

Eq. (92) can be expressed in matrix form as:

$$\begin{pmatrix} \boldsymbol{F}^{*}_{\boldsymbol{x}} & \boldsymbol{F}^{*}_{\dot{\boldsymbol{x}}} & \boldsymbol{F}^{*}_{\ddot{\boldsymbol{x}}} \end{pmatrix} \begin{pmatrix} \delta \boldsymbol{x} \\ \delta \dot{\boldsymbol{x}} \\ \delta \ddot{\boldsymbol{x}} \end{pmatrix} = \boldsymbol{0}. \tag{93}$$

The objective of the linearization procedure is to express Eq. (93) only in terms of the independent coordinates. To this end, the variational form of the holonomic constraints at position, velocity and acceleration levels, given by Eqs. (160)–(162) in Appendix A, are considered. Assembling Eqs. (160)–(162), and using the coordinate partition (26), the following relation between the complete set of variations at position, velocity and acceleration levels, $\delta \boldsymbol{X} = \begin{pmatrix} \delta \boldsymbol{x} & \delta \dot{\boldsymbol{x}} & \delta \ddot{\boldsymbol{x}} \end{pmatrix}^{\mathrm{T}}$, and the variations of the independent coordinates $\delta \boldsymbol{X}_{ai} = \begin{pmatrix} \delta \boldsymbol{x}_{ai} & \delta \dot{\boldsymbol{x}}_{ai} & \delta \ddot{\boldsymbol{x}}_{ai} \end{pmatrix}^{\mathrm{T}}$, is obtained:

$$\boldsymbol{\mathcal{N}}\delta \boldsymbol{X} = \boldsymbol{\mathcal{M}}\delta \boldsymbol{X}_{ai}. \tag{94}$$

The expressions of matrices $\boldsymbol{\mathcal{N}}$ and $\boldsymbol{\mathcal{M}}$ are detailed in Eqs. (163) and (164) of Appendix A.

Eq. (94) is used to solve for $\begin{pmatrix} \delta \boldsymbol{x} & \delta \dot{\boldsymbol{x}} & \delta \ddot{\boldsymbol{x}} \end{pmatrix}^{\mathrm{T}}$ in terms of the independent variations $\delta \boldsymbol{x}_{ai}$ and their time derivatives. Substituting in Eq. (93), the following linearized equations of motion are obtained:

$$\hat{\boldsymbol{M}}\delta \ddot{\boldsymbol{x}}_{ai} + \hat{\boldsymbol{C}}\delta \dot{\boldsymbol{x}}_{ai} + \hat{\boldsymbol{K}}\delta \boldsymbol{x}_{ai} = \boldsymbol{0}, \tag{95}$$

where $\hat{\boldsymbol{M}}$, $\hat{\boldsymbol{C}}$ and $\hat{\boldsymbol{K}}$ are the mass, damping and stiffness matrices, respectively. Eq. (95) provides $2(n-m)$ eigenvalues, which corresponds to the real spectrum of the problem, associated with the $n_g = n - m$ degrees of freedom of the multibody system.

In contrast to Eqs. (86)–(87), where the variations of the dependent coordinates explicitly appear, the linear equations of motion (95) are only expressed in terms of the independent variations $\delta \boldsymbol{x}_{ai}$ and the time derivatives $\delta \dot{\boldsymbol{x}}_{ai}$ and $\delta \ddot{\boldsymbol{x}}_{ai}$. The dependent coordinates have not been ignored in Eq. (95), since the dependency with the independent ones has been considered by means of the variational form of the holonomic constraints at position, velocity and acceleration levels, given by Eqs. (160)–(162).

Procedure by Cossalter et al. [27]

The linearization procedure by Cossalter et al. [27] is also presented for multibody systems with holonomic constraints. Consider the linear index-3 DAE given by Eqs. (31)–(32). Cossalter et al. [27] write Eqs. (31)–(32) as follows:

$$\boldsymbol{M}_a\ddot{\tilde{\boldsymbol{x}}} + \boldsymbol{C}_a\dot{\tilde{\boldsymbol{x}}} + \boldsymbol{K}_a\tilde{\boldsymbol{x}} + \boldsymbol{K}_\phi\tilde{\boldsymbol{x}} + \boldsymbol{C}^{\mathrm{T}}\left(\boldsymbol{x}^0\right)\tilde{\boldsymbol{\Lambda}} = \boldsymbol{0}, \tag{96}$$

$$\left.\frac{\partial \boldsymbol{C}(\boldsymbol{x})}{\partial \boldsymbol{x}}\right|_0 \tilde{\boldsymbol{x}} = \boldsymbol{0}. \tag{97}$$

Comparing Eqs. (31)–(32) with Eqs. (96)–(97), the following definitions are used:

$$\boldsymbol{M}_a = \boldsymbol{M}\left(\boldsymbol{x}^0\right), \qquad \boldsymbol{C}_a = -\left.\frac{\partial \boldsymbol{Q}}{\partial \dot{\boldsymbol{x}}}\right|_0,$$
$$\boldsymbol{K}_a = \left.\frac{\partial\left(\boldsymbol{M}(\boldsymbol{x})\,\ddot{\boldsymbol{x}}^0\right)}{\partial \boldsymbol{x}}\right|_0 - \left.\frac{\partial \boldsymbol{Q}}{\partial \boldsymbol{x}}\right|_0, \qquad \boldsymbol{K}_\phi = \left.\frac{\partial\left(\boldsymbol{C}_{\boldsymbol{x}}^{\mathrm{T}}(\boldsymbol{x})\,\boldsymbol{\Lambda}^0\right)}{\partial \boldsymbol{x}}\right|_0. \tag{98}$$

In the particular case of $\boldsymbol{K}_\phi$, this matrix is presented in [27] as shown in Eq. (165) of Appendix A. Eq. (165) is equivalent to the definition of $\boldsymbol{K}_\phi$ presented in Eq. (98).

The coordinate partition in terms of independent and dependent coordinates of Eq. (26) is now used. By virtue of Eq. (26), the reference solution $\boldsymbol{x}^0(t)$ and its time derivatives $\dot{\boldsymbol{x}}^0(t)$, $\ddot{\boldsymbol{x}}^0(t)$ can be expressed as:

$$\boldsymbol{x}^0_{ai}(t),\ \dot{\boldsymbol{x}}^0_{ai}(t),\ \ddot{\boldsymbol{x}}^0_{ai}(t),\ \boldsymbol{x}^0_{d}(t),\ \dot{\boldsymbol{x}}^0_{d}(t). \tag{99}$$

The variations with respect to the reference solution in Eq. (99) are introduced:

$$\tilde{\boldsymbol{x}}_{ai} = \boldsymbol{x}_{ai} - \boldsymbol{x}^0_{ai}, \qquad \dot{\tilde{\boldsymbol{x}}}_{ai} = \dot{\boldsymbol{x}}_{ai} - \dot{\boldsymbol{x}}^0_{ai},$$
$$\ddot{\tilde{\boldsymbol{x}}}_{ai} = \ddot{\boldsymbol{x}}_{ai} - \ddot{\boldsymbol{x}}^0_{ai}, \qquad \tilde{\boldsymbol{x}}_{d} = \boldsymbol{x}_{d} - \boldsymbol{x}^0_{d}, \tag{100}$$
$$\dot{\tilde{\boldsymbol{x}}}_{d} = \dot{\boldsymbol{x}}_{d} - \dot{\boldsymbol{x}}^0_{d}.$$

The following transformation between the variations of the redundant set of coordinates and the independent ones is introduced:

$$\tilde{\boldsymbol{x}} = \boldsymbol{T}_0\tilde{\boldsymbol{x}}_{ai}, \tag{101}$$

where the transformation matrix $\boldsymbol{T}_0$ is the same as that of Eq. (65), particularized for the case of only holonomic constraints:

$$\boldsymbol{T}_0 = \begin{pmatrix} \boldsymbol{I}_{(n-m)} \\ -\left(\boldsymbol{C}_{\boldsymbol{x}_d}\left(\boldsymbol{x}^0\right)\right)^{-1}\boldsymbol{C}_{\boldsymbol{x}_{ai}}\left(\boldsymbol{x}^0\right) \end{pmatrix}. \tag{102}$$

Cossalter et al. [27] consider that Eq. (101) also holds for the variations of the velocities and accelerations:

$$\dot{\tilde{\boldsymbol{x}}} = \boldsymbol{T}_0\dot{\tilde{\boldsymbol{x}}}_{ai}, \tag{103}$$

$$\ddot{\tilde{\boldsymbol{x}}} = \boldsymbol{T}_0\ddot{\tilde{\boldsymbol{x}}}_{ai}. \tag{104}$$

Premultiplying Eq. (96) by $\boldsymbol{T}_0^{\mathrm{T}}$, and using the transformations between the redundant set of coordinates and the independent ones of Eqs. (101), (103) and (104), yields:

$$\hat{\boldsymbol{M}}_a\ddot{\tilde{\boldsymbol{x}}}_{ai} + \hat{\boldsymbol{C}}_a\dot{\tilde{\boldsymbol{x}}}_{ai} + \hat{\boldsymbol{K}}_a\tilde{\boldsymbol{x}}_{ai} = \boldsymbol{0}, \tag{105}$$

with

$$\hat{\boldsymbol{M}}_a = \boldsymbol{T}_0^{\mathrm{T}}\boldsymbol{M}_a\boldsymbol{T}_0, \qquad \hat{\boldsymbol{C}}_a = \boldsymbol{T}_0^{\mathrm{T}}\boldsymbol{C}_a\boldsymbol{T}_0,$$
$$\hat{\boldsymbol{K}}_a = \boldsymbol{T}_0^{\mathrm{T}}\left(\boldsymbol{K}_a + \boldsymbol{K}_\phi\right)\boldsymbol{T}_0. \tag{106}$$

Note that, in Eq. (105), the variations of the Lagrange multipliers $\tilde{\boldsymbol{\Lambda}}$ of Eq. (96) disappear, since $\boldsymbol{T}_0^{\mathrm{T}}\boldsymbol{C}^{\mathrm{T}}\left(\boldsymbol{x}^0\right) = \boldsymbol{0}$.

Eq. (105) leads to $2(n-m)$ eigenvalues, which corresponds to the real spectrum of the problem. As in the linearization approach of Bae et al. [26], the linear equations of motion (105) are obtained in terms of the independent variations $\tilde{\boldsymbol{x}}_{ai}$ and their time derivatives $\dot{\tilde{\boldsymbol{x}}}_{ai}$ and $\ddot{\tilde{\boldsymbol{x}}}_{ai}$. The dependent coordinates have been considered in the linearization by means of the transformations between the redundant set of variations $\tilde{\boldsymbol{x}}$ and the independent ones at position, velocity and acceleration level, given by Eqs. (101), (103) and (104), respectively.

Procedure by Agúndez et al. [13] (second symbolic approach)

Agúndez et al. [13] presented a second symbolic linearization approach that leads to the linear equations of motion in ODE form, expressed in terms of only the independent variations and their time derivatives. The approach was developed for multibody systems with holonomic and nonholonomic constraints. To keep the presentation of the procedure simpler, the case with only holonomic constraints is presented first.

The linearization of Eqs. (23)–(24) with respect to the reference solution of Eq. (99) yields the following linear DAE system:

$$\boldsymbol{m}_0 \ddot{\tilde{\boldsymbol{x}}}_{ai} = \left.\frac{\partial \left(\boldsymbol{f} - \boldsymbol{m}\ddot{\boldsymbol{x}}^0_{ai}\right)}{\partial \boldsymbol{x}_{ai}}\right|_0 \tilde{\boldsymbol{x}}_{ai} + \left.\frac{\partial \left(\boldsymbol{f} - \boldsymbol{m}\ddot{\boldsymbol{x}}^0_{ai}\right)}{\partial \boldsymbol{x}_{d}}\right|_0 \tilde{\boldsymbol{x}}_{d} + \left.\frac{\partial \boldsymbol{f}}{\partial \dot{\boldsymbol{x}}_{ai}}\right|_0 \dot{\tilde{\boldsymbol{x}}}_{ai}, \tag{107}$$

$$\left.\frac{\partial \boldsymbol{C}}{\partial \boldsymbol{x}_{ai}}\right|_0 \tilde{\boldsymbol{x}}_{ai} + \left.\frac{\partial \boldsymbol{C}}{\partial \boldsymbol{x}_{d}}\right|_0 \tilde{\boldsymbol{x}}_{d} = \boldsymbol{0}, \tag{108}$$

where $\boldsymbol{m}_0 = \boldsymbol{m}\left(\boldsymbol{x}^0_{ai}, \boldsymbol{x}^0_{d}\right)$.

The linearized holonomic constraints (108) can be used to express the variations of the dependent coordinates $\tilde{\boldsymbol{x}}_d$ as a function of the independent ones $\tilde{\boldsymbol{x}}_{ai}$:

$$\tilde{\boldsymbol{x}}_d = -\left(\left.\frac{\partial \boldsymbol{C}}{\partial \boldsymbol{x}_d}\right|_0\right)^{-1} \left.\frac{\partial \boldsymbol{C}}{\partial \boldsymbol{x}_{ai}}\right|_0 \tilde{\boldsymbol{x}}_{ai}. \tag{109}$$

The substitution of Eq. (109) in the linearized dynamic Eqs. (107) leads to:

$$\boldsymbol{m}_0 \ddot{\tilde{\boldsymbol{x}}}_{ai} = \left(\left.\frac{\partial \left(\boldsymbol{f} - \boldsymbol{m}\ddot{\boldsymbol{x}}^0_{ai}\right)}{\partial \boldsymbol{x}_{ai}}\right|_0 - \left.\frac{\partial \left(\boldsymbol{f} - \boldsymbol{m}\ddot{\boldsymbol{x}}^0_{ai}\right)}{\partial \boldsymbol{x}_{d}}\right|_0 \left(\left.\frac{\partial \boldsymbol{C}}{\partial \boldsymbol{x}_d}\right|_0\right)^{-1} \left.\frac{\partial \boldsymbol{C}}{\partial \boldsymbol{x}_{ai}}\right|_0 \right) \tilde{\boldsymbol{x}}_{ai} + \left.\frac{\partial \boldsymbol{f}}{\partial \dot{\boldsymbol{x}}_{ai}}\right|_0 \dot{\tilde{\boldsymbol{x}}}_{ai}. \tag{110}$$

Defining $\tilde{\boldsymbol{X}} = \begin{pmatrix} \tilde{\boldsymbol{x}}_{ai} & \dot{\tilde{\boldsymbol{x}}}_{ai} \end{pmatrix}^{\mathrm{T}}$, the linear second-order ODE of Eq. (110) can be written as a first-order ODE of the form $\dot{\tilde{\boldsymbol{X}}} = \boldsymbol{J}\tilde{\boldsymbol{X}}$, with the Jacobian matrix $\boldsymbol{J}$:

$$\boldsymbol{J} = \left(\begin{array}{c|c} \boldsymbol{0}_{(n-m)} & \boldsymbol{I}_{(n-m)} \\ \hline \boldsymbol{J}_{21} & \boldsymbol{J}_{22} \end{array}\right). \tag{111}$$

The expressions of the blocks $\boldsymbol{J}_{21}$ and $\boldsymbol{J}_{22}$ in Eq. (111) can be found in Eqs. (166) of Appendix A.

In the particular case of a multibody system including nonholonomic constraints, the linearization of Eqs. (23)–(25) leads to the linear ODE system given by Eqs. (167) of Appendix A. Note that, in contrast to the dependent variations $\tilde{\boldsymbol{x}}_d$, which were expressed as a function of $\tilde{\boldsymbol{x}}_{ai}$ by using the linearized holonomic constraints (109), the set $\tilde{\boldsymbol{x}}_{ad}$ cannot be removed in Eqs. (167), since the nonholonomic constraints are first-order differential equations that cannot be eliminated. Finally, defining $\tilde{\boldsymbol{X}} = \begin{pmatrix} \tilde{\boldsymbol{x}}_{ai} & \dot{\tilde{\boldsymbol{x}}}_{ai} & \tilde{\boldsymbol{x}}_{ad} \end{pmatrix}^{\mathrm{T}}$, the system of Eqs. (167) can be rewritten as a first-order system of the form $\dot{\tilde{\boldsymbol{X}}} = \boldsymbol{J}\tilde{\boldsymbol{X}}$, with the Jacobian matrix $\boldsymbol{J}$:

$$\boldsymbol{J} = \left(\begin{array}{c|c|c} \boldsymbol{0}_{(n-m-l)} & \boldsymbol{I}_{(n-m-l)} & \boldsymbol{0}_{(n-m-l)\times l} \\ \hline \boldsymbol{J}_{21} & \boldsymbol{J}_{22} & \boldsymbol{J}_{23} \\ \hline \boldsymbol{J}_{31} & \boldsymbol{J}_{32} & \boldsymbol{J}_{33} \end{array}\right). \tag{112}$$

The detailed expressions of the blocks in the Jacobian matrix (112) can be found in Eqs. (168) of Appendix A.

Procedure by Agúndez et al. [13] (third numerical approach)

Agúndez et al. [13] developed a counterpart procedure to the previous symbolic linearization approach, which eases the computation of the Jacobian matrix of Eq. (112), allowing the symbolic and numerical implementation. As in the symbolic version, this linearization approach makes use of the linearized holonomic constraints to express the dependent variations $\tilde{\boldsymbol{x}}_d$ as a function of the independent ones.

Starting from the linearized dynamic Eqs. (66), the objective of this approach is to express Eq. (66) in terms of the independent variations $\tilde{\boldsymbol{x}}_{ai}$ and the time derivatives $\dot{\tilde{\boldsymbol{x}}}_{ai}$, $\ddot{\tilde{\boldsymbol{x}}}_{ai}$. For that purpose, the linearized constraints at velocity and acceleration levels, given by Eqs. (79) and (80), are used to obtain the transformations presented in Eqs. (82) and (83). Next, as in the previous approach, the linearized holonomic constraints (108) allow for obtaining the variations of the dependent coordinates as a function of the independent ones, as shown in Eq. (109). The following transformation for the redundant set of variations $\tilde{\boldsymbol{x}}$ in terms of the independent ones $\tilde{\boldsymbol{x}}_{ai}$ is obtained using Eq. (109):

$$\tilde{\boldsymbol{x}} = \boldsymbol{V}_{h,ai}\left(\boldsymbol{x}^0\right) \tilde{\boldsymbol{x}}_{ai}, \tag{113}$$

where

$$\boldsymbol{V}_{h,ai}\left(\boldsymbol{x}^0\right) = \begin{pmatrix} \boldsymbol{I}_{(n-m)} \\ -\left(\left.\frac{\partial \boldsymbol{C}}{\partial \boldsymbol{x}_d}\right|_0\right)^{-1} \left.\frac{\partial \boldsymbol{C}}{\partial \boldsymbol{x}_{ai}}\right|_0 \end{pmatrix}. \tag{114}$$

Note that the relation at position level between $\tilde{\boldsymbol{x}}$ and $\tilde{\boldsymbol{x}}_{ai}$ in Eq. (113) is equivalent to that used by Cossalter et al. [27] in Eq. (101). Nevertheless, the relations at velocity and acceleration levels derived in Eqs. (82) and (83) differ from those used in the approach of Cossalter et al. shown in Eqs. (103) and (104). While Eqs. (103) and (104) are obtained by differentiating with respect to time Eq. (101), Eqs. (82) and (83) are not derived from the time derivative of Eq. (113), but from the linearized constraints at velocity and acceleration levels of Eqs. (79) and (80), respectively.

Substituting Eqs. (82), (83) and (113) in Eq. (66), the linearized equations of motion are obtained in terms of the independent variations $\tilde{\boldsymbol{x}}_{ai}$ and their time derivatives:

$$\boldsymbol{m}_0 \ddot{\tilde{\boldsymbol{x}}}_{ai} = \left(\boldsymbol{R}_0 \bar{\tilde{\boldsymbol{V}}}_0 + \boldsymbol{S}_0\right) \boldsymbol{V}_{h,ai}\left(\boldsymbol{x}^0\right) \tilde{\boldsymbol{x}}_{ai} + \boldsymbol{R}_0 \boldsymbol{T}_0 \dot{\tilde{\boldsymbol{x}}}_{ai}, \tag{115}$$

where the matrices $\boldsymbol{m}_0$, $\boldsymbol{R}_0$ and $\boldsymbol{S}_0$ were defined in Eq. (158) of Appendix A. Note that Eq. (115) presents the same structure as Eq. (110).

Defining $\tilde{\boldsymbol{X}} = \begin{pmatrix} \tilde{\boldsymbol{x}}_{ai} & \dot{\tilde{\boldsymbol{x}}}_{ai} \end{pmatrix}^{\mathrm{T}}$, the linear second-order ODE system (115) can be written as a first-order ODE system of the form $\dot{\tilde{\boldsymbol{X}}} = \boldsymbol{J}\tilde{\boldsymbol{X}}$, where the expression of the Jacobian matrix $\boldsymbol{J}$ can be found in Eq. (169) of Appendix A.

The Jacobian matrices (111) and (169) are $2(n-m) \times 2(n-m)$. Therefore, $2(n-m)$ eigenvalues are obtained, corresponding to the real spectrum of the problem. Note that, despite the linearized equations of motion (110) and (115) are only expressed in terms of the independent variations $\tilde{\boldsymbol{x}}_{ai}$ and their time derivatives, the dependent coordinates are not ignored in the linearization. The dependency with the independent ones is taken into account by means of the relations at velocity, acceleration and position levels of Eqs. (82), (83) and (113), respectively.

In the particular case of a multibody system with nonholonomic constraints, Eq. (115) is augmented with the linearized nonholonomic constraints, leading to:

$$\boldsymbol{m}_0 \ddot{\tilde{\boldsymbol{x}}}_{ai} = \left(\boldsymbol{R}_0 \bar{\tilde{\boldsymbol{V}}}_0 + \boldsymbol{S}_0\right) \boldsymbol{V}_{h,ai}\left(\boldsymbol{x}^0\right) \tilde{\boldsymbol{x}}_{ai} + \boldsymbol{R}_0 \boldsymbol{T}_0 \dot{\tilde{\boldsymbol{x}}}_{ai} + \left(\boldsymbol{R}_0 \bar{\tilde{\boldsymbol{V}}}_0 + \boldsymbol{S}_0\right) \boldsymbol{V}_{h,ad}\left(\boldsymbol{x}^0\right) \tilde{\boldsymbol{x}}_{ad}, \tag{116}$$

$$\dot{\tilde{\boldsymbol{x}}}_{ad} = \boldsymbol{V}_{nh,ai}\left(\boldsymbol{x}^0, \dot{\boldsymbol{x}}^0\right) \tilde{\boldsymbol{x}}_{ai} + \boldsymbol{U}_{nh,ai}\left(\boldsymbol{x}^0\right) \dot{\tilde{\boldsymbol{x}}}_{ai} + \boldsymbol{V}_{nh,ad}\left(\boldsymbol{x}^0, \dot{\boldsymbol{x}}^0\right) \tilde{\boldsymbol{x}}_{ad}. \tag{117}$$

The derivation of matrices $\boldsymbol{V}_{h,ad}$, $\boldsymbol{U}_{nh,ai}$, $\boldsymbol{V}_{nh,ai}$ and $\boldsymbol{V}_{nh,ad}$ in Eqs. (116) and (117) can be found in detail in [13]. Defining $\tilde{\boldsymbol{X}} = \begin{pmatrix} \tilde{\boldsymbol{x}}_{ai} & \dot{\tilde{\boldsymbol{x}}}_{ai} & \tilde{\boldsymbol{x}}_{ad} \end{pmatrix}^{\mathrm{T}}$, the system of Eqs. (116) and (117) can be rewritten as a first-order system of the form $\dot{\tilde{\boldsymbol{X}}} = \boldsymbol{J}\tilde{\boldsymbol{X}}$, with the Jacobian matrix $\boldsymbol{J}$ given by Eq. (170) of Appendix A.

Note that Eqs. (116) and (117) present the same structure as Eqs. (167). The Jacobian matrices of Eqs. (112) and (170) are $(2(n-m)-l) \times (2(n-m)-l)$. This size is the minimum that can be achieved, not being possible a further reduction, since the nonholonomic constraints are first-order differential equations that cannot be eliminated. Among the $2(n-m)-l$ eigenvalues obtained with these approaches, $2(n-m-l)$ correspond to the real spectrum of the problem, and l are spurious eigenvalues associated with the l linearized nonholonomic constraints.

The accuracy of the linearized equations of motion (116) and (117), and the equivalence between the Jacobian matrices of Eqs. (112)

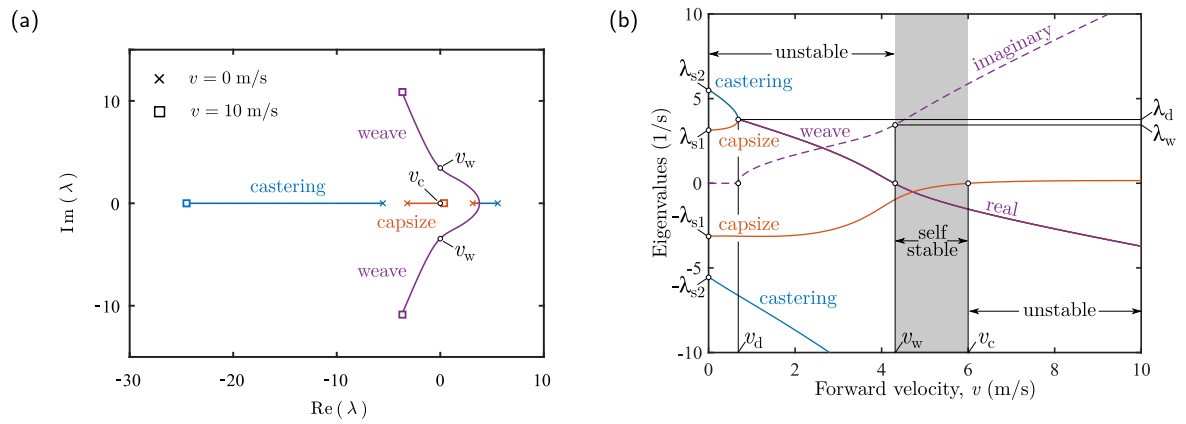

Fig. 2. Evolution of the eigenvalues in the forward speed range $0 < v < 10$ m/s: root locus of the bicycle (a) and evolution of the eigenvalues with the forward speed (b). The eigenvalues show that the uncontrolled bicycle is statically unstable at low speeds, asymptotic stable for medium speeds and oscillatory unstable at high speeds. In the root locus (a), the eigenvalues corresponding to $v = 0$ m/s are highlighted with crosses, and the eigenvalues associated with $v = 10$ m/s are represented with squares. The evolution of the eigenvalues with the forward speed shown in (b) corresponds to the same continuation diagram obtained in Meijaard et al. [14]. The real parts of the eigenvalues have been plotted with solid lines, while the imaginary parts are shown with dashed line. It can be seen that, for the forward speed v_d, the oscillatory unstable weave motion appears after the splitting of the two real eigenvalues λ_d into a complex conjugate pair. Once the weave speed v_w is reached, the complex conjugate pair traverses the imaginary axis at λ_w, so the weave mode is stabilized. The asymptotic stability of the bicycle benchmark continues until the capsize speed v_c, when the capsize real eigenvalue becomes positive, resulting in the instability of the bicycle. In this way, the asymptotic stability is achieved for the range $v_w < v < v_c$, with $v_w \simeq 4.29$ m/s and $v_c \simeq 6.02$ m/s. The points corresponding to v_w and v_c are also highlighted in the root locus (a).

and (170), were demonstrated with the stability results of the bicycle benchmark of Meijaard et al. [14].

4. Results and discussion

The importance of considering the set of dependent coordinates in the linearization is illustrated with the linear stability results of two case studies: the bicycle and the electric kickscooter (henceforth e-scooter). The bicycle multibody model considered in this study is based on the bicycle benchmark of Meijaard et al. [14] and includes toroidal wheels. The description of the bicycle multibody model is presented in Appendix B. The linearized equations along the steady forward motion are derived, considering different choices of independent and dependent coordinates. The role of the dependent coordinates in each scenario is discussed. Next, the second case study is the e-scooter multibody model, based on the e-scooter benchmark presented by García-Vallejo et al. [87]. The multibody model, which presents toroidal wheels and includes flexibility by means of the rear and front suspensions, is described in Appendix C. Considering different choices of independent and dependent coordinates, the linearized equations along the steady forward motion are obtained. Lastly, the role of the dependent coordinates is discussed with the linear stability results of the e-scooter.

4.1. Case study 1: the role of the dependent coordinates in the bicycle stability analysis

The role of the dependent coordinates in the linearization is illustrated with the bicycle model described in Appendix B.

Groups 1 and 2: as already shown, the linearization approaches described in Sections 3.1 and 3.2 (devoted to the linearization of the index-3 and index-1 DAE equations of motion, respectively) make use of the redundant set of coordinates. In these approaches, no coordinate partition in terms of independent and dependent coordinates is considered, and no distinction in the handling of the coordinates is made. The resulting Jacobian matrices include the partial derivatives with respect to the complete set of coordinates. Among the linearization approaches of Group 1, the procedure of Pappalardo et al. [10], summarized in Section 3.1, was used to analyze the stability of the steady forward motion of a bicycle multibody model. In the same way, the first of the numerical procedures proposed by Agúndez et al. [13], exposed in Section 3.2, was used to linearize the index-1 DAE equations of motion of the bicycle multibody model along the reference solution of Eq. (179).

Group 3: the approaches of the third group make use of a coordinate partition in terms of independent and dependent coordinates. In this case, it is important to clarify the handling of the dependent coordinates in the linearization.

Consider the vector of coordinates in Eq. (171) of Appendix B. The following coordinate partition is chosen:

$$\tilde{\boldsymbol{x}}_{ai} = \begin{pmatrix} \tilde{x}_b & \tilde{\phi}_b & \tilde{\delta} \end{pmatrix}^{\mathrm{T}},$$
$$\tilde{\boldsymbol{x}}_{dd} = \begin{pmatrix} \tilde{y}_b & \tilde{z}_b & \tilde{\psi}_b & \tilde{\theta}_b & \tilde{\theta}_R & \tilde{\theta}_F & \tilde{\xi}_R & \tilde{\xi}_F & \tilde{\eta}_R & \tilde{\eta}_F \end{pmatrix}^{\mathrm{T}}, \quad (118)$$

where $n - m - l = 3$ independent coordinates (the same number as degrees of freedom of the system) are considered. The forward motion, the lean and steering angles have been selected as independent coordinates. This partition is possible, since the submatrix $\boldsymbol{D}_{dd}(\boldsymbol{x})$ in Eq. (12) is non-singular. The Jacobian matrices of Eqs. (153) and (159), obtained with the symbolic and numerical approaches presented in [13], are computed for the steady forward motion of the bicycle, leading to equation in Box I, where the coefficients α_k, with $k = 1 \ldots 20$, are functions of the geometric and dynamic parameters of the bicycle. As shown in [13], the computation of the eigenvalues associated with the Jacobian matrix of Eq. (119), for the hoop-shaped wheels case ($\mu_i = 0$), yields the results of Fig. 2. Moreover, ten spurious null eigenvalues are obtained, associated with the $m + l = 10$ dependent coordinates in Eq. (118).

With the Jacobian matrix of Eq. (119), the following question arises: can the Jacobian matrix (119) be reduced by eliminating the blocks associated with the dependent coordinates? Note that, in the Jacobian matrices of Eqs. (153) and (159) of Appendix B, the blocks including the derivatives with respect to the dependent coordinates are $\boldsymbol{J}_{23} = \boldsymbol{m}_0^{-1} \left. \frac{\partial \left(\boldsymbol{f} - \boldsymbol{m}\ddot{\boldsymbol{x}}_{ai}^0 \right)}{\partial \boldsymbol{x}_{dd}} \right|_0 = \boldsymbol{m}_0^{-1} \left(\boldsymbol{R}_0 \bar{\bar{\boldsymbol{V}}}_0 + \boldsymbol{S}_0 \right) \boldsymbol{E}_{dd}$. In the particular case of the bicycle, with the selection of independent coordinates of Eq. (118), it can be seen that these blocks correspond to null submatrices (highlighted with red in Eq. (119)), and thus the dependent coordinates can be ignored. In this scenario, the Jacobian matrices of Eqs. (153) and

$$
\boldsymbol{J} = \left(\begin{array}{ccc|ccc|cccccccccc}
0 & 0 & 0 & 1 & 0 & 0 & 0 & 0 & 0 & 0 & 0 & 0 & 0 & 0 & 0 & 0 \\
0 & 0 & 0 & 0 & 1 & 0 & 0 & 0 & 0 & 0 & 0 & 0 & 0 & 0 & 0 & 0 \\
0 & 0 & 0 & 0 & 0 & 1 & 0 & 0 & 0 & 0 & 0 & 0 & 0 & 0 & 0 & 0 \\
\hline
0 & 0 & 0 & 0 & 0 & 0 & 0 & 0 & 0 & 0 & 0 & 0 & 0 & 0 & 0 & 0 \\
0 & \alpha_1 & \alpha_2 + \alpha_3\, v^2 & 0 & \alpha_4\, v & \alpha_5\, v & 0 & 0 & 0 & 0 & 0 & 0 & 0 & 0 & 0 & 0 \\
0 & \alpha_6 & \alpha_7 + \alpha_8\, v^2 & 0 & \alpha_9\, v & \alpha_{10}\, v & 0 & 0 & 0 & 0 & 0 & 0 & 0 & 0 & 0 & 0 \\
\hline
0 & 0 & \alpha_{11}\, v & 0 & \alpha_{12} & \alpha_{13} & 0 & 0 & \alpha_{14} v & 0 & 0 & 0 & 0 & 0 & 0 & 0 \\
0 & 0 & 0 & 0 & 0 & 0 & 0 & 0 & 0 & 0 & 0 & 0 & 0 & 0 & 0 & 0 \\
0 & 0 & \alpha_{15}\, v & 0 & 0 & \alpha_{16} & 0 & 0 & 0 & 0 & 0 & 0 & 0 & 0 & 0 & 0 \\
0 & 0 & 0 & 0 & 0 & 0 & 0 & 0 & 0 & 0 & 0 & 0 & 0 & 0 & 0 & 0 \\
0 & 0 & 0 & \alpha_{17} & 0 & 0 & 0 & 0 & 0 & 0 & 0 & 0 & 0 & 0 & 0 & 0 \\
0 & 0 & 0 & \alpha_{18} & 0 & 0 & 0 & 0 & 0 & 0 & 0 & 0 & 0 & 0 & 0 & 0 \\
0 & 0 & 0 & -\alpha_{17} & 0 & 0 & 0 & 0 & 0 & 0 & 0 & 0 & 0 & 0 & 0 & 0 \\
0 & 0 & 0 & -\alpha_{18} & 0 & 0 & 0 & 0 & 0 & 0 & 0 & 0 & 0 & 0 & 0 & 0 \\
0 & 0 & 0 & 0 & \alpha_{19} & 0 & 0 & 0 & 0 & 0 & 0 & 0 & 0 & 0 & 0 & 0 \\
0 & 0 & 0 & 0 & \alpha_{19} & \alpha_{20} & 0 & 0 & 0 & 0 & 0 & 0 & 0 & 0 & 0 & 0
\end{array}\right), \tag{119}
$$

Box I.

(159) can be simplified to:

$$
\boldsymbol{J} = \left(\begin{array}{c|c}
\boldsymbol{0}_{(n-m-l)} & \boldsymbol{I}_{(n-m-l)} \\
\hline
\left.\dfrac{\partial\left(\boldsymbol{f} - \boldsymbol{m}\ddot{\boldsymbol{x}}_{ai}^{0}\right)}{\partial \boldsymbol{x}_{ai}}\right|_0 & \boldsymbol{m}_0^{-1} \left.\dfrac{\partial \boldsymbol{f}}{\partial \dot{\boldsymbol{x}}_{ai}}\right|_0
\end{array}\right)
= \left(\begin{array}{c|c}
\boldsymbol{0}_{(n-m-l)} & \boldsymbol{I}_{(n-m-l)} \\
\hline
\boldsymbol{m}_0^{-1}\left(\boldsymbol{R}_0 \bar{\bar{\boldsymbol{V}}}_0 + \boldsymbol{S}_0\right) \boldsymbol{E}_{ai} & \boldsymbol{m}_0^{-1} \boldsymbol{R}_0 \boldsymbol{T}_0
\end{array}\right). \tag{120}
$$

In the bicycle example, Eq. (120) leads to:

$$
\boldsymbol{J} = \left(\begin{array}{ccc|ccc}
0 & 0 & 0 & 1 & 0 & 0 \\
0 & 0 & 0 & 0 & 1 & 0 \\
0 & 0 & 0 & 0 & 0 & 1 \\
\hline
0 & 0 & 0 & 0 & 0 & 0 \\
0 & \alpha_1 & \alpha_2 + \alpha_3\, v^2 & 0 & \alpha_4\, v & \alpha_5\, v \\
0 & \alpha_6 & \alpha_7 + \alpha_8\, v^2 & 0 & \alpha_9\, v & \alpha_{10}\, v
\end{array}\right). \tag{121}
$$

In the linear stability analysis of the bicycle performed by Escalona et al. [25], it is expressly mentioned that the dependent coordinates of Eq. (118) can be considered as null in the linearization, and therefore they can be ignored. This is demonstrated by obtaining the null submatrix in the block associated with the dependent coordinates, as shown in Eq. (119). The linearization approaches by Cuadrado et al. [15,16] and González et al. [7] described in Section 3.3, which do not include the blocks associated with the dependent coordinates, also lead to the Jacobian matrix of Eq. (121). Despite the reduction of the Jacobian matrix of Eq. (119) to Eq. (121), all the relevant stability information is retained. The same velocity continuation diagram of Fig. 2(b) is obtained. The Jacobian matrix in Eq. (119) is $(2n - m - l) \times (2n - m - l) = 16 \times 16$, while the Jacobian matrix (121) is $(2\,(n - m - l)) \times (2\,(n - m - l)) = 6 \times 6$, leading to the elimination of the ten spurious null eigenvalues obtained with Eq. (119).

Note that the fourth row of the Jacobian matrix of Eq. (121) is null. This row corresponds to the equation of the bicycle's forward motion, $\ddot{\tilde{x}}_b = 0$, which is decoupled from the others. Therefore, the Jacobian matrix (121) can be further reduced. The fifth and sixth rows of Eq. (121) correspond to the linearized lean and steer equations, which are equivalent to the linearized lean and steer equations derived by Meijaard et al. [14]:

$$
\ddot{\tilde{\phi}} = \alpha_1 \tilde{\phi} + \left(\alpha_2 + \alpha_3\, v^2\right) \tilde{\delta} + \alpha_4\, v \dot{\tilde{\phi}} + \alpha_5\, v \dot{\tilde{\delta}}, \tag{122}
$$

$$
\ddot{\tilde{\delta}} = \alpha_6 \tilde{\phi} + \left(\alpha_7 + \alpha_8\, v^2\right) \tilde{\delta} + \alpha_9\, v \dot{\tilde{\phi}} + \alpha_{10}\, v \dot{\tilde{\delta}}. \tag{123}
$$

Eqs. (122)–(123) contain all the information regarding the linear stability of the lateral motion of the bicycle.

Nevertheless, the dependent coordinates cannot generally be ignored. Consider now the following coordinate partition:

$$
\begin{aligned}
\tilde{\boldsymbol{x}}_{ai} &= \begin{pmatrix} \tilde{x}_b & \tilde{\psi}_b & \tilde{\phi}_b \end{pmatrix}^{\mathrm{T}}, \\
\tilde{\boldsymbol{x}}_{dd} &= \begin{pmatrix} \tilde{y}_b & \tilde{z}_b & \tilde{\theta}_b & \tilde{\delta} & \tilde{\theta}_R & \tilde{\theta}_F & \tilde{\xi}_R & \tilde{\xi}_F & \tilde{\eta}_R & \tilde{\eta}_F \end{pmatrix}^{\mathrm{T}},
\end{aligned} \tag{124}
$$

where the forward motion, the yaw and lean angles are selected as independent coordinates. The coordinate partition of Eq. (124) is also possible, since the submatrix $\boldsymbol{D}_{dd}(\boldsymbol{x})$ in Eq. (12) is non-singular. The Jacobian matrices of Eqs. (153) and (159), using the coordinate partition in Eq. (124), are given by equation in Box II.

In Eq. (125), the coefficients β_k, with $k = 1 \ldots 21$, are functions of the geometric and dynamic parameters of the bicycle. Despite a different coordinate partition to that of Eq. (118) is used, the Jacobian matrix (125) yields the same velocity continuation diagram of Fig. 2(b). Moreover, as in Eq. (119), ten spurious null eigenvalues are obtained.

The following question is now posed: can the Jacobian matrix of Eq. (125) be reduced by eliminating the blocks associated with the dependent coordinates? Note that, in this case, this block is a non-null submatrix, highlighted with red in Eq. (125). If the derivatives with respect to the dependent coordinates are ignored in Eq. (125), the following reduced Jacobian matrix is obtained:

$$
\boldsymbol{J} = \left(\begin{array}{ccc|ccc}
0 & 0 & 0 & 1 & 0 & 0 \\
0 & 0 & 0 & 0 & 1 & 0 \\
0 & 0 & 0 & 0 & 0 & 1 \\
\hline
0 & 0 & 0 & 0 & 0 & 0 \\
0 & 0 & \beta_1 & 0 & \beta_2\, v & \beta_3\, v \\
0 & 0 & \beta_6 & 0 & \beta_7\, v & \beta_8\, v
\end{array}\right). \tag{126}
$$

The resulting velocity continuation diagram associated with the Jacobian matrix of Eq. (126) does not correspond to that of Fig. 2(b), obtaining completely incorrect results. Due to the symmetry of the bicycle system, the selection of independent coordinates in Eq. (118) allowed obtaining the correct linearized equations of motion despite eliminating the dependent coordinates. Nevertheless, with the coordinate partition of Eq. (124), the dependent coordinates cannot be ignored and they are required in the computation of the exact linearized equations of motion. Therefore, the Jacobian matrix (125) cannot be reduced to Eq. (126).

Group 4: the use of the approaches described in Section 3.4 allows the elimination of m dependent coordinates. In the particular case of the bicycle multibody model, $m = 6$. This is accomplished by using Eq. (109), which makes use of the linearized holonomic constraints

$$
\boldsymbol{J} = \left(\begin{array}{ccc|ccc|ccc|c|ccc|ccc}
0 & 0 & 0 & 1 & 0 & 0 & 0 & 0 & 0 & 0 & 0 & 0 & 0 & 0 & 0 & 0 \\
0 & 0 & 0 & 0 & 1 & 0 & 0 & 0 & 0 & 0 & 0 & 0 & 0 & 0 & 0 & 0 \\
0 & 0 & 0 & 0 & 0 & 1 & 0 & 0 & 0 & 0 & 0 & 0 & 0 & 0 & 0 & 0 \\
\hline
0 & 0 & 0 & 0 & 0 & 0 & 0 & 0 & 0 & 0 & 0 & 0 & 0 & 0 & 0 & 0 \\
0 & 0 & \beta_1 & 0 & \beta_2\, v & \beta_3\, v & 0 & 0 & 0 & \beta_4 + \beta_5 v^2 & 0 & 0 & 0 & 0 & 0 & 0 \\
0 & 0 & \beta_6 & 0 & \beta_7\, v & \beta_8\, v & 0 & 0 & 0 & \beta_9 + \beta_{10} v^2 & 0 & 0 & 0 & 0 & 0 & 0 \\
\hline
0 & \beta_{11} v & 0 & 0 & \beta_{12} & \beta_{13} & 0 & 0 & 0 & 0 & 0 & 0 & 0 & 0 & 0 & 0 \\
0 & 0 & 0 & 0 & 0 & 0 & 0 & 0 & 0 & 0 & 0 & 0 & 0 & 0 & 0 & 0 \\
0 & 0 & 0 & 0 & 0 & 0 & 0 & 0 & 0 & 0 & 0 & 0 & 0 & 0 & 0 & 0 \\
0 & 0 & 0 & 0 & \beta_{14} & 0 & 0 & 0 & 0 & \beta_{15} v & 0 & 0 & 0 & 0 & 0 & 0 \\
0 & 0 & 0 & \beta_{16} & 0 & 0 & 0 & 0 & 0 & 0 & 0 & 0 & 0 & 0 & 0 & 0 \\
0 & 0 & 0 & \beta_{17} & 0 & 0 & 0 & 0 & 0 & 0 & 0 & 0 & 0 & 0 & 0 & 0 \\
0 & 0 & 0 & -\beta_{16} & 0 & 0 & 0 & 0 & 0 & 0 & 0 & 0 & 0 & 0 & 0 & 0 \\
0 & 0 & 0 & -\beta_{17} & 0 & 0 & 0 & 0 & 0 & 0 & 0 & 0 & 0 & 0 & 0 & 0 \\
0 & 0 & 0 & 0 & 0 & \beta_{18} & 0 & 0 & 0 & 0 & 0 & 0 & 0 & 0 & 0 & 0 \\
0 & 0 & 0 & 0 & \beta_{19} & \beta_{20} & 0 & 0 & 0 & \beta_{21}\, v & 0 & 0 & 0 & 0 & 0 & 0
\end{array}\right). \tag{125}
$$

Box II.

to express the variations of the dependent coordinates $\tilde{\boldsymbol{x}}_d$ in terms of $\tilde{\boldsymbol{x}}_{ai}$ and $\tilde{\boldsymbol{x}}_{ad}$. Choosing as independent coordinates the forward motion, the lean and steering angles, a possible coordinate partition, based on Eq. (18), is:

$$
\begin{aligned}
\tilde{\boldsymbol{x}}_{ai} &= \begin{pmatrix} \tilde{x}_b & \tilde{\phi}_b & \tilde{\delta} \end{pmatrix}^{\mathrm{T}}, \\
\tilde{\boldsymbol{x}}_{ad} &= \begin{pmatrix} \tilde{y}_b & \tilde{\psi}_b & \tilde{\theta}_R & \tilde{\theta}_F \end{pmatrix}^{\mathrm{T}}, \\
\tilde{\boldsymbol{x}}_{d} &= \begin{pmatrix} \tilde{z}_b & \tilde{\theta}_b & \tilde{\xi}_R & \tilde{\xi}_F & \tilde{\eta}_R & \tilde{\eta}_F \end{pmatrix}^{\mathrm{T}}.
\end{aligned} \tag{127}
$$

The use of Eq. (170), considering the coordinate partition in Eq. (127), leads to the following Jacobian matrix:

$$
\boldsymbol{J} = \left(\begin{array}{ccc|ccc|cccc}
0 & 0 & 0 & 1 & 0 & 0 & 0 & 0 & 0 & 0 \\
0 & 0 & 0 & 0 & 1 & 0 & 0 & 0 & 0 & 0 \\
0 & 0 & 0 & 0 & 0 & 1 & 0 & 0 & 0 & 0 \\
\hline
0 & 0 & 0 & 0 & 0 & 0 & 0 & 0 & 0 & 0 \\
0 & \gamma_1 & \gamma_2 + \gamma_3\, v^2 & 0 & \gamma_4\, v & \gamma_5\, v & 0 & 0 & 0 & 0 \\
0 & \gamma_6 & \gamma_7 + \gamma_8\, v^2 & 0 & \gamma_9\, v & \gamma_{10}\, v & 0 & 0 & 0 & 0 \\
\hline
0 & 0 & \gamma_{11}\, v & 0 & \gamma_{12} & \gamma_{13} & 0 & \gamma_{14} v & 0 & 0 \\
0 & 0 & \gamma_{15} v & 0 & 0 & \gamma_{16} & 0 & 0 & 0 & 0 \\
0 & 0 & 0 & \gamma_{17} & 0 & 0 & 0 & 0 & 0 & 0 \\
0 & 0 & 0 & \gamma_{18} & 0 & 0 & 0 & 0 & 0 & 0
\end{array}\right), \tag{128}
$$

where γ_k, with $k = 1 \ldots 18$, are functions of the geometric and dynamic parameters of the bicycle. The eigenvalues associated with Eq. (128) correspond to those of the velocity continuation diagram of Fig. 2(b). In this case, the Jacobian matrix (128) is $(2\,(n-m)-l)\times(2\,(n-m)-l) = 10\times10$, and the number of spurious null eigenvalues is reduced from ten to four, associated with the $l = 4$ linearized nonholonomic constraints.

In Eq. (128), the dependent coordinates $\tilde{\boldsymbol{x}}_d$ of Eq. (127) are eliminated with the use of the linearized holonomic constraints. Moreover, the block associated with the coordinates $\tilde{\boldsymbol{x}}_{ad}$ is a null submatrix, highlighted with color red. This block corresponds to $\boldsymbol{J}_{23}$ in the Jacobian matrices of Eqs. (112) and (170), obtained with the symbolic and counterpart approaches presented in [13]. As in Eq. (119), the Jacobian matrix (128) can be reduced to Eq. (121). This reduced Jacobian matrix leads to the correct eigenvalues of the system.

Nevertheless, as in the approaches of Group 3, the reduction ignoring the coordinates $\tilde{\boldsymbol{x}}_{ad}$ cannot always be done. Consider the following coordinate partition:

$$
\begin{aligned}
\tilde{\boldsymbol{x}}_{ai} &= \begin{pmatrix} \tilde{x}_b & \tilde{\psi}_b & \tilde{\phi}_b \end{pmatrix}^{\mathrm{T}}, \\
\tilde{\boldsymbol{x}}_{ad} &= \begin{pmatrix} \tilde{y}_b & \tilde{\delta} & \tilde{\theta}_R & \tilde{\theta}_F \end{pmatrix}^{\mathrm{T}}, \\
\tilde{\boldsymbol{x}}_{d} &= \begin{pmatrix} \tilde{z}_b & \tilde{\theta}_b & \tilde{\xi}_R & \tilde{\xi}_F & \tilde{\eta}_R & \tilde{\eta}_F \end{pmatrix}^{\mathrm{T}},
\end{aligned} \tag{129}
$$

where the forward motion, the yaw and lean angles are selected as independent coordinates. In this case, the Jacobian matrices of Eqs. (112) and (170) are given by:

$$
\boldsymbol{J} = \left(\begin{array}{ccc|ccc|cccc}
0 & 0 & 0 & 1 & 0 & 0 & 0 & 0 & 0 & 0 \\
0 & 0 & 0 & 0 & 1 & 0 & 0 & 0 & 0 & 0 \\
0 & 0 & 0 & 0 & 0 & 1 & 0 & 0 & 0 & 0 \\
\hline
0 & 0 & 0 & 0 & 0 & 0 & 0 & 0 & 0 & 0 \\
0 & 0 & \delta_1 & 0 & \delta_2\, v & \delta_3\, v & 0 & \delta_4 + \delta_5 v^2 & 0 & 0 \\
0 & 0 & \delta_6 & 0 & \delta_7\, v & \delta_8\, v & 0 & \delta_9 + \delta_{10} v^2 & 0 & 0 \\
\hline
0 & \delta_{11} v & 0 & 0 & \delta_{12} & \delta_{13} & 0 & 0 & 0 & 0 \\
0 & 0 & 0 & 0 & \delta_{14} & 0 & 0 & \delta_{15} v & 0 & 0 \\
0 & 0 & 0 & \delta_{16} & 0 & 0 & 0 & 0 & 0 & 0 \\
0 & 0 & 0 & \delta_{17} & 0 & 0 & 0 & 0 & 0 & 0
\end{array}\right). \tag{130}
$$

In Eq. (130), the coefficients δ_k, with $k = 1 \ldots 17$, are functions of the geometric and dynamic parameters of the bicycle. In contrast to Eq. (128), the block associated with the coordinates $\tilde{\boldsymbol{x}}_{ad}$ is a non-null submatrix, highlighted with color red in Eq. (130). The Jacobian matrix (130) leads to the same velocity continuation diagram of Fig. 2(b). However, eliminating this block results in completely incorrect results, as in Eq. (126).

This analysis clearly shows that the dependent coordinates need to be carefully handled in the linearization of the equations of motion of constrained multibody systems. If one of the approaches of Group 1 (Subsect. 3.1) and Group 2 (Subsect. 3.2) is used, no distinction between coordinates is considered and the handling of the dependent coordinates does not require further attention. As a drawback, a bulky Jacobian matrix is obtained. In the approaches of Group 3 (Subsect. 3.3), it is shown that, in general, the dependent coordinates cannot be ignored. In the particular case of the bicycle, the selection of the forward motion, the lean and steering angles as independent coordinates allows for ignoring the derivatives with respect to the dependent coordinates, due to the symmetry of the bicycle system along the steady forward motion. However, a different admissible choice of independent coordinates, as the one shown in Eq. (124), inhibits ignoring the derivatives with respect to the dependent coordinates. Lastly, by using the linearization approaches of Group 4 (Subsect. 3.4), the linearized holonomic constraints can be used to eliminate m dependent coordinates. In the particular case of a multibody system with only holonomic constraints, this allows obtaining the linearized equations

Table 1
Comparison of the results obtained in the linear stability analysis of the bicycle multibody model with toroidal wheels, using the linearization approaches illustrated in the overview of Section 3. Since the bicycle model of this study is an example of nonholonomic multibody system, those procedures that explicitly include nonholonomic constraints have been employed. The procedures illustrated in the overview that do not appear in Table 1, although they can be extended to the nonholonomic case, are developed by their authors in the respective works for multibody systems with holonomic constraints. Among the procedures of Group 1, the linearization approach by Pappalardo et al. [8,9] is used. In Group 2, the symbolic linearization of the index-1 DAE, the first numerical procedure by Agúndez et al. [13] and the approach by Van Khang et al. [12] are considered. Next, among the procedures of Group 3, the first symbolic and second numerical approaches by Agúndez et al. [13] have been employed. Lastly, the second symbolic and third numerical procedures by Agúndez et al. [13], which belong to Group 4, have been used. The size of the Jacobian matrix, the number of spurious eigenvalues and the eigenvalues of the spectrum, obtained by using the linearization approaches of each group, are detailed for the bicycle case.

Bicycle: $n = 13$, $m = 6$, $l = 4$	Group 1 Pappalardo et al. [8,9]	Group 2 Symbolic linearization index-1 DAE system First numerical approach by Agúndez et al. [13] Van Khang et al. [12]	Group 3 First symbolic approach Second numerical approach by Agúndez et al. [13]	Group 4 Second symbolic approach Third numerical approach by Agúndez et al. [13]
Size of Jacobian matrix	$2(n+m+l)$ 46×46	2n 26×26	2n-m-l 16×16	$2(n-m)-l$ 10×10
Number of spurious eigenvalues	$4(m+l)$ 40	$2(m+l)$ 20	m+l 10	l 4
Eigenvalues of the spectrum	$2(n-m-l)$ 6	$2(n-m-l)$ 6	$2(n-m-l)$ 6	$2(n-m-l)$ 6

of motion only in terms of the $n-m$ independent coordinates and their time derivatives, eliminating the dependent ones. Nevertheless, in a multibody system with nonholonomic constraints as the bicycle, the linearized nonholonomic constraints cannot be used to express the remaining dependent coordinates as a function of the independent ones, since these constraints are non-integrable. The approaches of Group 4 lead to the maximum possible reduction of the linearized equations of motion. As shown with the bicycle, in some multibody systems with a low number of coordinates and in presence of symmetries, a selection of independent coordinates can be intuitively found to ignore the dependent coordinates. However, this is not the usual case, and the systematic linearization of constrained multibody systems requires considering these dependent coordinates.

A comparison of the results obtained in the linear stability analysis of the bicycle multibody model with toroidal wheels, using the linearization approaches illustrated in the overview of Section 3, is shown in Table 1. Given that the bicycle model of this study is a nonholonomic multibody system, those procedures that explicitly include nonholonomic constraints have been employed. The procedures included in the overview of Section 3 that do not appear in Table 1, although they can be extended to the nonholonomic case, are developed by their authors in the respective works for multibody systems with holonomic constraints.

Among the procedures of Group 1, the linearization approach by Pappalardo et al. [8,9] is used. For a multibody system modeled with n generalized coordinates, m holonomic constraints and l nonholonomic constraints, this approach leads to a Jacobian matrix of size $2(n+m+l) \times 2(n+m+l)$, which in the case of the bicycle results in $2(n+m+l) = 46$ eigenvalues. A total of $4(m+l) = 40$ spurious eigenvalues are obtained, and the remaining six constitute the spectrum of the problem. Concerning Group 2, the symbolic linearization of the index-1 DAE, the first numerical procedure by Agúndez et al. [13] and the approach by Van Khang et al. [12] are considered. The use of these procedures result in a Jacobian matrix of size $2n \times 2n$, which leads to $2n = 26$ eigenvalues in the bicycle case, with $2(m+l) = 20$ spurious eigenvalues. A further reduction of the Jacobian matrix is obtained with the first symbolic and second numerical approaches by Agúndez et al. [13], which belong to Group 3. In this case, the Jacobian matrix is $(2n-m-l)\times(2n-m-l)$, resulting in $2n-m-l = 16$ eigenvalues for the bicycle. The number of spurious eigenvalues is reduced from $2(m+l) = 20$ with the approaches of Group 2 to $m+l = 10$, and the remaining six eigenvalues constitute the spectrum of the problem. Lastly, the procedures of Group 4 lead to the maximum possible reduction of the linearized equations, obtaining a $(2(n-m)-l)\times(2(n-m)-l)$ Jacobian matrix. A total of $2(n-m)-l = 10$ eigenvalues are obtained in the linear stability analysis of the bicycle, where $l = 4$ are spurious eigenvalues (associated with the $l = 4$ linearized nonholonomic constraints) and six correspond to the spectrum of the problem. Table 1 summarizes these results. In terms of computational efficiency, the use of numerical procedures is highly recommended over the symbolic approaches. The linearization approaches based on symbolic computation involve the calculation of inverse matrices, the computation of the time derivative of inverse matrices and the partial derivatives of cumbersome mathematical expressions, being their use generally not possible for moderately complex multibody systems as the bicycle with toroidal wheels. Nevertheless, these obstacles are avoided by using the numerical linearization approaches. Their power allow for generating the Jacobian matrix of the multibody system under study in terms of the geometric and dynamic parameters. In the particular case of the bicycle with toroidal wheels, the average time of computation of the Jacobian matrices of Eqs. (55), (159) and (170), derived from the first, second and third numerical approaches by Agúndez et al. [13], respectively, was of 0.02 s. The assessment was carried out by using a computer HP with Intel(R) Core(TM) i7-6700HQ 2.6 GHz and 12 GB of RAM.

4.2. Case study 2: the role of the dependent coordinates in the e-scooter stability analysis

The role of the dependent coordinates in the linearization is also illustrated with the e-scooter model described in Appendix C and the use of the approaches of Group 4, which allow for eliminating m dependent coordinates. In the particular case of the e-scooter multibody model, $m = 6$. This is accomplished by using Eq. (109), which makes use of the linearized holonomic constraints to express the variations of the dependent coordinates $\tilde{\boldsymbol{x}}_d$ in terms of $\tilde{\boldsymbol{x}}_{ai}$ and $\tilde{\boldsymbol{x}}_{ad}$. A possible coordinate partition, based on Eq. (18), is:

$$\begin{aligned}
\tilde{\boldsymbol{x}}_{ai} &= \begin{pmatrix} \tilde{x}_b & \tilde{\phi}_b & \tilde{\delta} & \tilde{s} & \tilde{\theta}_{S_R} \end{pmatrix}^{\mathrm{T}}, \\
\tilde{\boldsymbol{x}}_{ad} &= \begin{pmatrix} \tilde{y}_b & \tilde{\psi}_b & \tilde{\theta}_R & \tilde{\theta}_F \end{pmatrix}^{\mathrm{T}}, \\
\tilde{\boldsymbol{x}}_{d} &= \begin{pmatrix} \tilde{z}_b & \tilde{\theta}_b & \tilde{\xi}_R & \tilde{\xi}_F & \tilde{\eta}_R & \tilde{\eta}_F \end{pmatrix}^{\mathrm{T}},
\end{aligned} \tag{131}$$

where $n-m-l = 5$ independent coordinates (the same number as degrees of freedom of the system) are considered. The forward motion, the lean and steering angles, and the coordinates s and θ_{S_R}, associated with the front and rear suspensions, respectively, have been selected as independent coordinates.

$$
\boldsymbol{J} = \left(\begin{array}{ccccc|ccccc|cccc}
0 & 0 & 0 & 0 & 0 & 1 & 0 & 0 & 0 & 0 & 0 & 0 & 0 & 0 \\
0 & 0 & 0 & 0 & 0 & 0 & 1 & 0 & 0 & 0 & 0 & 0 & 0 & 0 \\
0 & 0 & 0 & 0 & 0 & 0 & 0 & 1 & 0 & 0 & 0 & 0 & 0 & 0 \\
0 & 0 & 0 & 0 & 0 & 0 & 0 & 0 & 1 & 0 & 0 & 0 & 0 & 0 \\
0 & 0 & 0 & 0 & 0 & 0 & 0 & 0 & 0 & 1 & 0 & 0 & 0 & 0 \\
\hline
0 & 0 & 0 & \chi_1 & \chi_2 & 0 & 0 & 0 & \chi_3 & \chi_4 & 0 & 0 & 0 & 0 \\
0 & \chi_5 & \chi_6 + \chi_7\, v^2 & 0 & 0 & 0 & \chi_8\, v & \chi_9\, v & 0 & 0 & 0 & 0 & 0 & 0 \\
0 & \chi_{10} & \chi_{11} + \chi_{12}\, v^2 & 0 & 0 & 0 & \chi_{13}\, v & \chi_{14}\, v & 0 & 0 & 0 & 0 & 0 & 0 \\
0 & 0 & 0 & \chi_{15} & \chi_{16} & 0 & 0 & 0 & \chi_{17} & \chi_{18} & 0 & 0 & 0 & 0 \\
0 & 0 & 0 & \chi_{19} & \chi_{20} & 0 & 0 & 0 & \chi_{21} & \chi_{22} & 0 & 0 & 0 & 0 \\
\hline
0 & 0 & \chi_{23}\, v & 0 & 0 & 0 & \chi_{24} & \chi_{25} & 0 & 0 & 0 & v & 0 & 0 \\
0 & 0 & \chi_{26}\, v & 0 & 0 & 0 & 0 & \chi_{27} & 0 & 0 & 0 & 0 & 0 & 0 \\
0 & 0 & 0 & 0 & 0 & \chi_{28} & 0 & 0 & \chi_{29} & \chi_{30} & 0 & 0 & 0 & 0 \\
0 & 0 & 0 & 0 & 0 & \chi_{31} & 0 & 0 & \chi_{32} & \chi_{33} & 0 & 0 & 0 & 0
\end{array}\right), \tag{132}
$$

Box III.

The Jacobian matrices of Eqs. (112) and (170), considering the coordinate partition of Eq. (131) and particularized for the steady forward motion of the e-scooter, are given by equation in Box III. The coefficients χ_k, with $k = 1 \dots 33$, are functions of the geometric and dynamic parameters of the e-scooter. The computation of the eigenvalues associated with the Jacobian matrix of Eq. (132) yields the results of Fig. 3. Moreover, four spurious null eigenvalues are obtained, associated with the $l = 4$ linearized nonholonomic constraints. Figs. 3 (a) and (b) show the evolution of the real part of the eigenvalues of the e-scooter with the forward velocity v, in the hoop-shaped and toroidal wheels scenarios, respectively. Both the rigid case and the case with suspensions are shown in Figs. 3 (a) and (b). It can be seen that, in contrast to the bicycle benchmark, and for the numerical values of the e-scooter benchmark parameters provided in García-Vallejo et al. [87], no self-stability velocity range exists for the uncontrolled e-scooter, obtaining eigenvalues with positive real parts in all the cases. The most important aspect to highlight due to the introduction of the suspensions is the appearance of two complex conjugate pairs of eigenvalues. The numerical values of the real parts of these pairs are independent of the forward speed and are highly dependent on the damping coefficients d_r and d_f. Moreover, the imaginary parts of these complex conjugate pairs are highly dependent on the stiffness constants of the rear and front suspensions, k_r and k_f. Concerning the remaining eigenvalues, it can be seen that the suspensions scenarios (labeled as 'Susp' in Fig. 3) do not lead to major differences with respect to the rigid scenario (labeled as 'Rigid' in Figs. 3).

The block associated with the coordinates $\tilde{\boldsymbol{x}}_{ad}$ in Eq. (132) is a null submatrix, highlighted with color red. This block corresponds to $\boldsymbol{J}_{23}$ in the Jacobian matrices of Eqs. (112) and (170), obtained with the second symbolic and third numerical approaches presented in [13]. In this scenario, the Jacobian matrix of Eq. (132) can be simplified to:

$$
\boldsymbol{J} = \left(\begin{array}{ccccc|ccccc}
0 & 0 & 0 & 0 & 0 & 1 & 0 & 0 & 0 & 0 \\
0 & 0 & 0 & 0 & 0 & 0 & 1 & 0 & 0 & 0 \\
0 & 0 & 0 & 0 & 0 & 0 & 0 & 1 & 0 & 0 \\
0 & 0 & 0 & 0 & 0 & 0 & 0 & 0 & 1 & 0 \\
0 & 0 & 0 & 0 & 0 & 0 & 0 & 0 & 0 & 1 \\
\hline
0 & 0 & 0 & \chi_1 & \chi_2 & 0 & 0 & 0 & \chi_3 & \chi_4 \\
0 & \chi_5 & \chi_6 + \chi_7\, v^2 & 0 & 0 & 0 & \chi_8\, v & \chi_9\, v & 0 & 0 \\
0 & \chi_{10} & \chi_{11} + \chi_{12}\, v^2 & 0 & 0 & 0 & \chi_{13}\, v & \chi_{14}\, v & 0 & 0 \\
0 & 0 & 0 & \chi_{15} & \chi_{16} & 0 & 0 & 0 & \chi_{17} & \chi_{18} \\
0 & 0 & 0 & \chi_{19} & \chi_{20} & 0 & 0 & 0 & \chi_{21} & \chi_{22}
\end{array}\right). \tag{133}
$$

This reduced Jacobian matrix leads to the eigenvalues shown in Fig. 3, eliminating the $l = 4$ spurious null eigenvalues obtained with the Jacobian matrix of Eq. (132).

Nevertheless, as shown with the bicycle, the reduction of the Jacobian matrix (132) ignoring the coordinates $\tilde{\boldsymbol{x}}_{ad}$ cannot always be done. Consider now the following coordinate partition:

$$
\begin{aligned}
\tilde{\boldsymbol{x}}_{ai} &= \begin{pmatrix} \tilde{x}_b & \tilde{\psi}_b & \tilde{\phi}_b & \tilde{s} & \tilde{\theta}_{S_R} \end{pmatrix}^{\mathrm{T}}, \\
\tilde{\boldsymbol{x}}_{ad} &= \begin{pmatrix} \tilde{y}_b & \tilde{\delta} & \tilde{\theta}_R & \tilde{\theta}_F \end{pmatrix}^{\mathrm{T}}, \\
\tilde{\boldsymbol{x}}_{d} &= \begin{pmatrix} \tilde{z}_b & \tilde{\theta}_b & \tilde{\xi}_R & \tilde{\xi}_F & \tilde{\eta}_R & \tilde{\eta}_F \end{pmatrix}^{\mathrm{T}},
\end{aligned} \tag{134}
$$

where the forward motion, the yaw and lean angles, and the coordinates s and θ_{S_R}, associated with the front and rear suspensions, respectively, have been chosen as independent coordinates. In this case, the Jacobian matrices of Eqs. (112) and (170) are given by equation in Box IV, where the coefficients ϱ_k, with $k = 1 \dots 33$, are functions of the geometric and dynamic parameters of the e-scooter. In contrast to Eq. (132), the block associated with the coordinates $\tilde{\boldsymbol{x}}_{ad}$ in Eq. (135) is a non-null submatrix, highlighted with color red. The Jacobian matrix (135) leads to the velocity continuation diagrams shown in Fig. 3. However, eliminating this block results in completely incorrect results. As was also demonstrated with the bicycle, in the particular case of the e-scooter, a convenient selection of independent coordinates can be intuitively found to ignore the dependent coordinates. This can be done in some multibody systems with a low number of coordinates and in the presence of symmetries. Nevertheless, as shown with the coordinate partition of Eq. (134) and the Jacobian matrix of Eq. (135), this is not the usual case, and the systematic linearization of constrained multibody systems requires considering these dependent coordinates.

Lastly, as it was done with the bicycle, a comparison of the results obtained in the linear stability analysis of the e-scooter multibody model with rear and front suspensions, using the linearization approaches illustrated in the overview of Section 3, is shown in Table 2. Given that the e-scooter model of this study is a nonholonomic multibody system, those procedures that explicitly include nonholonomic constraints have been employed. The procedures included in the overview of Section 3 that do not appear in Table 2, although they can be extended to the nonholonomic case, are developed by their authors in the respective works for multibody systems with holonomic constraints. As can be seen in Table 2, the linearization procedures of Group 4 lead to the maximum possible reduction of the linearized equations, obtaining a $(2(n-m)-l) \times (2(n-m)-l)$ Jacobian matrix. A total of $2(n-m)-l = 14$ eigenvalues are obtained in the linear stability analysis of the e-scooter, where $l = 4$ are spurious eigenvalues (associated with the $l = 4$ linearized nonholonomic constraints) and ten correspond to the spectrum of the problem.

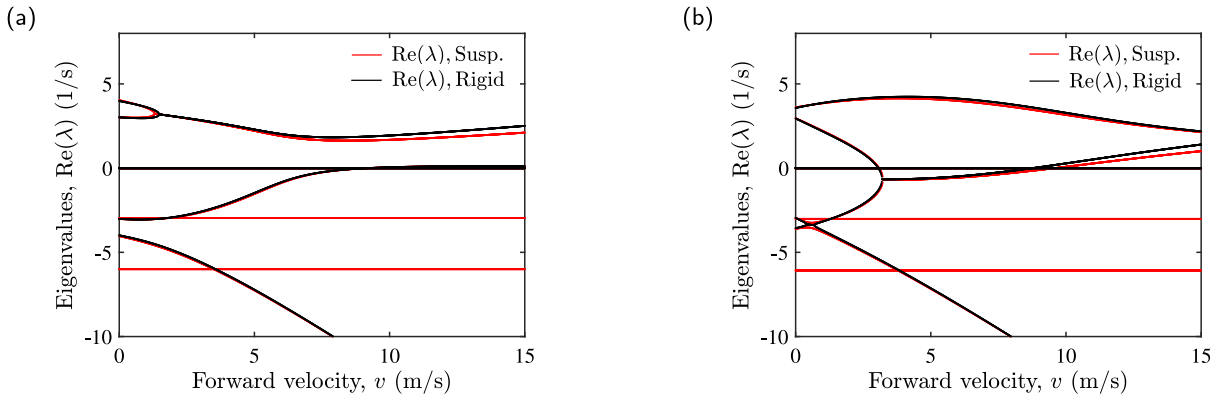

Fig. 3. Linearized speed analysis of the e-scooter multibody model with rear and front suspensions. The evolution of the real part of the eigenvalues ($\mathrm{Re}(\lambda)$) with the forward velocity v is shown in the hoop-shaped scenario (a), corresponding to $\mu_i = 0$, and the toroidal wheels scenarios (b), with $\mu_i = 0.3$. While the uncontrolled bicycle benchmark is asymptotically stable between the weave speed v_w and the capsize speed v_c, the uncontrolled e-scooter is completely unstable in the velocity range $0 < v < 15$ m/s. Both the rigid case and the case with suspensions are shown. It can be seen that the suspensions scenarios (labeled as 'Susp') do not lead to major differences with respect to the rigid scenario (labeled as 'Rigid').

$$
\boldsymbol{J} = \left(\begin{array}{ccccc|ccccc|cccc}
0 & 0 & 0 & 0 & 0 & 1 & 0 & 0 & 0 & 0 & 0 & 0 & 0 & 0 \\
0 & 0 & 0 & 0 & 0 & 0 & 1 & 0 & 0 & 0 & 0 & 0 & 0 & 0 \\
0 & 0 & 0 & 0 & 0 & 0 & 0 & 1 & 0 & 0 & 0 & 0 & 0 & 0 \\
0 & 0 & 0 & 0 & 0 & 0 & 0 & 0 & 1 & 0 & 0 & 0 & 0 & 0 \\
0 & 0 & 0 & 0 & 0 & 0 & 0 & 0 & 0 & 1 & 0 & 0 & 0 & 0 \\
\hline
0 & 0 & 0 & \varrho_1 & \varrho_2 & 0 & 0 & 0 & \varrho_3 & \varrho_4 & 0 & 0 & 0 & 0 \\
0 & 0 & \varrho_5 & 0 & 0 & 0 & \varrho_6\, v & \varrho_7\, v & 0 & 0 & 0 & \varrho_8 + \varrho_9\, v^2 & 0 & 0 \\
0 & 0 & \varrho_{10} & 0 & 0 & 0 & \varrho_{11}\, v & \varrho_{12}\, v & 0 & 0 & 0 & \varrho_{13} + \varrho_{14}\, v^2 & 0 & 0 \\
0 & 0 & 0 & \varrho_{15} & \varrho_{16} & 0 & 0 & 0 & \varrho_{17} & \varrho_{18} & 0 & 0 & 0 & 0 \\
0 & 0 & 0 & \varrho_{19} & \varrho_{20} & 0 & 0 & 0 & \varrho_{21} & \varrho_{22} & 0 & 0 & 0 & 0 \\
\hline
0 & \varrho_{23}\, v & 0 & 0 & 0 & 0 & \varrho_{24} & \varrho_{25} & 0 & 0 & 0 & 0 & 0 & 0 \\
0 & 0 & 0 & 0 & 0 & 0 & \varrho_{26} & 0 & 0 & 0 & 0 & \varrho_{27}\, v & 0 & 0 \\
0 & 0 & 0 & 0 & 0 & \varrho_{28} & 0 & 0 & \varrho_{29} & \varrho_{30} & 0 & 0 & 0 & 0 \\
0 & 0 & 0 & 0 & 0 & \varrho_{31} & 0 & 0 & \varrho_{32} & \varrho_{33} & 0 & 0 & 0 & 0
\end{array}\right), \tag{135}
$$

Box IV.

Table 2
Comparison of the results obtained in the linear stability analysis of the e-scooter multibody model with rear and front suspensions, using the linearization approaches illustrated in the overview of Section 3. As in the bicycle case, the e-scooter model of this work is an example of nonholonomic multibody system, and therefore those procedures that explicitly include nonholonomic constraints have been employed. The procedures illustrated in the overview that do not appear in Table 1, although they can be extended to the nonholonomic case, are developed by their authors in the respective works for holonomic multibody systems. The size of the Jacobian matrix, the number of spurious eigenvalues and the eigenvalues of the spectrum, obtained by using the linearization approaches of each group, are shown for the e-scooter case.

E-scooter: $n = 15$, $m = 6$, $l = 4$	Group 1 Pappalardo et al. [8,9]	Group 2 Symbolic linearization index-1 DAE system First numerical approach by Agúndez et al. [13] Van Khang et al. [12]	Group 3 First symbolic approach Second numerical approach by Agúndez et al. [13]	Group 4 Second symbolic approach Third numerical approach by Agúndez et al. [13]
Size of Jacobian matrix	$2(n+m+l)$ 50×50	2n 30×30	2n-m-l 20×20	$2(n-m)-l$ 14×14
Number of spurious eigenvalues	$4(m+l)$ 40	$2(m+l)$ 20	m+l 10	l 4
Eigenvalues of the spectrum	$2(n-m-l)$ 10	$2(n-m-l)$ 10	$2(n-m-l)$ 10	$2(n-m-l)$ 10

5. Conclusions

In this work, the handling of the dependent coordinates in the linearization of the equations of motion of constrained multibody systems has been clarified. For that purpose, a comprehensive overview of notable linearization approaches for constrained multibody systems with Lagrange multipliers was presented. This overview summarizes the approaches of previous works by using a common notation. The linearization approaches are classified into four groups, according to the initial form of the nonlinear equations of motion and the use of a redundant or a minimal set of coordinates. The first group (presented in Subsect. 3.1) includes approaches that linearize the index-3 DAE system, using a redundant set of coordinates. The second group (Subsect. 3.2) covers procedures based on the linearization of the index-1 DAE system, also considering a redundant set of coordinates. Next, a third group of procedures (Subsect. 3.3) is considered, based on a coordinate partition in terms of independent and dependent coordinates, which lead to a reduced linear ODE system. Finally, a fourth group of approaches, described in Subsect. 3.4, allows for obtaining the linearized equations of motion in ODE form, only expressed in terms of the independent coordinates and their time derivatives, by eliminating the dependent coordinates with the use of the linearized holonomic constraints. The role of the dependent coordinates in each of these procedures was discussed.

The importance of considering the set of dependent coordinates was demonstrated with the linear stability results of a well-acknowledged bicycle benchmark multibody model. To this end, the Jacobian matrices and the evolution of the eigenvalues with the forward speed in the steady forward motion of the bicycle were computed, considering different choices of independent and dependent coordinates. The use of the approaches of Group 1 and Group 2 do not involve risks in the handling of the dependent coordinates, since these approaches make use of an augmented Jacobian matrix with the redundant set of coordinates. Therefore, no distinction between independent and dependent coordinates is considered. In the approaches of Group 3, it was shown that, in the particular case of the bicycle, the selection of the forward motion, the lean and steering angles as independent coordinates allows for ignoring the derivatives with respect to the dependent coordinates in the linearization, due to the symmetry of the bicycle system along the steady forward motion. However, it was shown that, for a different admissible coordinate partition, the dependent coordinates cannot be ignored, leading to incorrect eigenvalues in the linear stability analysis. Lastly, the approaches of Group 4 allow for expressing the dependent coordinates in terms of the independent ones with the linearized holonomic constraints. By doing this, in the particular case of a multibody system with only holonomic constraints, the linearized equations of motion are obtained only in terms of the independent coordinates and their time derivatives, eliminating the dependent ones. Nevertheless, in a nonholonomic multibody system as the bicycle, the linearized nonholonomic constraints cannot be used to express the remaining dependent coordinates as a function of the independent ones, since these constraints are non-integrable. As in the third group, it was shown that, in some multibody systems as the bicycle (with low number of coordinates and in presence of symmetries), one can intuitively find a set of independent coordinates that allows for ignoring the derivatives with respect to the dependent ones. Nevertheless, this is not the general case, and the correct linearization of constrained multibody systems requires considering the dependent coordinates. A comparison between the linearization approaches included in the overview of Section 3 was also performed, showing the size of the Jacobian matrices and the number of spurious eigenvalues obtained for the bicycle case. The computational efficiency of those procedures based on numerical computation was also highlighted.

Lastly, the role of the dependent coordinates was also shown with an e-scooter multibody model with rear and front suspensions and the application of the linearization approaches of Group 4. As in the bicycle case, a convenient coordinate partition that allowed for ignoring the derivatives with respect to the dependent coordinates was found, exploiting the symmetry of the e-scooter along the steady forward motion. However, a different admissible choice of independent coordinates showed that, in general, the derivatives with respect to the dependent coordinates cannot be ignored to correctly compute the linearized equations of motion.

CRediT authorship contribution statement

A.G. Agúndez: Writing – review & editing, Writing – original draft, Visualization, Validation, Supervision, Software, Resources, Project administration, Methodology, Investigation, Funding acquisition, Formal analysis, Data curation, Conceptualization. **D. García-Vallejo:** Writing – review & editing, Writing – original draft, Visualization, Validation, Supervision, Software, Resources, Project administration, Methodology, Investigation, Funding acquisition, Formal analysis, Data curation, Conceptualization. **E. Freire:** Writing – review & editing, Writing – original draft, Visualization, Validation, Supervision, Software, Resources, Project administration, Methodology, Investigation, Funding acquisition, Formal analysis, Data curation, Conceptualization. **A. Mikkola:** Writing – review & editing, Writing – original draft, Visualization, Validation, Supervision, Software, Resources, Project administration, Methodology, Investigation, Funding acquisition, Formal analysis, Data curation, Conceptualization.

Declaration of competing interest

The authors declare that they have no known competing financial interests or personal relationships that could have appeared to influence the work reported in this paper.

Data availability

Data will be made available on request.

Acknowledgments

This work was supported by Grant FPU18/05598 of the Spanish Ministry of Science, Innovation and Universities and project US-1380740 of Consejería de Universidad, Investigación e Innovación, Junta de Andalucía, Spain.

Appendix A. Details of the linearization approaches of Section 3

Procedure by Escalona et al. [5,6] and González et al. [7] (RCS Formulation)

The $(2n+m)\times(2n+m)$ matrices $\boldsymbol{\mathcal{A}}_0$ and $\boldsymbol{\mathcal{B}}_0$ of Eq. (33) are given by (see the equation given in Box V):

These matrices are $(2n+m+l)\times(2n+m+l)$ if the multibody system presents nonholonomic constraints.

Procedure by Pappalardo et al. [8,9]

The $n+m+l$ composite mass, damping and stiffness matrices of Eq. (37), $\bar{\boldsymbol{M}}_0$, $\bar{\boldsymbol{C}}_0$ and $\bar{\boldsymbol{K}}_0$, respectively, are:

$$\bar{\boldsymbol{M}}_0 = \begin{pmatrix} \boldsymbol{M}\left(\boldsymbol{x}^0\right) & \boldsymbol{0}_{n\times(m+l)} \\ \boldsymbol{0}_{(m+l)\times n} & \boldsymbol{0}_{(m+l)} \end{pmatrix},$$

$$\bar{\boldsymbol{C}}_0 = \begin{pmatrix} -\left.\dfrac{\partial \boldsymbol{Q}\left(\boldsymbol{x},\dot{\boldsymbol{x}}\right)}{\partial \dot{\boldsymbol{x}}}\right|_0 & \boldsymbol{0}_{n\times(m+l)} \\ \left.\boldsymbol{E}_{\dot{\boldsymbol{x}}}\right|_0 & \boldsymbol{0}_{(m+l)} \end{pmatrix}, \tag{138}$$

$$\bar{\boldsymbol{K}}_0 = \left(\begin{array}{c|c} -\left.\dfrac{\partial \boldsymbol{Q}\left(\boldsymbol{x},\dot{\boldsymbol{x}}\right)}{\partial \boldsymbol{x}}\right|_0 + \left.\dfrac{\partial\left(\boldsymbol{M}\left(\boldsymbol{x}\right)\ddot{\boldsymbol{x}}^0\right)}{\partial \boldsymbol{x}}\right|_0 + \left.\dfrac{\partial\left(\boldsymbol{D}^{\mathrm{T}}\left(\boldsymbol{x}\right)\boldsymbol{\Lambda}^0\right)}{\partial \boldsymbol{x}}\right|_0 & \boldsymbol{D}^{\mathrm{T}}\left(\boldsymbol{x}^0\right) \\ \hline \left.\boldsymbol{E}_{\boldsymbol{x}}\right|_0 & \boldsymbol{0}_{(m+l)} \end{array}\right).$$

$$\mathcal{A}_0 = \left(\begin{array}{c|c|c} \boldsymbol{I}_n & \boldsymbol{0}_n & \boldsymbol{0}_{n\times m} \\ \hline \boldsymbol{0}_n & \boldsymbol{M}\left(\boldsymbol{x}^0\right) & \boldsymbol{0}_{n\times m} \\ \hline \boldsymbol{0}_{m\times n} & \boldsymbol{0}_{m\times n} & \boldsymbol{0}_m \end{array}\right), \tag{136}$$

$$\mathcal{B}_0 = \left(\begin{array}{c|c|c} \boldsymbol{0}_n & \boldsymbol{I}_n & \boldsymbol{0}_{n\times m} \\ \hline \left.\dfrac{\partial \boldsymbol{Q}\left(\boldsymbol{x},\dot{\boldsymbol{x}}\right)}{\partial \boldsymbol{x}}\right|_0 - \left.\dfrac{\partial\left(\boldsymbol{M}\left(\boldsymbol{x}\right)\ddot{\boldsymbol{x}}^0\right)}{\partial \boldsymbol{x}}\right|_0 - \left.\dfrac{\partial\left(\boldsymbol{C}_{\boldsymbol{x}}^{\mathrm{T}}\left(\boldsymbol{x}\right)\boldsymbol{\Lambda}^0\right)}{\partial \boldsymbol{x}}\right|_0 & \left.\dfrac{\partial \boldsymbol{Q}\left(\boldsymbol{x},\dot{\boldsymbol{x}}\right)}{\partial \dot{\boldsymbol{x}}}\right|_0 & -\boldsymbol{C}_{\boldsymbol{x}}^{\mathrm{T}}\left(\boldsymbol{x}^0\right) \\ \hline -\boldsymbol{C}_{\boldsymbol{x}}\left(\boldsymbol{x}^0\right) & \boldsymbol{0}_{m\times n} & \boldsymbol{0}_m \end{array}\right). \tag{137}$$

Box V.

Matrices $\boldsymbol{C}_0$ and $\boldsymbol{D}_0$ in Eq. (38) are given by:

$$\boldsymbol{C}_0 = \begin{pmatrix} \bar{\boldsymbol{C}}_0 & \bar{\boldsymbol{M}}_0 \\ \bar{\boldsymbol{M}}_0 & \boldsymbol{0}_{(n+m+l)} \end{pmatrix}, \qquad \boldsymbol{D}_0 = \begin{pmatrix} -\bar{\boldsymbol{K}}_0 & \boldsymbol{0}_{(n+m+l)} \\ \boldsymbol{0}_{(n+m+l)} & \bar{\boldsymbol{M}}_0 \end{pmatrix}. \tag{139}$$

Procedure by Negrut et al. [4]

The partial derivatives $\dfrac{\partial \boldsymbol{F}}{\partial \dot{\boldsymbol{x}}_{ai}}$ and $\dfrac{\partial \boldsymbol{F}}{\partial \boldsymbol{x}_{ai}}$ in Eqs. (43) and (44) are computed as:

$$\frac{\partial \boldsymbol{F}}{\partial \dot{\boldsymbol{x}}_{ai}} = \begin{pmatrix} \boldsymbol{M}\left(\boldsymbol{x}\right)\dfrac{\partial \ddot{\boldsymbol{x}}}{\partial \dot{\boldsymbol{x}}_{ai}} + \boldsymbol{C}_{\boldsymbol{x}}^{\mathrm{T}}\left(\boldsymbol{x}\right)\dfrac{\partial \boldsymbol{\Lambda}}{\partial \dot{\boldsymbol{x}}_{ai}} + \boldsymbol{Y}_{\dot{\boldsymbol{x}}}\dfrac{\partial \dot{\boldsymbol{x}}}{\partial \dot{\boldsymbol{x}}_{ai}} + \boldsymbol{Y}_{\boldsymbol{x}}\dfrac{\partial \boldsymbol{x}}{\partial \dot{\boldsymbol{x}}_{ai}} \\ \ddot{\boldsymbol{C}}_{\dot{\boldsymbol{x}}}\dfrac{\partial \ddot{\boldsymbol{x}}}{\partial \dot{\boldsymbol{x}}_{ai}} + \ddot{\boldsymbol{C}}_{\dot{\boldsymbol{x}}}\dfrac{\partial \dot{\boldsymbol{x}}}{\partial \dot{\boldsymbol{x}}_{ai}} + \ddot{\boldsymbol{C}}_{\boldsymbol{x}}\dfrac{\partial \boldsymbol{x}}{\partial \dot{\boldsymbol{x}}_{ai}} \\ \dot{\boldsymbol{C}}_{\dot{\boldsymbol{x}}}\dfrac{\partial \dot{\boldsymbol{x}}}{\partial \dot{\boldsymbol{x}}_{ai}} + \dot{\boldsymbol{C}}_{\boldsymbol{x}}\dfrac{\partial \boldsymbol{x}}{\partial \dot{\boldsymbol{x}}_{ai}} \\ \boldsymbol{C}_{\boldsymbol{x}}\dfrac{\partial \boldsymbol{x}}{\partial \dot{\boldsymbol{x}}_{ai}} \\ \boldsymbol{B}_1\dfrac{\partial \dot{\boldsymbol{x}}}{\partial \dot{\boldsymbol{x}}_{ai}} \\ \boldsymbol{B}_0\dfrac{\partial \boldsymbol{x}}{\partial \dot{\boldsymbol{x}}_{ai}} \end{pmatrix}, \tag{140}$$

$$\frac{\partial \boldsymbol{F}}{\partial \boldsymbol{x}_{ai}} = \begin{pmatrix} \boldsymbol{M}\left(\boldsymbol{x}\right)\dfrac{\partial \ddot{\boldsymbol{x}}}{\partial \boldsymbol{x}_{ai}} + \boldsymbol{C}_{\boldsymbol{x}}^{\mathrm{T}}\left(\boldsymbol{x}\right)\dfrac{\partial \boldsymbol{\Lambda}}{\partial \boldsymbol{x}_{ai}} + \boldsymbol{Y}_{\dot{\boldsymbol{x}}}\dfrac{\partial \dot{\boldsymbol{x}}}{\partial \boldsymbol{x}_{ai}} + \boldsymbol{Y}_{\boldsymbol{x}}\dfrac{\partial \boldsymbol{x}}{\partial \boldsymbol{x}_{ai}} \\ \ddot{\boldsymbol{C}}_{\dot{\boldsymbol{x}}}\dfrac{\partial \ddot{\boldsymbol{x}}}{\partial \boldsymbol{x}_{ai}} + \ddot{\boldsymbol{C}}_{\dot{\boldsymbol{x}}}\dfrac{\partial \dot{\boldsymbol{x}}}{\partial \boldsymbol{x}_{ai}} + \ddot{\boldsymbol{C}}_{\boldsymbol{x}}\dfrac{\partial \boldsymbol{x}}{\partial \boldsymbol{x}_{ai}} \\ \dot{\boldsymbol{C}}_{\dot{\boldsymbol{x}}}\dfrac{\partial \dot{\boldsymbol{x}}}{\partial \boldsymbol{x}_{ai}} + \dot{\boldsymbol{C}}_{\boldsymbol{x}}\dfrac{\partial \boldsymbol{x}}{\partial \boldsymbol{x}_{ai}} \\ \boldsymbol{C}_{\boldsymbol{x}}\dfrac{\partial \boldsymbol{x}}{\partial \boldsymbol{x}_{ai}} \\ \boldsymbol{B}_1\dfrac{\partial \dot{\boldsymbol{x}}}{\partial \boldsymbol{x}_{ai}} \\ \boldsymbol{B}_0\dfrac{\partial \boldsymbol{x}}{\partial \boldsymbol{x}_{ai}} \end{pmatrix}, \tag{141}$$

where $\boldsymbol{Y}_{\dot{\boldsymbol{x}}}$ and $\boldsymbol{Y}_{\boldsymbol{x}}$ are given by:

$$\boldsymbol{Y}_{\dot{\boldsymbol{x}}} = -\frac{\partial \boldsymbol{Q}\left(\boldsymbol{x},\dot{\boldsymbol{x}}\right)}{\partial \dot{\boldsymbol{x}}}, \qquad \boldsymbol{Y}_{\boldsymbol{x}} = \frac{\partial\left(\boldsymbol{M}\left(\boldsymbol{x}\right)\ddot{\boldsymbol{x}} + \boldsymbol{C}_{\boldsymbol{x}}^{\mathrm{T}}\left(\boldsymbol{x}\right)\boldsymbol{\Lambda} - \boldsymbol{Q}\left(\boldsymbol{x},\dot{\boldsymbol{x}}\right)\right)}{\partial \boldsymbol{x}}. \tag{142}$$

The partial derivatives $\dfrac{\partial \boldsymbol{b}}{\partial \dot{\boldsymbol{x}}_{ai}}$ and $\dfrac{\partial \boldsymbol{b}}{\partial \boldsymbol{x}_{ai}}$ are given by:

$$\frac{\partial \boldsymbol{b}}{\partial \dot{\boldsymbol{x}}_{ai}} = \begin{pmatrix} \boldsymbol{0}_{n\times(n-m)} \\ \boldsymbol{0}_{m\times(n-m)} \\ \boldsymbol{0}_{m\times(n-m)} \\ \boldsymbol{0}_{m\times(n-m)} \\ \boldsymbol{I}_{(n-m)} \\ \boldsymbol{0}_{(n-m)} \end{pmatrix}, \quad \frac{\partial \boldsymbol{b}}{\partial \boldsymbol{x}_{ai}} = \begin{pmatrix} \boldsymbol{0}_{n\times(n-m)} \\ \boldsymbol{0}_{m\times(n-m)} \\ \boldsymbol{0}_{m\times(n-m)} \\ \boldsymbol{0}_{m\times(n-m)} \\ \boldsymbol{0}_{(n-m)} \\ \boldsymbol{I}_{(n-m)} \end{pmatrix}. \tag{143}$$

The expressions of $\mathcal{A}_1$, $\boldsymbol{X}_1$ and $\boldsymbol{b}_1$ in Eqs. (45) are:

$$\mathcal{A}_1\left(\boldsymbol{x}\right) = \left(\begin{array}{c|c|c|c} \boldsymbol{M}\left(\boldsymbol{x}\right) & \boldsymbol{C}_{\boldsymbol{x}}^{\mathrm{T}}\left(\boldsymbol{x}\right) & \boldsymbol{Y}_{\dot{\boldsymbol{x}}} & \boldsymbol{Y}_{\boldsymbol{x}} \\ \hline \ddot{\boldsymbol{C}}_{\ddot{\boldsymbol{x}}} & \boldsymbol{0}_m & \ddot{\boldsymbol{C}}_{\dot{\boldsymbol{x}}} & \ddot{\boldsymbol{C}}_{\boldsymbol{x}} \\ \hline \boldsymbol{0}_{m\times n} & \boldsymbol{0}_m & \dot{\boldsymbol{C}}_{\dot{\boldsymbol{x}}} & \dot{\boldsymbol{C}}_{\boldsymbol{x}} \\ \hline \boldsymbol{0}_{m\times n} & \boldsymbol{0}_m & \boldsymbol{0}_{m\times n} & \boldsymbol{C}_{\boldsymbol{x}} \\ \hline \boldsymbol{0}_{(n-m)\times n} & \boldsymbol{0}_{(n-m)\times m} & \boldsymbol{B}_1 & \boldsymbol{0}_{(n-m)\times n} \\ \hline \boldsymbol{0}_{(n-m)\times n} & \boldsymbol{0}_{(n-m)\times m} & \boldsymbol{0}_{(n-m)\times n} & \boldsymbol{B}_0 \end{array}\right), \tag{144}$$

$$\boldsymbol{X}_1 = \begin{pmatrix} \dfrac{\partial \ddot{\boldsymbol{x}}}{\partial \dot{\boldsymbol{x}}_{ai}} & \dfrac{\partial \ddot{\boldsymbol{x}}}{\partial \boldsymbol{x}_{ai}} \\ \dfrac{\partial \boldsymbol{\Lambda}}{\partial \dot{\boldsymbol{x}}_{ai}} & \dfrac{\partial \boldsymbol{\Lambda}}{\partial \boldsymbol{x}_{ai}} \\ \dfrac{\partial \dot{\boldsymbol{x}}}{\partial \dot{\boldsymbol{x}}_{ai}} & \dfrac{\partial \dot{\boldsymbol{x}}}{\partial \boldsymbol{x}_{ai}} \\ \dfrac{\partial \boldsymbol{x}}{\partial \dot{\boldsymbol{x}}_{ai}} & \dfrac{\partial \boldsymbol{x}}{\partial \boldsymbol{x}_{ai}} \end{pmatrix}, \qquad \boldsymbol{b}_1 = \begin{pmatrix} \boldsymbol{0}_{n\times(n-m)} & \boldsymbol{0}_{n\times(n-m)} \\ \boldsymbol{0}_{m\times(n-m)} & \boldsymbol{0}_{m\times(n-m)} \\ \boldsymbol{0}_{m\times(n-m)} & \boldsymbol{0}_{m\times(n-m)} \\ \boldsymbol{0}_{m\times(n-m)} & \boldsymbol{0}_{m\times(n-m)} \\ \boldsymbol{I}_{(n-m)} & \boldsymbol{0}_{(n-m)} \\ \boldsymbol{0}_{(n-m)} & \boldsymbol{I}_{(n-m)} \end{pmatrix}. \tag{145}$$

Procedure by Agúndez et al. [13] (first numerical approach)

Matrices $\bar{\mathcal{A}}_0$ and $\bar{\mathcal{B}}_0$ of Eq. (53) are given by:

$$\bar{\mathcal{A}}_0 = \begin{pmatrix} \boldsymbol{M}\left(\boldsymbol{x}^0\right) & \boldsymbol{D}^{\mathrm{T}}\left(\boldsymbol{x}^0\right) \\ \boldsymbol{D}\left(\boldsymbol{x}^0\right) & \boldsymbol{0} \end{pmatrix}, \tag{146}$$

$$\bar{\mathcal{B}}_0 = \left(\begin{array}{c|c} \left.\dfrac{\partial \boldsymbol{Q}\left(\boldsymbol{x},\dot{\boldsymbol{x}}\right)}{\partial \boldsymbol{x}}\right|_0 - \left.\dfrac{\partial\left(\boldsymbol{M}\left(\boldsymbol{x}\right)\ddot{\boldsymbol{x}}^0\right)}{\partial \boldsymbol{x}}\right|_0 - \left.\dfrac{\partial\left(\boldsymbol{D}^{\mathrm{T}}\left(\boldsymbol{x}\right)\boldsymbol{\Lambda}^0\right)}{\partial \boldsymbol{x}}\right|_0 & \left.\dfrac{\partial \boldsymbol{Q}\left(\boldsymbol{x},\dot{\boldsymbol{x}}\right)}{\partial \dot{\boldsymbol{x}}}\right|_0 \\ \hline \left.\dfrac{\partial \boldsymbol{Q}_d\left(\boldsymbol{x},\dot{\boldsymbol{x}}\right)}{\partial \boldsymbol{x}}\right|_0 - \left.\dfrac{\partial\left(\boldsymbol{D}\left(\boldsymbol{x}\right)\ddot{\boldsymbol{x}}^0\right)}{\partial \boldsymbol{x}}\right|_0 & \left.\dfrac{\partial \boldsymbol{Q}_d\left(\boldsymbol{x},\dot{\boldsymbol{x}}\right)}{\partial \dot{\boldsymbol{x}}}\right|_0 \end{array}\right). \tag{147}$$

Procedure by Van Khang et al. [12]

The $n\times n$ composite mass, damping and stiffness matrices of Eq. (63), $\bar{\boldsymbol{M}}$, $\bar{\boldsymbol{C}}$ and $\bar{\boldsymbol{K}}$, respectively, are:

$$\bar{\boldsymbol{M}} = \begin{pmatrix} \left.\dfrac{\partial \boldsymbol{f}_1}{\partial \ddot{\boldsymbol{x}}}\right|_0 \\ \left.\dfrac{\partial \boldsymbol{f}_2}{\partial \ddot{\boldsymbol{x}}}\right|_0 \end{pmatrix}, \quad \bar{\boldsymbol{C}} = \begin{pmatrix} -\left.\dfrac{\partial \boldsymbol{k}_1}{\partial \dot{\boldsymbol{x}}}\right|_0 \\ -\left.\dfrac{\partial \boldsymbol{k}_2}{\partial \dot{\boldsymbol{x}}}\right|_0 \end{pmatrix}, \quad \bar{\boldsymbol{K}} = \begin{pmatrix} \left.\dfrac{\partial \boldsymbol{f}_1}{\partial \boldsymbol{x}}\right|_0 - \left.\dfrac{\partial \boldsymbol{k}_1}{\partial \boldsymbol{x}}\right|_0 \\ \left.\dfrac{\partial \boldsymbol{f}_2}{\partial \boldsymbol{x}}\right|_0 - \left.\dfrac{\partial \boldsymbol{k}_2}{\partial \boldsymbol{x}}\right|_0 \end{pmatrix}. \tag{148}$$

Combination of Van Khang et al. [12] and Agúndez et al. [13]

The detailed expressions of the $n\times n$ composite mass, damping and stiffness matrices of Eq. (63), $\bar{\boldsymbol{M}}$, $\bar{\boldsymbol{C}}$ and $\bar{\boldsymbol{K}}$, respectively, are given by:

$$\bar{\boldsymbol{M}} = \begin{pmatrix} \boldsymbol{T}_0^{\mathrm{T}}\boldsymbol{M}\left(\boldsymbol{x}^0\right) \\ \boldsymbol{D}\left(\boldsymbol{x}^0\right) \end{pmatrix}, \qquad \bar{\boldsymbol{C}} = \begin{pmatrix} -\boldsymbol{T}_0^{\mathrm{T}}\left.\dfrac{\partial \boldsymbol{Q}}{\partial \dot{\boldsymbol{x}}}\right|_0 \\ -\left.\dfrac{\partial \boldsymbol{Q}_d}{\partial \dot{\boldsymbol{x}}}\right|_0 \end{pmatrix},$$

$$\bar{\boldsymbol{K}} = \begin{pmatrix} \boldsymbol{T}_0^{\mathrm{T}} \left(\left. \frac{\partial \left(\boldsymbol{M}\left(\boldsymbol{x}\right) \ddot{\boldsymbol{x}}^0 \right)}{\partial \boldsymbol{x}} \right|_0 + \left. \frac{\partial \left(\boldsymbol{D}^{\mathrm{T}}\left(\boldsymbol{x}\right) \boldsymbol{\Lambda}^0 \right)}{\partial \boldsymbol{x}} \right|_0 - \left. \frac{\partial \boldsymbol{Q}}{\partial \boldsymbol{x}} \right|_0 \right) \\ \left. \frac{\partial \left(\boldsymbol{D}\left(\boldsymbol{x}\right) \ddot{\boldsymbol{x}}^0 \right)}{\partial \boldsymbol{x}} \right|_0 - \left. \frac{\partial \boldsymbol{Q}_d}{\partial \boldsymbol{x}} \right|_0 \end{pmatrix}. \tag{149}$$

Procedure by González et al. [7] (MCS Formulation)

The partial derivatives $\frac{\partial \boldsymbol{H}_1}{\partial \boldsymbol{x}_{ai}}$, $\frac{\partial \boldsymbol{H}_1}{\partial \dot{\boldsymbol{x}}_{ai}}$ and $\frac{\partial \boldsymbol{H}_1}{\partial \ddot{\boldsymbol{x}}_{ai}}$ in Eq. (75) are:

$$\begin{aligned} \frac{\partial \boldsymbol{H}_1}{\partial \boldsymbol{x}_{ai}} &= \left(\frac{\partial \boldsymbol{T}^{\mathrm{T}}}{\partial \boldsymbol{x}_{ai}} \boldsymbol{M} \boldsymbol{T} + \boldsymbol{T}^{\mathrm{T}} \frac{\partial \boldsymbol{M}}{\partial \boldsymbol{x}_{ai}} \boldsymbol{T} + \boldsymbol{T}^{\mathrm{T}} \boldsymbol{M} \frac{\partial \boldsymbol{T}}{\partial \boldsymbol{x}_{ai}} \right) \ddot{\boldsymbol{x}}_{ai} \\ &\quad - \frac{\partial \boldsymbol{T}^{\mathrm{T}}}{\partial \boldsymbol{x}_{ai}} \left(\boldsymbol{Q} - \boldsymbol{M} \dot{\boldsymbol{T}} \dot{\boldsymbol{x}}_{ai} \right) - \boldsymbol{T}^{\mathrm{T}} \left(\frac{\partial \boldsymbol{Q}}{\partial \boldsymbol{x}_{ai}} - \frac{\partial \boldsymbol{M}}{\partial \boldsymbol{x}_{ai}} \dot{\boldsymbol{T}} \dot{\boldsymbol{x}}_{ai} - \boldsymbol{M} \frac{\partial \left(\dot{\boldsymbol{T}} \dot{\boldsymbol{x}}_{ai} \right)}{\partial \boldsymbol{x}_{ai}} \right), \end{aligned} \tag{150}$$

$$\frac{\partial \boldsymbol{H}_1}{\partial \dot{\boldsymbol{x}}_{ai}} = -\boldsymbol{T}^{\mathrm{T}} \left(\frac{\partial \boldsymbol{Q}}{\partial \dot{\boldsymbol{x}}_{ai}} - \boldsymbol{M} \frac{\partial \left(\dot{\boldsymbol{T}} \dot{\boldsymbol{x}}_{ai} \right)}{\partial \dot{\boldsymbol{x}}_{ai}} \right), \tag{151}$$

$$\frac{\partial \boldsymbol{H}_1}{\partial \ddot{\boldsymbol{x}}_{ai}} = \boldsymbol{T}^{\mathrm{T}} \boldsymbol{M} \boldsymbol{T}. \tag{152}$$

As stated by González et al. [7], the expressions for the numerical evaluation of the partial derivatives of $\boldsymbol{T}$ can be found in [90].

Procedure by Agúndez et al. [13] (first symbolic approach)

The expression of the Jacobian matrix $\boldsymbol{J}$ resulting from the first symbolic approach of Agúndez et al. [13] is:

$$\boldsymbol{J} = \left(\begin{array}{c|c|c} \boldsymbol{0}_{(n-m-l)} & \boldsymbol{I}_{(n-m-l)} & \boldsymbol{0}_{(n-m-l)\times(m+l)} \\ \hline \boldsymbol{m}_0^{-1} \left. \frac{\partial \left(\boldsymbol{f} - \boldsymbol{m} \ddot{\boldsymbol{x}}_{ai}^0 \right)}{\partial \boldsymbol{x}_{ai}} \right|_0 & \boldsymbol{m}_0^{-1} \left. \frac{\partial \boldsymbol{f}}{\partial \dot{\boldsymbol{x}}_{ai}} \right|_0 & \boldsymbol{m}_0^{-1} \left. \frac{\partial \left(\boldsymbol{f} - \boldsymbol{m} \ddot{\boldsymbol{x}}_{ai}^0 \right)}{\partial \boldsymbol{x}_{dd}} \right|_0 \\ \hline \left. \frac{\partial \left(\boldsymbol{H} \ddot{\boldsymbol{x}}_{ai}^0 \right)}{\partial \boldsymbol{x}_{ai}} \right|_0 & \boldsymbol{H}_0 & \left. \frac{\partial \left(\boldsymbol{H} \ddot{\boldsymbol{x}}_{ai}^0 \right)}{\partial \boldsymbol{x}_{dd}} \right|_0 \end{array} \right). \tag{153}$$

Procedure by Agúndez et al. [13] (second numerical approach)

Matrices $\boldsymbol{T}_{dd}\left(\boldsymbol{x}^0\right)$ and $\bar{\boldsymbol{V}}\left(\boldsymbol{x}^0, \dot{\boldsymbol{x}}^0\right)$ in Eq. (81) are given by:

$$\begin{aligned} \boldsymbol{T}_{dd}\left(\boldsymbol{x}^0\right) &= -\left(\boldsymbol{D}_{dd}\left(\boldsymbol{x}^0\right)\right)^{-1} \boldsymbol{D}_{ai}\left(\boldsymbol{x}^0\right), \\ \bar{\boldsymbol{V}}\left(\boldsymbol{x}^0, \dot{\boldsymbol{x}}^0\right) &= -\left(\boldsymbol{D}_{dd}\left(\boldsymbol{x}^0\right)\right)^{-1} \left. \frac{\partial \left(\boldsymbol{D}\left(\boldsymbol{x}\right) \dot{\boldsymbol{x}}^0 \right)}{\partial \boldsymbol{x}} \right|_0. \end{aligned} \tag{154}$$

The expressions of matrices $\bar{\bar{\boldsymbol{V}}}\left(\boldsymbol{x}^0, \dot{\boldsymbol{x}}^0\right)$, $\boldsymbol{U}\left(\boldsymbol{x}^0, \dot{\boldsymbol{x}}^0\right)$ and $\boldsymbol{V}\left(\boldsymbol{x}^0, \dot{\boldsymbol{x}}^0, \ddot{\boldsymbol{x}}^0\right)$ in Eqs. (82) and (83) are:

$$\bar{\bar{\boldsymbol{V}}}\left(\boldsymbol{x}^0, \dot{\boldsymbol{x}}^0\right) = \begin{pmatrix} \boldsymbol{0}_{(n-m-l)\times n} \\ \bar{\boldsymbol{V}}\left(\boldsymbol{x}^0, \dot{\boldsymbol{x}}^0\right) \end{pmatrix}, \tag{155}$$

$$\boldsymbol{U}\left(\boldsymbol{x}^0, \dot{\boldsymbol{x}}^0\right) = \begin{pmatrix} \boldsymbol{0}_{(n-m-l)\times n} \\ \left(\boldsymbol{D}_{dd}\left(\boldsymbol{x}^0\right)\right)^{-1} \left. \frac{\partial \boldsymbol{Q}_d}{\partial \dot{\boldsymbol{x}}} \right|_0 \end{pmatrix}, \tag{156}$$

$$\boldsymbol{V}\left(\boldsymbol{x}^0, \dot{\boldsymbol{x}}^0, \ddot{\boldsymbol{x}}^0\right) = \begin{pmatrix} \boldsymbol{0}_{(n-m-l)\times n} \\ \left(\boldsymbol{D}_{dd}\left(\boldsymbol{x}^0\right)\right)^{-1} \left(\left. \frac{\partial \boldsymbol{Q}_d}{\partial \boldsymbol{x}} \right|_0 - \left. \frac{\partial \left(\boldsymbol{D}\left(\boldsymbol{x}\right) \ddot{\boldsymbol{x}}^0 \right)}{\partial \boldsymbol{x}} \right|_0 \right) \end{pmatrix}. \tag{157}$$

Matrices $\boldsymbol{m}_0$, $\boldsymbol{R}_0$ and $\boldsymbol{S}_0$ in the linearized dynamic Eqs. (86) are computed as follows:

$$\begin{aligned} \boldsymbol{m}_0 &= \boldsymbol{T}_0^{\mathrm{T}} \boldsymbol{M}\left(\boldsymbol{x}^0\right) \boldsymbol{T}_0, \\ \boldsymbol{R}_0 &= \boldsymbol{T}_0^{\mathrm{T}} \left(\left. \frac{\partial \boldsymbol{Q}}{\partial \dot{\boldsymbol{x}}} \right|_0 - \boldsymbol{M}\left(\boldsymbol{x}^0\right) \boldsymbol{U}\left(\boldsymbol{x}^0, \dot{\boldsymbol{x}}^0\right) \right), \\ \boldsymbol{S}_0 &= \boldsymbol{T}_0^{\mathrm{T}} \left(\left. \frac{\partial \boldsymbol{Q}}{\partial \boldsymbol{x}} \right|_0 - \boldsymbol{M}\left(\boldsymbol{x}^0\right) \boldsymbol{V}\left(\boldsymbol{x}^0, \dot{\boldsymbol{x}}^0, \ddot{\boldsymbol{x}}^0\right) - \left. \frac{\partial \left(\boldsymbol{M}\left(\boldsymbol{x}\right) \ddot{\boldsymbol{x}}^0 \right)}{\partial \boldsymbol{x}} \right|_0 - \left. \frac{\partial \left(\boldsymbol{D}^{\mathrm{T}}\left(\boldsymbol{x}\right) \boldsymbol{\Lambda}^0 \right)}{\partial \boldsymbol{x}} \right|_0 \right). \end{aligned} \tag{158}$$

The expression of the Jacobian matrix $\boldsymbol{J}$ resulting from the second numerical approach of Agúndez et al. [13] is:

$$\boldsymbol{J} = \left(\begin{array}{c|c|c} \boldsymbol{0}_{(n-m-l)} & \boldsymbol{I}_{(n-m-l)} & \boldsymbol{0}_{(n-m-l)\times(m+l)} \\ \hline \boldsymbol{m}_0^{-1} \left(\boldsymbol{R}_0 \bar{\bar{\boldsymbol{V}}}_0 + \boldsymbol{S}_0 \right) \boldsymbol{E}_{ai} & \boldsymbol{m}_0^{-1} \boldsymbol{R}_0 \boldsymbol{T}_0 & \boldsymbol{m}_0^{-1} \left(\boldsymbol{R}_0 \bar{\bar{\boldsymbol{V}}}_0 + \boldsymbol{S}_0 \right) \boldsymbol{E}_{dd} \\ \hline \bar{\boldsymbol{V}}_0 \boldsymbol{E}_{ai} & \boldsymbol{T}_{dd}\left(\boldsymbol{x}^0\right) & \bar{\boldsymbol{V}}_0 \boldsymbol{E}_{dd} \end{array} \right). \tag{159}$$

Procedure by Bae et al. [26]

The variational form of the holonomic constraints at position, velocity and acceleration levels, used to obtain a relation between the complete set of variations, $\delta \boldsymbol{X} = \begin{pmatrix} \delta \boldsymbol{x} & \delta \dot{\boldsymbol{x}} & \delta \ddot{\boldsymbol{x}} \end{pmatrix}^{\mathrm{T}}$, and the variations of the independent coordinates $\delta \boldsymbol{X}_{ai} = \begin{pmatrix} \delta \boldsymbol{x}_{ai} & \delta \dot{\boldsymbol{x}}_{ai} & \delta \ddot{\boldsymbol{x}}_{ai} \end{pmatrix}^{\mathrm{T}}$ in Eq. (94), is given by:

$$\boldsymbol{C}_{\boldsymbol{x}} \delta \boldsymbol{x} = \boldsymbol{0}, \tag{160}$$

$$\dot{\boldsymbol{C}}_{\boldsymbol{x}} \delta \boldsymbol{x} + \boldsymbol{C}_{\boldsymbol{x}} \delta \dot{\boldsymbol{x}} = \boldsymbol{0}, \tag{161}$$

$$\ddot{\boldsymbol{C}}_{\boldsymbol{x}} \delta \boldsymbol{x} + 2 \dot{\boldsymbol{C}}_{\boldsymbol{x}} \delta \dot{\boldsymbol{x}} + \boldsymbol{C}_{\boldsymbol{x}} \delta \ddot{\boldsymbol{x}} = \boldsymbol{0}. \tag{162}$$

The expressions of matrices $\mathcal{N}$ and $\mathcal{M}$ in Eq. (94) are:

$$\mathcal{N} = \left(\begin{array}{c|c|c} \boldsymbol{C}_{\boldsymbol{x}} & \boldsymbol{0}_{m\times n} & \boldsymbol{0}_{m\times n} \\ \hline \dot{\boldsymbol{C}}_{\boldsymbol{x}} & \boldsymbol{C}_{\boldsymbol{x}} & \boldsymbol{0}_{m\times n} \\ \hline \ddot{\boldsymbol{C}}_{\boldsymbol{x}} & 2\dot{\boldsymbol{C}}_{\boldsymbol{x}} & \boldsymbol{C}_{\boldsymbol{x}} \\ \hline \boldsymbol{B}_0 & \boldsymbol{0}_{(n-m)\times n} & \boldsymbol{0}_{(n-m)\times n} \\ \hline \boldsymbol{0}_{(n-m)\times n} & \boldsymbol{B}_1 & \boldsymbol{0}_{(n-m)\times n} \\ \hline \boldsymbol{0}_{(n-m)\times n} & \boldsymbol{0}_{(n-m)\times n} & \boldsymbol{B}_2 \end{array} \right), \tag{163}$$

$$\mathcal{M} = \left(\begin{array}{c|c|c} \boldsymbol{0}_{3m\times(n-m)} & \boldsymbol{0}_{3m\times(n-m)} & \boldsymbol{0}_{3m\times(n-m)} \\ \hline \boldsymbol{I}_{(n-m)} & \boldsymbol{0}_{(n-m)} & \boldsymbol{0}_{(n-m)} \\ \hline \boldsymbol{0}_{(n-m)} & \boldsymbol{I}_{(n-m)} & \boldsymbol{0}_{(n-m)} \\ \hline \boldsymbol{0}_{(n-m)} & \boldsymbol{0}_{(n-m)} & \boldsymbol{I}_{(n-m)} \end{array} \right). \tag{164}$$

In Eq. (163), $\boldsymbol{B}_0$, $\boldsymbol{B}_1$ and $\boldsymbol{B}_2$ are $(n-m)\times n$ Boolean matrices. Note that the matrices $\boldsymbol{B}_0$ and $\boldsymbol{B}_1$ were already used in the linearization procedure of Negrut et al. [4].

Procedure by Cossalter et al. [27]

Matrix $\boldsymbol{K}_\phi$ in Eq. (96) is defined by Cossalter et al. [27] as:

$$\boldsymbol{K}_\phi = \sum_{k=1}^{n-m} \Lambda_k^0 \boldsymbol{H}_k, \tag{165}$$

where $\boldsymbol{H}_k$ is the Hessian of kth constraint and Λ_k^0 is the Lagrange multiplier associated with this constraint.

Procedure by Agúndez et al. [13] (second symbolic approach)

The blocks $\boldsymbol{J}_{21}$ and $\boldsymbol{J}_{22}$ of the Jacobian matrix (111) are given by:

$$\begin{aligned} \boldsymbol{J}_{21} &= \boldsymbol{m}_0^{-1} \left(\left. \frac{\partial \left(\boldsymbol{f} - \boldsymbol{m} \ddot{\boldsymbol{x}}_{ai}^0 \right)}{\partial \boldsymbol{x}_{ai}} - \frac{\partial \left(\boldsymbol{f} - \boldsymbol{m} \ddot{\boldsymbol{x}}_{ai}^0 \right)}{\partial \boldsymbol{x}_d} \left(\frac{\partial \boldsymbol{C}}{\partial \boldsymbol{x}_d} \right)^{-1} \frac{\partial \boldsymbol{C}}{\partial \boldsymbol{x}_{ai}} \right) \right|_0, \\ \boldsymbol{J}_{22} &= \boldsymbol{m}_0^{-1} \left. \frac{\partial \boldsymbol{f}}{\partial \dot{\boldsymbol{x}}_{ai}} \right|_0. \end{aligned} \tag{166}$$

The linearized equations of motion of a multibody system with nonholonomic constraints, using the second symbolic approach, are:

$$\begin{aligned} \boldsymbol{m}_0 \ddot{\tilde{\boldsymbol{x}}}_{ai} &= \left(\frac{\partial \left(\boldsymbol{f} - \boldsymbol{m} \ddot{\boldsymbol{x}}_{ai}^0 \right)}{\partial \boldsymbol{x}_{ai}} - \frac{\partial \left(\boldsymbol{f} - \boldsymbol{m} \ddot{\boldsymbol{x}}_{ai}^0 \right)}{\partial \boldsymbol{x}_d} \left(\frac{\partial \boldsymbol{C}}{\partial \boldsymbol{x}_d} \right)^{-1} \frac{\partial \boldsymbol{C}}{\partial \boldsymbol{x}_{ai}} \right) \Bigg|_0 \tilde{\boldsymbol{x}}_{ai} \\ &\quad + \left(\frac{\partial \left(\boldsymbol{f} - \boldsymbol{m} \ddot{\boldsymbol{x}}_{ai}^0 \right)}{\partial \boldsymbol{x}_{ad}} - \frac{\partial \left(\boldsymbol{f} - \boldsymbol{m} \ddot{\boldsymbol{x}}_{ai}^0 \right)}{\partial \boldsymbol{x}_d} \left(\frac{\partial \boldsymbol{C}}{\partial \boldsymbol{x}_d} \right)^{-1} \frac{\partial \boldsymbol{C}}{\partial \boldsymbol{x}_{ad}} \right) \Bigg|_0 \tilde{\boldsymbol{x}}_{ad} + \left. \frac{\partial \boldsymbol{f}}{\partial \dot{\boldsymbol{x}}_{ai}} \right|_0 \dot{\tilde{\boldsymbol{x}}}_{ai}, \\ \dot{\tilde{\boldsymbol{x}}}_{ad} &= \boldsymbol{G}_0 \dot{\tilde{\boldsymbol{x}}}_{ai} + \left(\frac{\partial \left(\boldsymbol{G} \dot{\boldsymbol{x}}_{ai}^0 \right)}{\partial \boldsymbol{x}_{ai}} - \frac{\partial \left(\boldsymbol{G} \dot{\boldsymbol{x}}_{ai}^0 \right)}{\partial \boldsymbol{x}_d} \left(\frac{\partial \boldsymbol{C}}{\partial \boldsymbol{x}_d} \right)^{-1} \frac{\partial \boldsymbol{C}}{\partial \boldsymbol{x}_{ai}} \right) \Bigg|_0 \tilde{\boldsymbol{x}}_{ai} \\ &\quad + \left(\frac{\partial \left(\boldsymbol{G} \dot{\boldsymbol{x}}_{ai}^0 \right)}{\partial \boldsymbol{x}_{ad}} - \frac{\partial \left(\boldsymbol{G} \dot{\boldsymbol{x}}_{ai}^0 \right)}{\partial \boldsymbol{x}_d} \left(\frac{\partial \boldsymbol{C}}{\partial \boldsymbol{x}_d} \right)^{-1} \frac{\partial \boldsymbol{C}}{\partial \boldsymbol{x}_{ad}} \right) \Bigg|_0 \tilde{\boldsymbol{x}}_{ad}, \end{aligned} \tag{167}$$

where $\boldsymbol{G}_0 = \boldsymbol{G}\left(\boldsymbol{x}_{ai}^0, \boldsymbol{x}_{ad}^0, \boldsymbol{x}_d^0\right)$.

The detailed expressions of the blocks of the Jacobian matrix (112) are as follows:

$$
\begin{aligned}
\boldsymbol{J}_{21} &= \boldsymbol{m}_0^{-1}\left(\frac{\partial\left(\boldsymbol{f}-\boldsymbol{m}\ddot{\boldsymbol{x}}_{ai}^0\right)}{\partial \boldsymbol{x}_{ai}} - \frac{\partial\left(\boldsymbol{f}-\boldsymbol{m}\ddot{\boldsymbol{x}}_{ai}^0\right)}{\partial \boldsymbol{x}_d}\left(\frac{\partial \boldsymbol{C}}{\partial \boldsymbol{x}_d}\right)^{-1}\frac{\partial \boldsymbol{C}}{\partial \boldsymbol{x}_{ai}}\right)\Bigg|_0,\\
\boldsymbol{J}_{22} &= \boldsymbol{m}_0^{-1}\left.\frac{\partial \boldsymbol{f}}{\partial \dot{\boldsymbol{x}}_{ai}}\right|_0,\\
\boldsymbol{J}_{23} &= \boldsymbol{m}_0^{-1}\left(\frac{\partial\left(\boldsymbol{f}-\boldsymbol{m}\ddot{\boldsymbol{x}}_{ai}^0\right)}{\partial \boldsymbol{x}_{ad}} - \frac{\partial\left(\boldsymbol{f}-\boldsymbol{m}\ddot{\boldsymbol{x}}_{ai}^0\right)}{\partial \boldsymbol{x}_d}\left(\frac{\partial \boldsymbol{C}}{\partial \boldsymbol{x}_d}\right)^{-1}\frac{\partial \boldsymbol{C}}{\partial \boldsymbol{x}_{ad}}\right)\Bigg|_0,\\
\boldsymbol{J}_{31} &= \left(\frac{\partial\left(\boldsymbol{G}\dot{\boldsymbol{x}}_{ai}^0\right)}{\partial \boldsymbol{x}_{ai}} - \frac{\partial\left(\boldsymbol{G}\dot{\boldsymbol{x}}_{ai}^0\right)}{\partial \boldsymbol{x}_d}\left(\frac{\partial \boldsymbol{C}}{\partial \boldsymbol{x}_d}\right)^{-1}\frac{\partial \boldsymbol{C}}{\partial \boldsymbol{x}_{ai}}\right)\Bigg|_0,\\
\boldsymbol{J}_{32} &= \boldsymbol{G}_0,\\
\boldsymbol{J}_{33} &= \left(\frac{\partial\left(\boldsymbol{G}\dot{\boldsymbol{x}}_{ai}^0\right)}{\partial \boldsymbol{x}_{ad}} - \frac{\partial\left(\boldsymbol{G}\dot{\boldsymbol{x}}_{ai}^0\right)}{\partial \boldsymbol{x}_d}\left(\frac{\partial \boldsymbol{C}}{\partial \boldsymbol{x}_d}\right)^{-1}\frac{\partial \boldsymbol{C}}{\partial \boldsymbol{x}_{ad}}\right)\Bigg|_0.
\end{aligned}
\tag{168}
$$

Procedure by Agúndez et al. [13] (third numerical approach)

In the particular case of a holonomic multibody system, the Jacobian matrix $\boldsymbol{J}$ is:

$$
\boldsymbol{J} = \left(\begin{array}{c|c} \boldsymbol{0}_{(n-m)} & \boldsymbol{I}_{(n-m)} \\ \hline \boldsymbol{m}_0^{-1}\left(\boldsymbol{R}_0\bar{\boldsymbol{V}}_0 + \boldsymbol{S}_0\right)\boldsymbol{V}_{h,ai} & \boldsymbol{m}_0^{-1}\boldsymbol{R}_0\boldsymbol{T}_0 \end{array}\right). \tag{169}
$$

For a multibody system with holonomic and nonholonomic constraints, the Jacobian matrix $\boldsymbol{J}$ is given by:

$$
\boldsymbol{J} = \left(\begin{array}{c|c|c} \boldsymbol{0}_{(n-m-l)} & \boldsymbol{I}_{(n-m-l)} & \boldsymbol{0}_{(n-m-l)\times l} \\ \hline \boldsymbol{m}_0^{-1}\left(\boldsymbol{R}_0\bar{\boldsymbol{V}}_0 + \boldsymbol{S}_0\right)\boldsymbol{V}_{h,ai}\left(\boldsymbol{x}^0\right) & \boldsymbol{m}_0^{-1}\boldsymbol{R}_0\boldsymbol{T}_0 & \boldsymbol{m}_0^{-1}\left(\boldsymbol{R}_0\bar{\boldsymbol{V}}_0 + \boldsymbol{S}_0\right)\boldsymbol{V}_{h,ad}\left(\boldsymbol{x}^0\right) \\ \hline \boldsymbol{V}_{nh,ai}\left(\boldsymbol{x}^0, \dot{\boldsymbol{x}}^0\right) & \boldsymbol{U}_{nh,ai}\left(\boldsymbol{x}^0\right) & \boldsymbol{V}_{nh,ad}\left(\boldsymbol{x}^0, \dot{\boldsymbol{x}}^0\right) \end{array}\right). \tag{170}
$$

Appendix B. Description of the bicycle multibody model

The bicycle multibody model presents five rigid bodies: the inertial frame is designated as body 1; the rear and front wheels, modeled as tori rolling without slipping, are bodies R and F, respectively; the rear body and frame assembly, including the rider, is body B; and the front handlebar is represented by H. The centres of mass G_j, with $j = \{B, H, R, F\}$, correspond to the origins of the body frames. The $n \times 1$ vector of coordinates $\boldsymbol{x} \in \mathbb{R}^n$ is given by:

$$
\boldsymbol{x} = \begin{pmatrix} x_b & y_b & z_b & \psi_b & \phi_b & \theta_b & \delta & \theta_R & \theta_F & \xi_R & \xi_F & \eta_R & \eta_F \end{pmatrix}^{\mathrm{T}}. \tag{171}
$$

The coordinates x_b, y_b and z_b locate G_B; ψ_b, ϕ_b and θ_b are the yaw, lean and pitch angles, which allow orientating body B in space; the steering angle δ represents the rotation of the handlebar with respect to body B; θ_R and θ_F correspond to the rotations of the rear and front wheels with respect to bodies B and H, respectively; and ξ_R, ξ_F, η_R, η_F are angular coordinates, used to describe the toroidal geometry of the wheels. The set of generalized coordinates of the multibody system and the body reference frames are shown in Fig. 4.

The major and minor radii of the toroidal wheel are ρ_i and a_i, respectively, with $i = \{R, F\}$. The geometry of the wheel is completely described by the torus aspect ratio $\mu_i = \frac{a_i}{\rho_i}$. Note that the hoop-shaped wheel case of the bicycle benchmark [14] is also captured with this model, and is obtained by degenerating the tori for $\mu_i = 0$. Fig. 5(a) shows a three-dimensional view of the toroidal wheel, with the angular coordinates ξ_i and η_i, the local reference frames and the middle plane of the torus, denoted as π_m. A cross-section of the toroidal wheel, showing the major and minor radii of the torus, ρ_i and a_i, is depicted in Fig. 5(b).

The set of holonomic constraints arise from the contact of the bicycle wheels with the ground:

$$
\boldsymbol{C}(\boldsymbol{x}) = \begin{pmatrix} r_{P_Z} & r_{Q_Z} & \boldsymbol{n}\cdot\boldsymbol{t}_{L_R} & \boldsymbol{n}\cdot\boldsymbol{t}_{T_R} & \boldsymbol{n}\cdot\boldsymbol{t}_{L_F} & \boldsymbol{n}\cdot\boldsymbol{t}_{T_F} \end{pmatrix}^{\mathrm{T}} = \boldsymbol{0}, \tag{172}
$$

where r_{P_Z} and r_{Q_Z} are the Z-components of the position vectors $\boldsymbol{r}_P$ and $\boldsymbol{r}_Q$ of the contact points P and Q; $\boldsymbol{t}_{L_i}$ and $\boldsymbol{t}_{T_i}$ are the longitudinal and transversal tangent vectors to the contact points; and $\boldsymbol{n}$ is the normal vector to the ground surface. These vectors are given by:

$$
\begin{aligned}
\boldsymbol{r}_P &= \boldsymbol{r}_{G_R} + \boldsymbol{R}_R\bar{\boldsymbol{r}}_{G_RP}^R, & \boldsymbol{r}_Q &= \boldsymbol{r}_{G_F} + \boldsymbol{R}_F\bar{\boldsymbol{r}}_{G_FQ}^F,\\
\boldsymbol{t}_{L_R} &= \boldsymbol{R}_R\frac{\partial\bar{\boldsymbol{r}}_{G_RP}^R}{\partial\xi_R}, & \boldsymbol{t}_{T_R} &= \boldsymbol{R}_R\frac{\partial\bar{\boldsymbol{r}}_{G_RP}^R}{\partial\eta_R},\\
\boldsymbol{t}_{L_F} &= \boldsymbol{R}_F\frac{\partial\bar{\boldsymbol{r}}_{G_FQ}^F}{\partial\xi_F}, & \boldsymbol{t}_{T_F} &= \boldsymbol{R}_F\frac{\partial\bar{\boldsymbol{r}}_{G_FQ}^F}{\partial\eta_F}.
\end{aligned}
\tag{173}
$$

In Eqs. (173), $\boldsymbol{R}_R$ and $\boldsymbol{R}_F$ are the orientation matrices of bodies R and F, respectively. Moreover, $\bar{\boldsymbol{r}}_{G_RP}^R$ and $\bar{\boldsymbol{r}}_{G_FQ}^F$ are vectors, expressed in the local reference frames of bodies R and F, respectively, computed as follows:

$$
\begin{aligned}
\bar{\boldsymbol{r}}_{G_RP}^R &= \boldsymbol{R}_{\xi_R}\left(\boldsymbol{\rho}_R + \boldsymbol{R}_{\eta_R}\boldsymbol{r}_R\right), & \bar{\boldsymbol{r}}_{G_FQ}^F &= \boldsymbol{R}_{\xi_F}\left(\boldsymbol{\rho}_F + \boldsymbol{R}_{\eta_F}\boldsymbol{r}_F\right),\\
\boldsymbol{\rho}_R &= \begin{pmatrix} \rho_R & 0 & 0 \end{pmatrix}^{\mathrm{T}}, & \boldsymbol{\rho}_F &= \begin{pmatrix} \rho_F & 0 & 0 \end{pmatrix}^{\mathrm{T}},\\
\boldsymbol{r}_R &= \begin{pmatrix} a_R & 0 & 0 \end{pmatrix}^{\mathrm{T}}, & \boldsymbol{r}_F &= \begin{pmatrix} a_F & 0 & 0 \end{pmatrix}^{\mathrm{T}},
\end{aligned}
\tag{174}
$$

where $\boldsymbol{R}_{\xi_i}$ and $\boldsymbol{R}_{\eta_i}$ are rotation matrices, associated with the coordinates ξ_i and η_i.

The wheels are assumed to roll without slipping, leading to the following nonholonomic constraints:

$$
\boldsymbol{C}_{nh}(\boldsymbol{x}, \dot{\boldsymbol{x}}) = \begin{pmatrix} v_{P_x} & v_{P_y} & v_{Q_x} & v_{Q_y} \end{pmatrix}^{\mathrm{T}} = \boldsymbol{0}. \tag{175}
$$

In Eq. (175), $\boldsymbol{v}_P$ and $\boldsymbol{v}_Q$ are the velocity of the contact points P and Q, respectively, computed as follows:

$$
\boldsymbol{v}_P = \boldsymbol{v}_{G_R} + \boldsymbol{R}_R\left(\bar{\boldsymbol{\omega}}_R \times \bar{\boldsymbol{r}}_{G_RP}^R\right), \qquad \boldsymbol{v}_Q = \boldsymbol{v}_{G_F} + \boldsymbol{R}_F\left(\bar{\boldsymbol{\omega}}_F \times \bar{\boldsymbol{r}}_{G_FQ}^F\right), \tag{176}
$$

where $\boldsymbol{v}_{G_R}$ and $\boldsymbol{v}_{G_F}$ are the absolute velocities of G_R and G_F, and $\bar{\boldsymbol{\omega}}_R$ and $\bar{\boldsymbol{\omega}}_F$ are the angular velocities of the rear and front wheels, respectively, expressed in the body reference frames.

Therefore, $n = 13$, $m = 6$ and $l = 4$ in the bicycle multibody model. The equations of motion of the bicycle constitute an index-3 DAE system, given by the dynamic Eqs. (1) (derived as explained in Schiehlen [91]), the holonomic constraints (172) and the nonholonomic constraints (175):

$$
\begin{aligned}
&\boldsymbol{M}(\boldsymbol{x})\ddot{\boldsymbol{x}} + \boldsymbol{D}^{\mathrm{T}}(\boldsymbol{x})\boldsymbol{\Lambda} = \boldsymbol{Q}(\boldsymbol{x}, \dot{\boldsymbol{x}}),\\
&\boldsymbol{C}(\boldsymbol{x}) = \boldsymbol{0},\\
&\boldsymbol{C}_{nh}(\boldsymbol{x}, \dot{\boldsymbol{x}}) = \boldsymbol{B}(\boldsymbol{x})\dot{\boldsymbol{x}} = \boldsymbol{0}.
\end{aligned}
\tag{177}
$$

The steady forward motion of the uncontrolled bicycle is given by:

$$
\boldsymbol{x}^0 = \begin{pmatrix} x_b^0 & y_b^0 & z_b^0 & \psi_b^0 & \phi_b^0 & \theta_b^0 & \delta^0 & \theta_R^0 & \theta_F^0 & \xi_R^0 & \xi_F^0 & \eta_R^0 & \eta_F^0 \end{pmatrix}^{\mathrm{T}}, \tag{178}
$$

with

$$
\begin{aligned}
x_b^0 &= vt, & \psi_b^0 &= 0,\\
y_b^0 &= 0, & \phi_b^0 &= 0,\\
z_b^0 &= z_B, & \theta_b^0 &= 0,\\
\delta^0 &= 0, & \theta_R^0 &= \frac{v}{R_R}t,\\
\theta_F^0 &= \frac{v}{R_F}t, & \xi_R^0 &= \frac{\pi}{2} - \theta_R^0,\\
\xi_F^0 &= \nu + \frac{\pi}{2} - \theta_F^0, & \eta_R^0 &= 0,\\
\eta_F^0 &= 0.
\end{aligned}
\tag{179}
$$

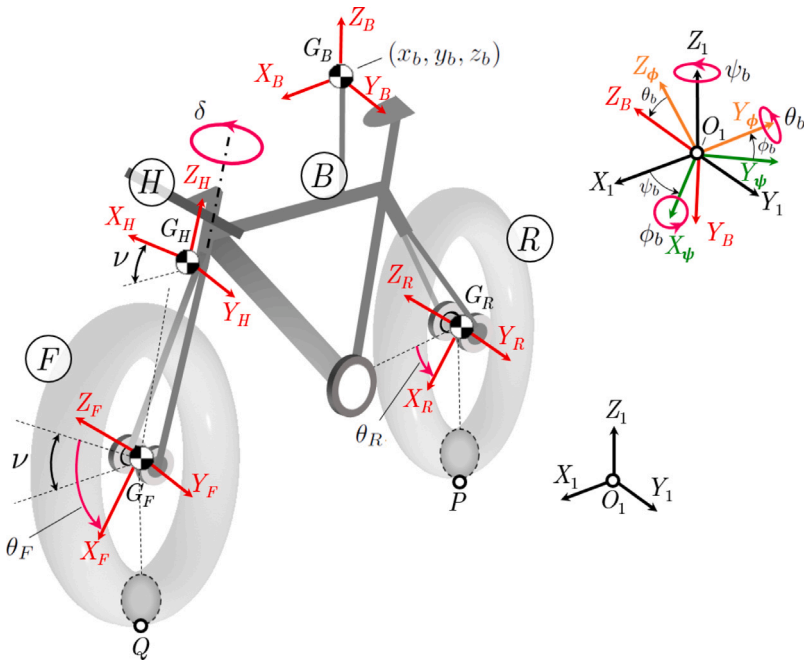

Fig. 4. Multibody model of the bicycle with toroidal wheels. The global reference frame is designated as body 1, with origin O_1; the rear body and frame assembly, including the rider, is body B; the front handlebar is body H; and the rear and front wheels, modeled as tori rolling without slipping, are bodies R and F, respectively. The generalized coordinates of the multibody system, presented in Eq. (171), are shown, except for the angular coordinates ξ_R, ξ_F, η_R and η_F, which are shown in detail in Fig. 5. The body reference frames, whose origins are the centres of mass G_j, with $j = \{B, H, R, F\}$, are depicted. The geometric and dynamic parameters of the model are those of the bicycle benchmark of Meijaard et al. [14].

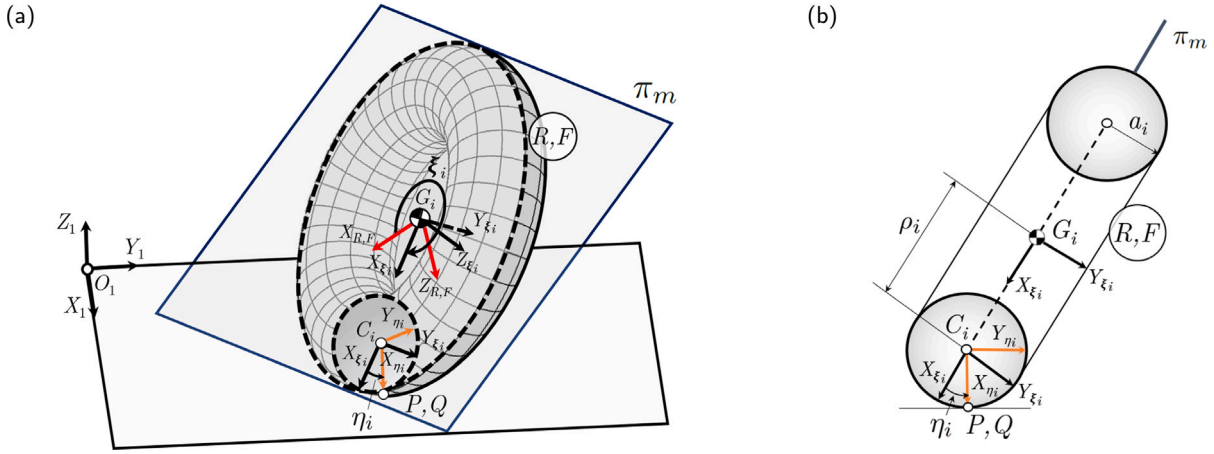

Fig. 5. Model of the toroidal wheel: three-dimensional view (a) and cross-section of the wheel (b). The angular coordinates ξ_i and η_i, with $i = \{R, F\}$, describe the toroidal geometry and are depicted in (a). The plane π_m corresponds to the middle plane of the torus. The local reference frames, the centre of mass G_i, the centre of the torus tube C_i, and the contact points with the ground, denoted as P and Q for the rear and front wheels, respectively, are also shown in (a). The cross section (b) illustrates the major and minor radii of the torus, ρ_i and a_i, with $i = \{R, F\}$.

In Eqs. (179), v is the forward speed of the bicycle; t represents time; ν is the steering axis tilt angle; z_B is the vertical distance between the rear contact point P and the centre of mass G_B; and $R_i = \rho_i + a_i$, with $i = \{R, F\}$.

The reference solution given by Eq. (178) fulfills the equations of motion (177). The forward dynamics simulation of the bicycle along the forward motion has been performed, for both the nonlinear and linear cases. To carry out the forward dynamics simulation of the nonlinear system, the index-1 DAE form of the equations of motion, given by Eq. (8), has been used. Since working with the constraints at acceleration level in Eq. (8) may result in the violation of the holonomic and nonholonomic constraints, Baumgarte's stabilization method [92] has been used to avoid numerical drift. The linear stability results of the bicycle benchmark of Meijaard et al. [14] showed that the system is asymptotically stable for the velocity range $v_w < v < v_c$, with $v_w \simeq 4.29$ m/s and $v_c \simeq 6.02$ m/s. The results of the forward dynamics simulation are shown below, for different initial values of forward velocity, $\dot{x}_b(0) = v_0$, within and outside the self-stability velocity range: $v_0 = 5$ m/s and $v_0 = 7.5$ m/s.

In the numerical integration, performed using the ode45 solver of MATLAB, the initial conditions considered are the values of the generalized coordinates and their velocities in the reference solution (178). A perturbation in the time derivative of the lean angle, $\dot{\phi}_b(0)$, has been considered. Fig. 6(a) shows the time evolution of the lean angle, ϕ_b, in both the linear and nonlinear cases, for an initial forward velocity of $v_0 = 5$ m/s and a perturbation $\dot{\phi}_b(0) = 0.1$ rad/s. It can be seen that the linear response accurately reproduces the nonlinear result and that the initial oscillations caused by the perturbation diminish over

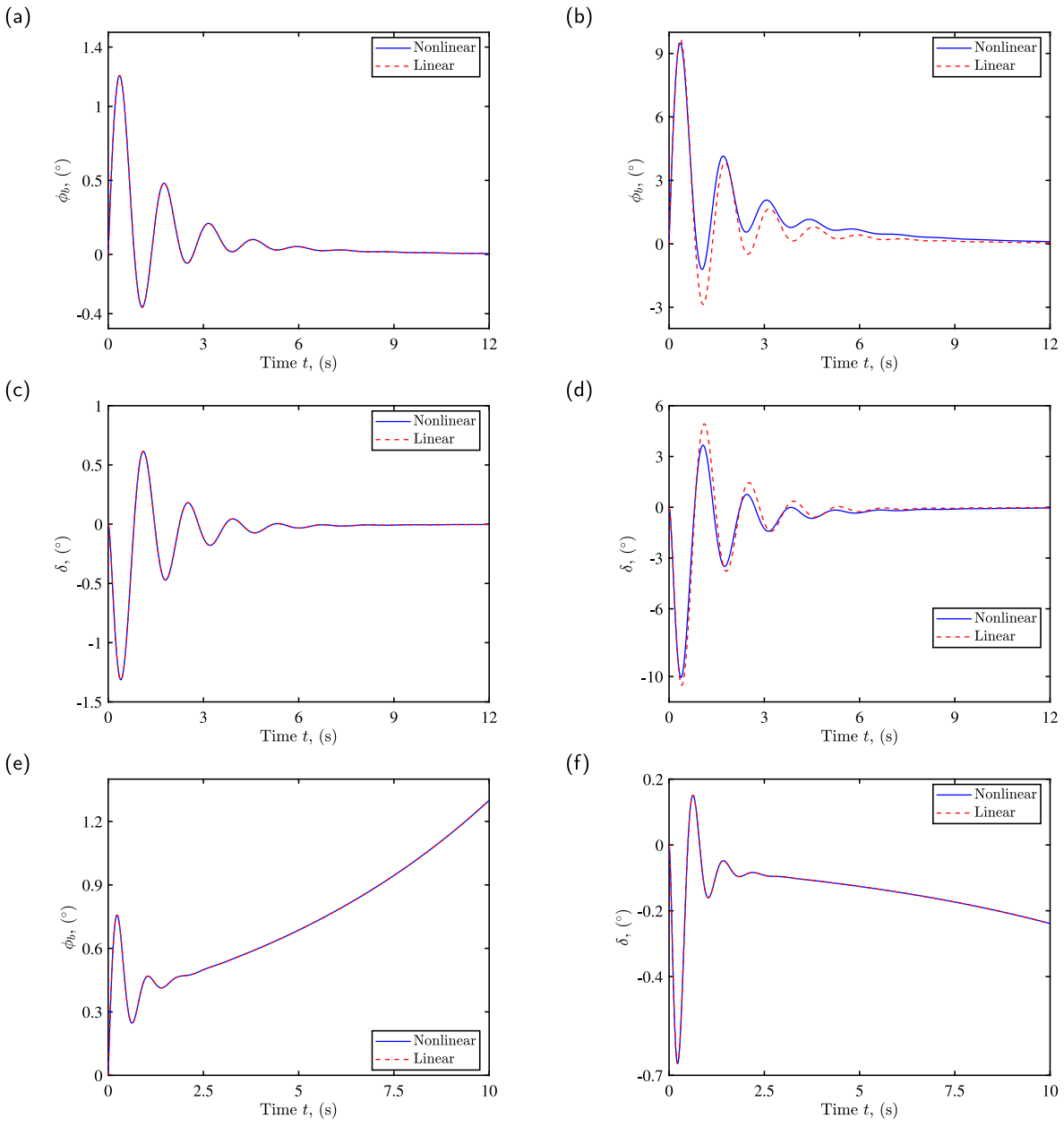

Fig. 6. Results of the forward dynamics simulation of the bicycle benchmark multibody model: time evolution of the lean angle ϕ_b (a) and steering angle δ (c), for a small perturbation, $\dot{\phi}_b(0) = 0.1$ rad/s; and time evolution of ϕ_b (b) and δ (d), for a larger value of the perturbation, $\dot{\phi}_b(0) = 0.8$ rad/s. The dynamic simulations in (a), (b), (c) and (d) are performed for an initial velocity $v_0 = 5$ m/s, within the self-stability velocity range of the bicycle benchmark: $v_w < v < v_c$, with $v_w \simeq 4.29$ m/s and $v_c \simeq 6.02$ m/s. Both the linear and nonlinear cases are shown. In (a) and (c), which correspond to the small perturbation, it can be seen that the linear responses accurately reproduce the nonlinear results and that the initial oscillations diminish over time. In contrast, for a larger perturbation, the linear responses in (b) and (d) reproduce the nonlinear results with less accuracy. Lastly, (e) and (f) show the time evolution of ϕ_b and δ, respectively, in both the linear and nonlinear cases, for an initial velocity outside the self-stability velocity range of the bicycle benchmark: $v_0 = 7.5$ m/s. The results in (e) and (f) are shown for a small perturbation of $\dot{\phi}_b(0) = 0.1$ rad/s. It can be seen that the linear responses accurately reproduce the nonlinear results and that the system is unstable, since the lean and steering angles increase over time.

time. Fig. 6(b) shows the time evolution of ϕ_b, in both the linear and nonlinear cases, for $v_0 = 5$ m/s and a larger value of the perturbation, $\dot{\phi}_b(0) = 0.8$ rad/s. In this scenario, the linear response reproduces the nonlinear result with less accuracy. Analogous results for the steering angle δ can be seen in Fig. 6. The time evolution of δ, in both the linear and nonlinear cases, is shown in Fig. 6(c) for an initial forward velocity of $v_0 = 5$ m/s and a perturbation of $\dot{\phi}_b(0) = 0.1$ rad/s. The linear response accurately reproduces the nonlinear result and the initial oscillations caused by the perturbation vanish over time. In contrast, when a larger perturbation is considered ($\dot{\phi}_b(0) = 0.8$ rad/s), the linear response reproduces the nonlinear result with less accuracy, as can be seen in Fig. 6(d). Furthermore, the results of the forward dynamics simulation, considering an initial velocity $v_0 = 7.5$ m/s outside the self-stability velocity range of the bicycle benchmark, are shown in Fig. 6. Fig. 6(e) represents the time evolution of the lean angle, ϕ_b, in both the linear and nonlinear cases, for a perturbation $\dot{\phi}_b(0) = 0.1$ rad/s. It can be seen that the linear response accurately reproduces the nonlinear result and that the system is unstable, since the lean angle increases over time. The unstable behavior can also be observed for the steering angle δ, whose time evolution is shown in Fig. 6(f), for both the linear and nonlinear cases. Lastly, the time evolution of the 2-norm of the holonomic and nonholonomic constraints is shown in Figs. 7 (a) and (b), respectively. It can be seen that the constraints are fulfilled throughout the forward dynamics simulation.

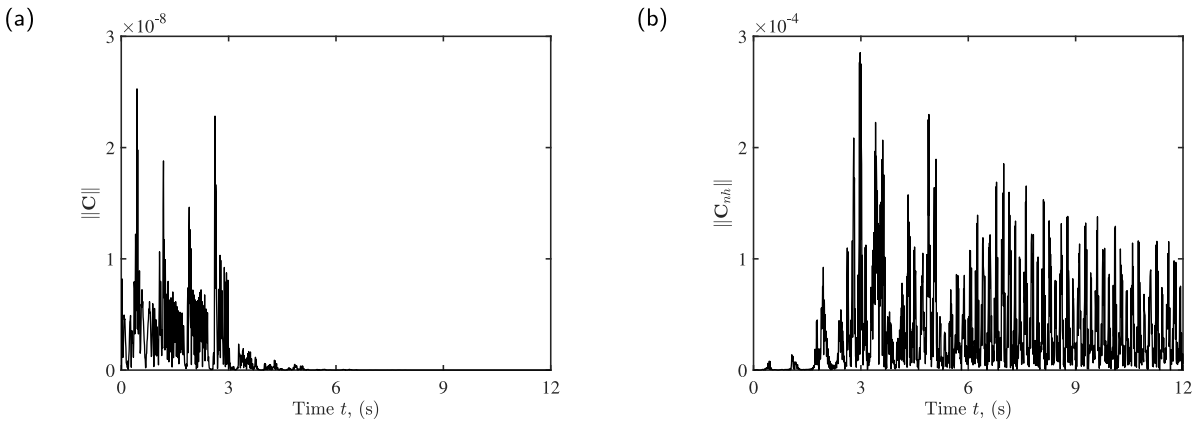

Fig. 7. Fulfillment of the holonomic and nonholonomic constraints throughout the forward dynamics simulation, considering an initial velocity $v_0 = 5$ m/s and a perturbation $\dot{\phi}_b(0) = 0.1$ rad/s. The time evolution of the 2-norm of the holonomic (a) and nonholonomic (b) constraints is shown. Since working with the constraints at acceleration level in the index-1 DAE of Eq. (8) may result in the violation of the holonomic and nonholonomic constraints, Baumgarte's stabilization method [92] has been used to avoid numerical drift.

Appendix C. Description of the electric kickscooter multibody model with rear and front suspensions

The e-scooter multibody model presents toroidal wheels, rear and front suspensions. The geometric and dynamic parameters are those of the e-scooter benchmark of García-Vallejo et al. [87], based on the SEAT eXS Kickscooter ES2. As in the bicycle case, the equations of motion are derived as explained in Schiehlen [91]. The multibody model presents seven bodies: the rear and front wheels are bodies R and F, respectively; the rear body and frame assembly, which includes the rider, is body B; the front handlebar is designated as body H; the rear and front suspensions are represented as bodies S_R and S_F, respectively; and lastly, the global reference frame is denoted as body 1. The origin of the inertial frame is O_1, and the origins of the body reference frames are located at the respective centres of mass G_j, with $j = \{R, F, B, H, S_R, S_F\}$.

To describe the system, a set of $n = 15$ coordinates is used, with the $n \times 1$ vector of coordinates $\boldsymbol{x}$ given by:

$$\boldsymbol{x} = \begin{pmatrix} x_b & y_b & z_b & \psi_b & \phi_b & \theta_b & \delta & s & \theta_{S_R} & \theta_R & \theta_F \\ & & \xi_R & \xi_F & \eta_R & \eta_F & & & & & \end{pmatrix}^{\mathrm{T}}. \tag{180}$$

The coordinates x_b, y_b and z_b are Cartesian coordinates that locate the centre of mass G_B; ψ_b is the yaw angle; ϕ_b is the lean angle; and θ_b is the pitch angle. The triplet $\{\psi_b, \phi_b, \theta_b\}$ allows for orientating body B in space. The steering angle δ corresponds to the rotation of the handlebar with respect to body B. Moreover, the coordinate s represents the distance between G_H and G_F and considers the spring elongation of the front suspension. Furthermore, θ_{S_R} represents the rotation of body S_R with respect to body B, due to the rear suspension. The rotations of the rear and front wheels are given by θ_R and θ_F, respectively. As in the bicycle case, the wheels of the e-scooter are modeled with toroidal geometry. Therefore, the same model described in Appendix B for the toroidal wheels of the bicycle is used. To parameterize the surfaces of the wheels, the angular coordinates ξ_i and η_i, presented in Eq. (180), with $i = \{R, F\}$, are used. Fig. 8 shows the numbering of the bodies, the set of generalized coordinates of the system and the body reference frames. The rider model used in the e-scooter benchmark [87] has been considered in this work. The shape of the rider has been simplified in Fig. 8, in order to ease the visualization of the multibody model.

The rear suspension is modeled by means of a torsion spring, with stiffness constant k_r, and a damper with damping coefficient d_r. A detailed view of the rear suspension is shown in Fig. 9. In particular, Fig. 9(a) shows a view of the rear suspension of a SEAT eXS Kickscooter ES2, and Fig. 9(b) illustrates a scheme with body S_R and the coordinate θ_{S_R}. The front suspension is modeled as a linear spring with stiffness

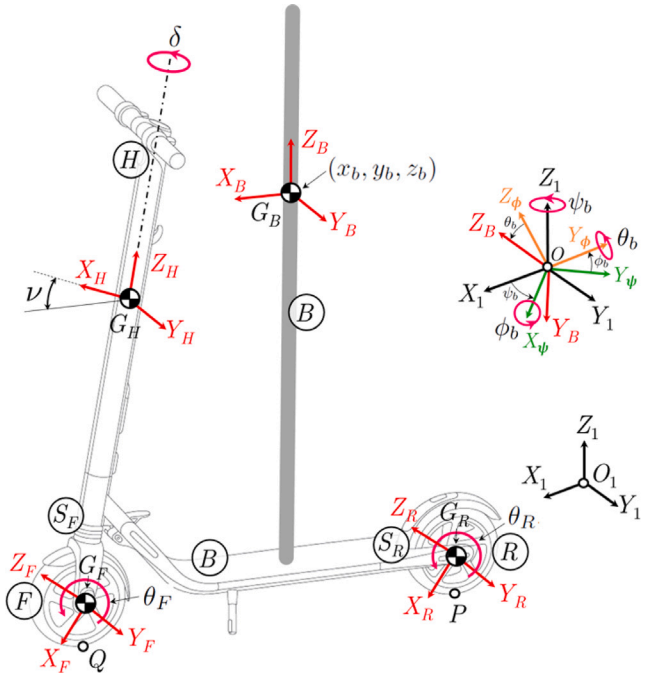

Fig. 8. Multibody model of the SEAT eXS Kickscooter ES2: numbering of the bodies, generalized coordinates and body reference frames. The global reference frame is designated as body 1, with origin O_1; the rear body and frame assembly, including the rider, is body B; the front handlebar is body H; the rear and front suspensions are represented as bodies S_R and S_F, respectively; and the rear and front wheels, modeled as tori rolling without slipping, are bodies R and F, respectively. The generalized coordinates of the multibody system, presented in Eq. (180), are shown, except for the coordinate θ_{S_R}, associated with the rear suspension, shown in Fig. 9(b); the coordinate s, associated with the front suspension, depicted in Fig. 10(b); and the angular coordinates that describe the toroidal geometry of the wheels, ξ_R, ξ_F, η_R and η_F, which are the same as those in the bicycle case and are shown in detail in Fig. 5. The body reference frames, whose origins are the centres of mass G_j, with $j = \{R, F, B, H, S_R, S_F\}$, are depicted. The rider is represented in a simplified manner to facilitate the visualization of the multibody model.

constant k_f and a damper with damping coefficient d_f. Fig. 10(a) shows the front suspension of the SEAT eXS Kickscooter ES2, and Fig. 10(b) presents a scheme with body S_F and the coordinate s.

The set of holonomic constraints arise from the contact of the e-scooter wheels with the ground:

$$\boldsymbol{C}(\boldsymbol{x}) = \begin{pmatrix} r_{P_Z} & r_{Q_Z} & \boldsymbol{n} \cdot \boldsymbol{t}_{L_R} & \boldsymbol{n} \cdot \boldsymbol{t}_{T_R} & \boldsymbol{n} \cdot \boldsymbol{t}_{L_F} & \boldsymbol{n} \cdot \boldsymbol{t}_{T_F} \end{pmatrix}^{\mathrm{T}} = \boldsymbol{0}, \tag{181}$$

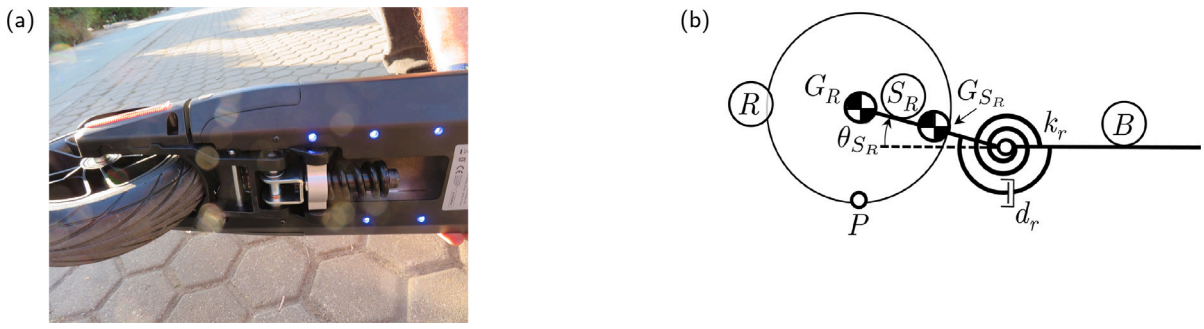

Fig. 9. Rear suspension of the e-scooter multibody model: view of the rear suspension of a SEAT eXS Kickscooter ES2 (a) and scheme with body S_R and the coordinate θ_{S_R} (b). Note that, as shown in (b), the rear suspension is modeled by means of a torsion spring, with stiffness constant k_r, and a damper with damping coefficient d_r.

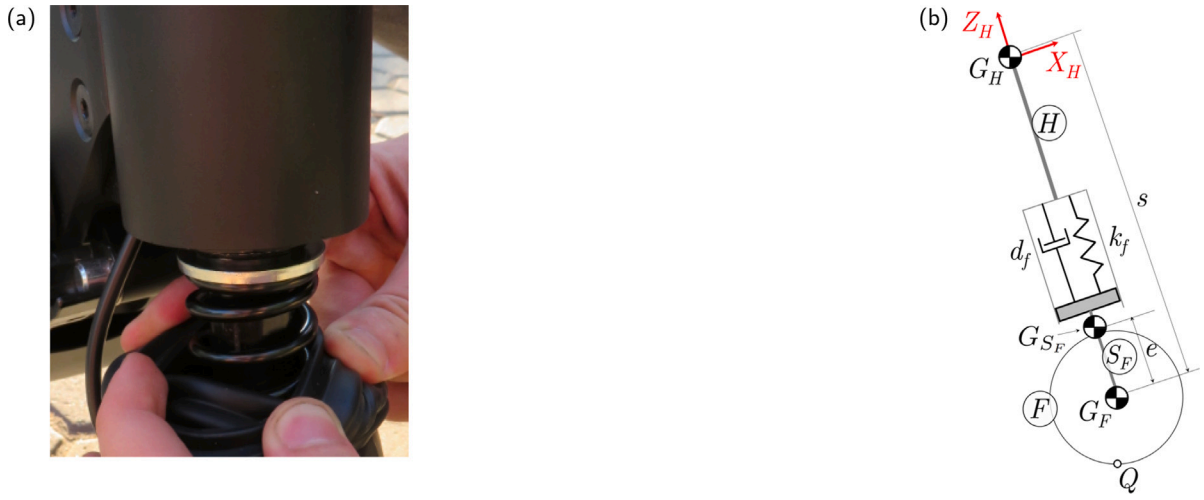

Fig. 10. Front suspension of the e-scooter multibody model: front suspension of the SEAT eXS Kickscooter ES2 (a) and scheme with body S_F and the coordinate s (b). The front suspension is modeled as a linear spring with stiffness constant k_f and a damper with damping coefficient d_f.

where r_{P_Z} and r_{Q_Z} are the Z-components of the position vectors $\boldsymbol{r}_P$ and $\boldsymbol{r}_Q$ of the contact points P and Q; $\boldsymbol{t}_{L_i}$ and $\boldsymbol{t}_{T_i}$ are the longitudinal and transversal tangent vectors to the contact points; and $\boldsymbol{n}$ is the normal vector to the ground surface. The expressions of these vectors are the same as in the bicycle case and can be found in Eqs. (173). The wheels are assumed to roll without slipping, leading to the following nonholonomic constraints:

$$\boldsymbol{C}_{nh}(\boldsymbol{x}, \dot{\boldsymbol{x}}) = \begin{pmatrix} v_{P_x} & v_{P_y} & v_{Q_x} & v_{Q_y} \end{pmatrix}^{\mathrm{T}} = \boldsymbol{0}, \tag{182}$$

where $\boldsymbol{v}_P$ and $\boldsymbol{v}_Q$ are the velocity of the contact points P and Q, respectively, computed as shown in Eq. (176).

The e-scooter multibody model presents $n = 15$ coordinates, $m = 6$ holonomic constraints and $l = 4$ nonholonomic constraints, which results in $n_g = n - m - l = 5$ degrees of freedom. The equations of motion of the e-scooter constitute an index-3 DAE system, given by the dynamic Eqs. (1) (derived as explained in Schiehlen [91]), the holonomic constraints (181) and the nonholonomic constraints (182):

$$\begin{aligned} &\boldsymbol{M}(\boldsymbol{x})\ddot{\boldsymbol{x}} + \boldsymbol{D}^{\mathrm{T}}(\boldsymbol{x})\boldsymbol{\Lambda} = \boldsymbol{Q}(\boldsymbol{x}, \dot{\boldsymbol{x}}), \\ &\boldsymbol{C}(\boldsymbol{x}) = \boldsymbol{0}, \\ &\boldsymbol{C}_{nh}(\boldsymbol{x}, \dot{\boldsymbol{x}}) = \boldsymbol{B}(\boldsymbol{x})\dot{\boldsymbol{x}} = \boldsymbol{0}. \end{aligned} \tag{183}$$

The steady forward motion of the uncontrolled e-scooter is expressed as:

$$\boldsymbol{x}^0 = \begin{pmatrix} x_b^0 & y_b^0 & z_b^0 & \psi_b^0 & \phi_b^0 & \theta_b^0 & s^0 & \theta_{S_R}^0 & \theta_R^0 & \theta_F^0 & \xi_R^0 \\ & & \xi_F^0 & \eta_R^0 & \eta_F^0 & & & & & & \end{pmatrix}^{\mathrm{T}}, \tag{184}$$

with

$$\begin{aligned} &x_b^0(t) = vt, && \theta_{S_R}^0(t) = \theta_{S_R}^0, \\ &y_b^0(t) = 0, && \theta_R^0(t) = \frac{v}{R_R}t, \\ &z_b^0(t) = z_0, && \theta_F^0(t) = \frac{v}{R_F}t, \\ &\psi_b^0(t) = 0, && \xi_R^0(t) = \zeta_R^0 - \theta_R^0(t), \\ &\phi_b^0(t) = 0, && \xi_F^0(t) = \zeta_F^0 - \theta_F^0(t), \\ &\theta_b^0(t) = \theta_0, && \eta_R^0(t) = 0, \\ &\delta^0(t) = 0, && \eta_F^0(t) = 0, \\ &s^0(t) = s_0. \end{aligned} \tag{185}$$

In Eqs. (185), v is the forward speed; t represents time; and z_0, θ_0, s_0, $\theta_{S_R}^0$, ζ_R^0 and ζ_F^0 are constants. The reference solution (184) verifies the equations of motion (183).

References

[1] Wehage RA, Haug EJ. Generalized coordinate partitioning for dimension reduction in analysis of constrained dynamic systems. ASME J Mech Des 1982;104(1):247–55.
[2] Blajer W, Schiehlen W, Schirm W. A projective criterion to the coordinate partitioning method for multibody dynamics. Arch Appl Mech 1994;64(2):86–98.
[3] De Jalon JG, Bayo E. Kinematic and dynamic simulation of multibody systems: the real-time challenge. Springer Science & Business Media; 2012.
[4] Negrut D, Ortiz JL. A practical approach for the linearization of the constrained multibody dynamics equations. J Comput Nonlinear Dyn 2006;1(3):230–9. http://dx.doi.org/10.1115/1.2198876.
[5] Escalona JL, Chamorro R. Stability analysis of vehicles on circular motions using multibody dynamics. Nonlinear Dynam 2008;53(3):237–50.

[6] Chamorro R, Escalona JL, Recuero AM. Stability analysis of multibody systems with long flexible bodies using the moving modes method and its application to railroad dynamics. J Comput Nonlinear Dyn 2014;9(1).

[7] González F, Masarati P, Cuadrado J, Naya MA. Assessment of linearization approaches for multibody dynamics formulations. J Comput Nonlinear Dyn 2017;12(4).

[8] Pappalardo CM, Lettieri A, Guida D. Stability analysis of rigid multibody mechanical systems with holonomic and nonholonomic constraints. Arch Appl Mech 2020.

[9] Pappalardo CM, Lettieri A, Guida D. A general multibody approach for the linear and nonlinear stability analysis of bicycle systems. Part I: methods of constrained dynamics. J Appl Comput Mech 2021;7(2):655–70.

[10] Pappalardo CM, Lettieri A, Guida D. A general multibody approach for the linear and nonlinear stability analysis of bicycle systems. Part II: application to the whipple-carvallo bicycle model. J Appl Comput Mech 2021;7(2):671–700.

[11] Xiong J, Wang N, Liu C. Bicycle dynamics and its circular solution on a revolution surface. Acta Mech Sin 2020;36(1):220–33.

[12] Van Khang N, Nam NS, Van Quyen N. Symbolic linearization and vibration analysis of constrained multibody systems. Arch Appl Mech 2018;88(8):1369–84.

[13] García-Agúndez A, García-Vallejo D, Freire E. Linearization approaches for general multibody systems validated through stability analysis of a benchmark bicycle model. Nonlinear Dynam 2021;103(1):557–80.

[14] Meijaard JP, Papadopoulos JM, Ruina A, Schwab AL. Linearized dynamics equations for the balance and steer of a bicycle: A benchmark and review. Proc R Soc A Math Phys Eng Sci 2007;463(2084):1955–82. http://dx.doi.org/10.1098/rspa.2007.1857, URL https://www.scopus.com/inward/record.uri?eid=2-s2.0-36349022162&doi=10.1098%2frspa.2007.1857&partnerID=40&md5=98e61532aacaadb476b77b495a67759b.

[15] Cuadrado J, Dopico D, Barreiro A, Delgado E. Real-time state observers based on multibody models and the extended Kalman filter. J Mech Sci Technol 2009;23(4):894–900.

[16] Cuadrado J, Dopico D, Perez JA, Pastorino R. Automotive observers based on multibody models and the extended Kalman filter. Multibody Syst Dyn 2012;27(1):3–19.

[17] Sanjurjo E, Naya MÁ, Blanco-Claraco JL, Torres-Moreno JL, Giménez-Fernández A. Accuracy and efficiency comparison of various nonlinear Kalman filters applied to multibody models. Nonlinear Dynam 2017;88(3):1935–51.

[18] Naya MÁ, Sanjurjo E, Rodríguez AJ, Cuadrado J. Kalman filters based on multibody models: linking simulation and real world. A comprehensive review. Multibody Syst Dyn 2023;1–43.

[19] Pyrhönen L, Jaiswal S, Garcia-Agundez A, García Vallejo D, Mikkola A. Linearization-based state-transition model for the discrete extended Kalman filter applied to multibody simulations. Multibody Syst Dyn 2023;57(1):55–72.

[20] Jaiswal S, Sanjurjo E, Cuadrado J, Sopanen J, Mikkola A. State estimator based on an indirect Kalman filter for a hydraulically actuated multibody system. Multibody Syst Dyn 2022;54(4):373–98.

[21] Sanjurjo E, Dopico D, Luaces A, Naya MÁ. State and force observers based on multibody models and the indirect Kalman filter. Mech Syst Signal Process 2018;106:210–28.

[22] Rodríguez AJ, Sanjurjo E, Pastorino R, Naya MÁ. State, parameter and input observers based on multibody models and Kalman filters for vehicle dynamics. Mech Syst Signal Process 2021;155:107544.

[23] Peterson DL, Gede G, Hubbard M. Symbolic linearization of equations of motion of constrained multibody systems. Multibody Syst Dyn 2015;33(2):143–61.

[24] Kane TR, Levinson DA. Dynamics, theory and applications. McGraw Hill; 1985.

[25] Escalona JL, Recuero AM. A bicycle model for education in multibody dynamics and real-time interactive simulation. Multibody Syst Dyn 2012;27(3):383–402.

[26] Bae D. An implementation method of linearized equations of motion for multibody systems with closed loops. Trans Korean Soc Mach Tool Eng 2003;12(2):71–8.

[27] Cossalter V, Lot R, Maggio F. The modal analysis of a motorcycle in straight running and on a curve. Meccanica 2004;39(1):1–16.

[28] Bayo E, De Jalon JG, Serna MA. A modified Lagrangian formulation for the dynamic analysis of constrained mechanical systems. Comput Methods Appl Mech Engrg 1988;71(2):183–95.

[29] González F, Masarati P, Cuadrado J. On the linearization of multibody dynamics formulations. In: International design engineering technical conferences and computers and information in engineering conference, vol. 50183. American Society of Mechanical Engineers; 2016, V006T09A008.

[30] Xiong J, Wang N, Liu C. Stability analysis for the Whipple bicycle dynamics. Multibody Syst Dyn 2020;48(3):311–35.

[31] Desloge EA. The Gibbs–Appell equations of motion. Amer J Phys 1988;56(9):841–6.

[32] Van Khang N. About the Gibbs-Appel equations for multibody systems. Vietnam J Mech 2006;28(4):225–9.

[33] Xiong J, Liu C. Symmetry and relative equilibria of a bicycle system moving on a surface of revolution. Nonlinear Dynam 2021;106(4):2859–78.

[34] Voronets P. On the equations of motion for nonholonomic systems. Mat Sb 1901;22(4):681–97.

[35] Bos M, Traversaro S, Pucci D, Saccon A. Efficient geometric linearization of moving-base rigid robot dynamics. 2022, arXiv preprint arXiv:2204.05092.

[36] Angeli A, Desmet W, Naets F. Deep learning of multibody minimal coordinates for state and input estimation with Kalman filtering. Multibody Syst Dyn 2021;53(2):205–23.

[37] Khadim Q, Kiani-Oshtorjani M, Jaiswal S, Matikainen MK, Mikkola A. Estimating the characteristic curve of a directional control valve in a combined multibody and hydraulic system using an augmented discrete extended Kalman filter. Sensors 2021;21(15):5029.

[38] Adduci R, Vermaut M, Naets F, Croes J, Desmet W. A discrete-time extended Kalman filter approach tailored for multibody models: state-input estimation. Sensors 2021;21(13):4495.

[39] Tang Y, Hu H, Tian Q. Model order reduction based on successively local linearizations for flexible multibody dynamics. Internat J Numer Methods Engrg 2019;118(3):159–80.

[40] Bauchau OA, Wang J. Stability analysis of complex multibody systems. J Comput Nonlinear Dyn 2006;1(1):71–80.

[41] Bauchau OA, Nikishkov YG. An implicit transition matrix approach to stability analysis of flexible multi-body systems. Multibody Syst Dyn 2001;5:279–301.

[42] Coddington EA, Levinson N. Theory of ordinary differential equations. New York, USA: McGraw-Hill; 1955.

[43] Nayfeh A. Nonlinear interactions: Analytical, computational, and experimental methods. New York, USA: Wiley; 2000.

[44] Bauchau OA, Nikishkov YG. An implicit floquet analysis for rotorcraft stability evaluation. J Am Helicopter Soc 2001;46(3):200–9.

[45] Han S, Bauchau OA. Simulation and stability analysis of periodic flexible multibody systems. Multibody Syst Dyn 2020;50:381–413.

[46] Cossalter V, Lot R, Massaro M. An advanced multibody code for handling and stability analysis of motorcycles. Meccanica 2011;46(5):943–58.

[47] Nishimi T, Aoki A, Katayama T. Analysis of straight running stability of motorcycles. Technical report, SAE Technical Paper; 1985.

[48] Splerings P. The effects of lateral front fork flexibility on the vibrational modes of straight-running single-track vehicles. Veh Syst Dyn 1981;10(1):21–35.

[49] Sharp RS. Vibrational modes of motorcycles and their design parameter sensitivities. In: Institution of mechanical engineers conference publications, vol. 3. Medical Engineering Publications Ltd; 1994, p. 107.

[50] Cossalter V, Lot R, Massaro M. The influence of frame compliance and rider mobility on the scooter stability. Veh Syst Dyn 2007;45(4):313–26.

[51] Sharp RS. The stability and control of motorcycles. J Mech Eng Sci 1971;13(5):316–29.

[52] Sharp RS. Stability, control and steering responses of motorcycles. Veh Syst Dyn 2001;35(4–5):291–318.

[53] Sharp RS, Limebeer DJ. A motorcycle model for stability and control analysis. Multibody Syst Dyn 2001;6(2):123–42.

[54] Agúndez A, García-Vallejo D, Freire E, Mikkola A. A reduced and linearized high fidelity waveboard multibody model for stability analysis. J Comput Nonlinear Dyn 2022;17(5):051010.

[55] Agúndez A, García-Vallejo D, Freire E, Mikkola A. Stability analysis of a waveboard multibody model with toroidal wheels. Multibody Syst Dyn 2021;1–31.

[56] Lu H, Stepan G, Lu J, Takacs D. Dynamics of vehicle stability control subjected to feedback delay. Eur J Mech A Solids 2022;96:104678.

[57] Lu H, Lu J, Stepan G, Denes T. Stability analysis and optimization of vehicle active motion control system with feedback time delay. In: Vehicle and automotive engineering. Springer; 2022, p. 111–25.

[58] Horvath HZ, Takacs D. Stability and local bifurcation analyses of two-wheeled trailers considering the nonlinear coupling between lateral and vertical motions. Nonlinear Dynam 2022;1–18.

[59] Mantaras DA, Luque P, Alonso M. Phase plane analysis applied to non-explicit multibody vehicle models. Multibody Syst Dyn 2022;56(2):173–88.

[60] Masarati P, Tamer A. Sensitivity of trajectory stability estimated by Lyapunov characteristic exponents. Aerosp Sci Technol 2015;47:501–10.

[61] Tamer A, Masarati P. Stability of nonlinear, time-dependent rotorcraft systems using Lyapunov characteristic exponents. J Am Helicopter Soc 2016;61(2):1–12.

[62] Tamer A, Masarati P. Sensitivity of Lyapunov exponents in design optimization of nonlinear dampers. J Comput Nonlinear Dyn 2019;14(2):021002.

[63] Cassoni G, Zanoni A, Tamer A, Masarati P. Stability of rotorcraft ground resonance by estimating Lyapunov characteristic exponents from multibody dynamics. In: International design engineering technical conferences and computers and information in engineering conference. 86304, American Society of Mechanical Engineers; 2022, V009T09A025.

[64] Masarati P, Cassoni G, Zanoni A, Tamer A, et al. Stability analysis of arbitrarily complex multibody problems using Lyapunov exponents. In: 3rd international nonlinear dynamics conference. 2023, p. 1–10.

[65] Cassoni G, Cocco A, Tamer A, Zanoni A, Masarati P, et al. Tiltrotor whirl-flutter stability analysis using the maximum Lyapunov characteristic exponent estimated from time series. Mater Res Proc 2023;37:30–3.

[66] Cassoni G, Zanoni A, Tamer A, Masarati P. Stability analysis of nonlinear rotating systems using Lyapunov characteristic exponents estimated from multibody dynamics. J Comput Nonlinear Dyn 2023;18(8):081002.

[67] Hung NB, Lim O. A review of history, development, design and research of electric bicycles. Appl Energy 2020;260:114323.

[68] Ventura R, Ghirardi A, Vetturi D, Maternini G, Barabino B. Comparing the vibrational behaviour of e-kick scooters and e-bikes. Evidence from Italy. Int J Transp Sci Technol 2023.
[69] Eccarius T, Lu C-C. Powered two-wheelers for sustainable mobility: A review of consumer adoption of electric motorcycles. Int J Sustain Transp 2020;14(3):215–31.
[70] Manrique-Escobar CA, Pappalardo CM, Guida D. On the analytical and computational methodologies for modelling two-wheeled vehicles within the multibody dynamics framework: a systematic literature review. J Appl Comput Mech 2022;8(1):153–81.
[71] Kooijman J, Schwab A, Meijaard JP. Experimental validation of a model of an uncontrolled bicycle. Multibody Syst Dyn 2008;19(1–2):115–32.
[72] Basu-Mandal P, Chatterjee A, Papadopoulos JM. Hands-free circular motions of a benchmark bicycle. Proc R Soc A Math Phys Eng Sci 2007;463(2084):1983–2003.
[73] Meijaard J, Schwab A. Linearized equations for an extended bicycle model. In: III european conference on computational mechanics. Springer; 2006, p. 772.
[74] Schwab A, Meijaard J, Kooijman J. Some recent developments in bicycle dynamics. In: Proceedings of the 12th world congress in mechanism and machine science. Citeseer; 2007, p. 1–6.
[75] Sharp RS. On the stability and control of the bicycle. Appl Mech Rev 2008;61(6).
[76] Moore JK. Human control of a bicycle. Davis Davis, CA: University of California; 2012.
[77] Bulsink VE, Doria A, van de Belt D, Koopman B. The effect of tyre and rider properties on the stability of a bicycle. Adv Mech Eng 2015;7(12):1687814015622596.
[78] Agúndez A, García-Vallejo D, Freire E. Linear stability analysis of a bicycle multibody model with toroidal wheels. In: Advances in nonlinear dynamics: Proceedings of the second international nonlinear dynamics conference (NODYCON 2021), volume 2. Springer; 2021, p. 477–87.
[79] Griffin R, Parks CT, Rue III LW, McGwin Jr G. Comparison of severe injuries between powered and nonpowered scooters among children aged 2 to 12 in the United States. Ambul Pediatr 2008;8(6):379–82.
[80] Unkuri J, Salminen P, Kallio P, Kosola S. Kick scooter injuries in children and adolescents: minor fractures and bruise. Scand J Surg 2018;107(4):350–5.
[81] Mebert RV, Klukowska-Roetzler J, Ziegenhorn S, Exadaktylos AK. Push scooter-related injuries in adults: an underestimated threat? Two decades analysed by an emergency department in the capital of Switzerland. BMJ Open Sport Exercise Med 2018;4(1):e000428.
[82] Kowalczewska J, Rzepczyk S, Żaba C. E-scooters and the city–head to toe injuries. J Med Sci 2022;91(2):e672.
[83] Kostrzewska M, Macikowski B. Towards hybrid urban mobility: Kick scooter as a means of individual transport in the city. In: IOP conference series: materials science and engineering, vol. 245, no. 5. IOP Publishing; 2017, 052073.
[84] Kazemzadeh K, Haghani M, Sprei F. Electric scooter safety: An integrative review of evidence from transport and medical research domains. Sustainable Cities Soc 2023;89:104313.
[85] Paudel M, Yap FF, Rosli TBM, Tan KH, Xu H, Vahdati N, et al. A computational study on the basis for a safe speed limit for bicycles on shared paths considering the severity of pedestrian head injuries in bicyclist-pedestrian collisions. Accid Anal Prev 2022;176:106792.
[86] Paudel M, Yap FF, Rosli TBM, Tan KH, Xu H. A computational investigation of the dynamic factors governing severity of head injury to pedestrians involved in e-scooter collisions. Transp Res Interdiscip Perspect 2023;22:100972.
[87] García-Vallejo D, Schiehlen W, García-Agúndez A. Dynamics, control and stability of motion of electric scooters. In: The IAVSD international symposium on dynamics of vehicles on roads and tracks. Springer; 2019, p. 1199–209.
[88] Klinger F, Klinger M, Edelmann J, Plöchl M. Electric scooter dynamics–From a vehicle safety perspective. In: The IAVSD international symposium on dynamics of vehicles on roads and tracks. Springer; 2022, p. 1102–12.
[89] Paudel M, Fah Yap F. Front steering design guidelines formulation for e-scooters considering the influence of sitting and standing riders on self-stability and safety performance. Proc Inst Mech Eng D 2021;235(9):2551–67.
[90] Dopico D, Zhu Y, Sandu A, Sandu C. Direct and adjoint sensitivity analysis of ordinary differential equation multibody formulations. J Comput Nonlinear Dyn 2015;10(1).
[91] Schiehlen W. Multibody system dynamics: roots and perspectives. Multibody Syst Dyn 1997;1:149–88.
[92] Baumgarte J. Stabilization of constraints and integrals of motion in dynamical systems. Comput Methods Appl Mech Engrg 1972;1(1):1–16.